6-1-2010

Damage detection via structural model updating using frequency response functions and genetic algorithms

Bassam Elsaid

The American University in Cairo
School of Sciences and Engineering

Damage Detection via Structural Model Updating using Frequency Response Functions and Genetic Algorithms

By

Bassam Sabry Fawzy Elsaid

A thesis submitted in partial fulfillment of the requirements for the degree of

Master of Science in Engineering

With specialization in:

Mechanical Engineering

Under supervision of:

Dr. Mustafa H. Arafa
Associate Professor, Mechanical Engineering Department

Fall 2009

ACKNOWLEDGMENTS

I would like to thank my supervisor Dr. Mustafa H. Arafa for his support and guidance which made this work possible, in addition to his continued encouragement through my entire study period at the AUC.

I dedicate this work to my wife and family who their unlimited support enabled me to achieve my goal of pursuing graduate education.

ABSTRACT

This thesis covers the development of a model updating technique which relies on the introduction of correction factors to the elemental stiffness matrix of a beam Finite Element Model (FEM). A Genetic Algorithm selects the values of correction factors by minimizing the difference between an experimentally measured Frequency Response Function (FRF) and the FRF calculated from the FEM being updated.

The model updating technique was employed as a damage detection algorithm. The first phase of damage detection is to use model updating to eliminate experimental and modeling errors between the FRF of a beam measured experimentally and the FRF of the same beam calculated by FEM. The second step of damage detection is to employ the model updating process to match the FRF of a damaged beam measured experimentally to the response of the updated FEM. A damage index based on the change in FEM correction factors during the second phase is applied to locate damage.

Three different cost functions were evaluated and tuned against two different damage cases measured experimentally. Later the best cost function was tested against two damage cases with smaller damage magnitude. The damage detection algorithm showed reasonable accuracy in determining the damage location in all cases. Additionally, this thesis covers the adaptation of strain gauges for dynamic measurement and the associated signal processing and filtering.

CONTENTS

Figures iv
Tables ix
Nomenclature x
1. Introduction 1
    1.1 Damage Indicators 1
    1.2 Damage Location And Quantification 3
    1.3 Optimization Methods 4
    1.4 Challenges Facing Damage Detection Algorithms 5
    1.5 Research Objectives 5
    1.6 Thesis Organization 6
2. Experimental Procedure 7
    2.1 Experimental Setup 7
    2.2. Signal Conditioning And Processing 11
        2.2.1 Filtering 11
        2.2.2 Fast Fourier Transform 12
        2.2.3 Automatic Mode Detection 17
    2.3 Vibration Modeling 18
        2.3.1 Response To A General Excitation 18
        2.3.2 FEM Of Beam Element 20
        2.3.3 Calculation FRF Using FEM 21
3. Model Updating Using Genetic Algorithms 23
        3.1 Optimization Problem Definition 23
        3.2 Encoding 23
        3.3 Genetic Operators 24
        3.3.1 Arithmetic Crossover 24
        3.3.2 Mutation 25
        3.3.3 Individual Selection 25
        3.3.4 Elitism 25
    3.4 Algorithm 25
    3.5 Fitness Function 26
        3.5.1 Frequency Fitness Function 27
        3.5.2 Peak Vector 27
        3.5.3 Weighted Peak Vector 28
    3.6 Optimization Constraints 28
    3.7 Solver Parameters 29
4. Damage Detection 33
    4.1 Introduction 33
    4.2 Damage Cases 34
    4.2 Damage Index 37
    4.3 Large Structural Damage 37
    4.4 Fitness Function Adjustment 50
    4.5 Small Structural Damage 57
    4.6 Effect of Excitation Location 63
    4.7 Multi-Channel Inputs 68
5. Conclusion And Recommendations For Future Work 73
    5.1 Conclusions 73

5.2 Recommendations For Future Work 73
References 74

FIGURES

Figure (2.1) Experiment Schematic 7
Figure (2.2) Sample Beam Fixation 8
Figure (2.3) Experimental Setup 8
Figure (2.4) Sample beam no. 1 with damage case 1 10
Figure (2.5) Sample beam no. 2 with damage case 2 10
Figure (2.6) Sample beam no. 1 with damage case 3 10
Figure (2.7) Chebyshev Filter Characteristics 11
Figure (2.8) Comparison between Various Windowing Functions 13
Figure (2.9) Comparison between Raw Strain Data before and after Filtering 14
Figure (2.10) FFT for Data after filtering and windowing 15
Figure (2.11) Averaging Technique 15
Figure (2.12) Final FRF for a sample beam 16
Figure (2.13) Automatic Mode Shape Detection Algorithm 17
Figure (2.14) Highest Amplitude Method applied to an intact beam and Damage Case4 18
Figure (2.15) Beam Element 20
Figure (2.16): Force applied to finite model 21
Figure (2.17): Comparison bet. Theoretical and Experimental FRF for Intact Beam 1 22
Figure (2.18): Comparison bet. Theoretical and Experimental FRF for Intact Beam 2. 22
Figure (3.1): Problem GA Encoding 24
Figure (3.2): Arithmetic Crossover 24
Figure (3.3): Geometric Probability Distribution 25
Figure (3.4): Genetic Solver Algorithm 26
Figure (3.5) Peak Vector Definetion 28
Figure (3.8): Model Updating Result for Intact Beam 1 31
Figure (3.9): Model Updating Convergence for Intact Beam 1 32
Figure (4.1): Damage Detection Algorithm 33
Figure (4.2): Top View of Damage Location and size 34
Figure (4.3) FRF Comparison for Case 1 35
Figure (4.4) FRF Comparison for Case 2 35
Figure (4.5) FRF Comparison for Case 3 36
Figure (4.6) FRF Comparison for Case 4 36
Figure (4.7): Damage Detection Run1 Results 38
Figure (4.8): Final Correction Factors For Damage Detection Run1 39

Figure (4.9): Damage Detection Run 2 Results 40
Figure (4.10): Final Correction Factors For Damage Detection Run 2 40
Figure (4.11): Model Tuning Results for Run 3 41
Figure (4.12): Final Correction Factors For Damage Detection Run 3 41
Figure (4.13): Damage Detection Results for Run 3 42
Figure (4.14): Model Tuning Results for Run 4 43
Figure (4.15): Final Correction Factors For Damage Detection Run 4 43
Figure (4.16): Damage Detection Results for Run 4 44
Figure (4.17): Model Tuning Detection Results for Run 5 45
Figure (4.18): Final Correction Factors For Damage Detection Run 5 46
Figure (4.19): Damage Detection Results for Run 5 47
Figure (4.20): Model Tuning Results for Run 6 48
Figure (4.21): Final Correction Factors For Damage Detection Run 6 48
Figure (4.22): Damage Detection Results for Run 6 49
Figure (4.23): Model Tuning Results for Run 7 51
Figure (4.24): Final Correction Factors For Damage Detection Run 7 51
Figure (4.25): Damage Detection Results for Run 7 52
Figure (4.26): Model Tuning Results for Run 8 53
Figure (4.27): Final Correction Factors For Damage Detection Run 8 53
Figure (4.28): Damage Detection Results for Run 8 54
Figure (4.29): Model Tuning Results for Run 9 55
Figure (4.30): Final Correction Factors For Damage Detection Run 9 55
Figure (4.31): Damage Detection Results for Run 9 56
Figure (4.32): Model Tuning Results for Run 10 57
Figure (4.33): Final Correction Factors For Damage Detection Run 10 58
Figure (4.34): Damage Detection Results for Run 10 59
Figure (4.35): Model Tuning Results for Run 11 60
Figure (4.36): Final Correction Factors For Damage Detection Run 11 61
Figure (4.37): Damage Detection Results for Run 11 62
Figure (4.38): Model Tuning Results for Scenario #3 using Base Excitation 64
Figure (4.39): Final Correction Factors for Scenario #3 using Base Excitation 64
Figure (4.40): Damage Detection Results for Scenario #3 using Base Excitation 65
Figure (4.41): Model Tuning Results for Scenario #4 using Base Excitation 66
Figure (4.42): Final Correction Factors for Scenario #4 using Base Excitation 67
Figure (4.43): Damage Detection Results for Scenario #4 using Base Excitation 67
Figure (4.44): Model Tuning Results for Scenario #3 using Base Excitation and Averaged Normalized Strain 68

Figure (4.45): Final Correction Factors for Scenario #3 using Base Excitation and Averaged Normalized Strain 69

Figure (4.46): Damage Detection Results for Scenario #3 using Base Excitation and Averaged Normalized Strain 70

Figure (4.47): Model Tuning Results for Scenario #4 using Base Excitation and Averaged Normalized Strain 71

Figure (4.48): Final Correction Factors for Scenario #4 using Base Excitation and Averaged Normalized Strain 71

Figure (4.49): Damage Detection Results for Scenario #4 using Base Excitation and Averaged Normalized Strain 72

TABELS

Table (2.1) Strain gauges location on a sample beam 9
Table (2.1) Strain gauges location on a sample beam 9
Table (2.3) Sample Beam Specifications 9
Table (2.4) Natural Frequencies of the sample beam calculated by FEA 10
Table (2.5) Filters used to remove unwanted frequency ranges. 12
Table (3.1): Genetic Solver Parameters 30
Table (3.2): Effect of Number of Elements on Solution Fitness 30
Table (4.1): Damage Cases Details 34
Table (4.2) Large Structural Damage Detection Runs 37
Table (4.3) Results for Damage Detection Run 1 38
Table (4.4) Results for Damage Detection Run 1 39
Table (4.5): Fitness Function Adjustment Runs Details 50
Table (4.6): Damage Detection for Minor Structural Damage. 57

NOMENCLATURES

a	Damage Location Measured from Beam Root
ACO	Ant Colony Optimization
B	Beam Shape Function
b	Damage Width
c	Damping coefficient
DFT	Discrete Fourier Transform
F	Total Fitness Function
FBDD	Frequency Based Damage Detection
FEA	Finite Element Analysis
FEM	Finite Element Modeling
FFT	Fast Fourier Transform
FRF	Frequency Response Function
F_{nc}	Fitness Function Measured by one senor
F_o	Applied force
G	Genetic Algorithm Offspring
GA	Genetic Algorithm
I_i	Damage index for element i
k	Stiffness coefficient
k_o	Stiffness coefficient before model updating
l	Full signal length
l_i	Signal interval length
m	Mass coefficient
MBDD	Modal Based Damage Detection
m_o	Mass coefficient before model updating
N	Number of averaging intervals
o	Averaging intervals overlap
P_{kD}	Stiffness correction factor at end of damage detection phase
P_{ki}	Stiffness correction factor for element number i

P_{kT}	Stiffness correction factor at end of model tuning phase
P_{mi}	Mass Correction factor for element i
PSO	Particle Swarm Optimization
q	Nodal Displacements
S_i	Fitness function sensitivity for the correction factor number i
VBDD	Vibration based damage detection
V_p	Peak Vector
X	Vibration Amplitude
x_e	Length of truncated segment from end of signal as result of averaging
x_s	Length of truncated segment from start of signal as result of averaging
y_E	Experimental mode shape amplitude
y_T	Theoretical mode shape amplitude
α	Damping stiffness proportionality coefficient
β	Damping mass proportionality coefficient
γ	Fitness function scale factor
λ	Interpolation factor
Φ	Vibration phase
ω	Excitation frequency
ω_E	Experimental mode shape frequency
ω_T	Theoretical mode shape frequency

CHAPTER ONE
INTRODUCTION

The sudden failure of an engineering structure usually constitutes a major economical loss and in some cases might constitute a danger to human life. As a result, the majority of engineering disciplines have interest in Non Destructive Damage Detection Methods [1, 2]. All available damage detection methods require prior knowledge of the possible damage vicinity. Additionally, In some applications such as aerospace structures or off shore oil structure visual inspection might be cumbersome or even impossible.

Any structural damage is associated with a change in the stiffness and mass characteristics of the damaged structural member. These changes have direct impact on the modal behavior of the structure under investigation. Consequently, detecting and quantifying the modal characteristics changes can be used to quantify and locate a structural damage [1-5]. Most of these methods, which are known as Vibration Based Damage Detection (VBDD) methods, involve comparing the modal behavior of the structure under investigation to the modal behavior of a reference structure which is known to be undamaged. The question of which parameters to measure and how to process and compare these parameters is still an active field of research and development.

1.1 Damage Indicators

Several VBDD methods which involve analyzing the changes in natural frequencies of the structure under investigation have been proposed in literature [1]. This group of methods is known as Frequency Based Damage Detection methods (FBDD). However, a group of factors adversely affect the quality of results achieved by these methods. One of factors is that the loss of mass from an unstressed parts in a structure can introduce large changes in frequencies without causing real threat to the structure integrity. Another factor is that the structure natural frequencies are very sensitive to the boundary conditions. Even a slight change in the rigidity of the supports will cause significant

changes in natural frequencies without a proportional change in the overall structure integrity. Additionally, according to Doebling and Farrar [1], using frequency shifts to detect damage is only advisable in application where frequencies can be measured accurately in a controlled environment.

Another group of VBDD methods are the Modal Based Damage Detection (MBDD). These types of methods monitor changes in modal parameters, such as mode shapes, as an damage indicator. These methods compare measured mode shapes from a reference structure to the mode shapes measured from the structure under investigation. One important example of MBDD methods is the structural translation and rotational error checking. This method relies on taking ratios of relative nodal displacements as an indicator for the difference in stiffness between experimental results and a FEM or between two experiments [6].

Several variants of the MBDD methods use mode shape curvature or strain mode shape changes as a damage ibdicator. This group of methods relies on using the derivatives of the mode shapes such as curvature, strain or strain energy. An example is the Strain Energy Damage Detection Method [5, 7] which is a very promising MBDD method based on measuring the change in relative strain energy. For sake of damage detection, the structure under consideration is divided into a group of elements, given the strain energy is known before and after the damage, a damage index can be formulated based on the change in the element's relative strain energy when compared to the whole structure.

Significant research was done on comparing the accuracy of FBDD and MBDD methods. The results indicated that the MBDD more accurate results when compared to FBDD Methods [4]. However, measuring mode shapes or its derivatives require a large number of sensors to attain a reasonable damage detection resolution. The accuracy of a method based on the mode shape or its derivatives will be directly proportional to the number of sensors used. From a practical point of view, installing a large number of sensors, related wiring, signal conditioning units and data acquisition units in a fielded structure is not always possible. Additionally, if this structure is a lightweight structure like space structures, the weight of this equipment might constitute a major design burden.

A third category of damage indicators introduced by Huynh et al.[8] uses the FRF from non destructive vibration tests. Based on the knowledge of the dynamic stiffness matrix of the intact structure and the change in the damaged structure FRF, a damage location vector can be evaluated. In the research work by by Huynh et al.[8], The dynamic stiffness matrix was calculated from the FEM of an intact structure while the FRF was measured by hammer testing.

1.2 Damage Location and Quantification

The damage indicators discussed in the previous section is not sufficient to accurately locate the damage on it is own. The change in frequencies or in modal properties can indicate the existence of some change in the structure. In order, to determine the damage location the problem becomes a type of pattern recognition problem [1].

There are many approaches to translate the change in damage indicator, whether it was an FBDD or MBDD, into damage location and size. The simplest of these methods is to study the sensitivity of the damage indicator to element attributes such as thickness and width [9, 10]. The most popular approach is to formulate an analytical damage index in terms of the damage indicator used. A third approach is solving the inverse problem of updating the structure FEM to have a response which matches that of the actual structure. Also, trained neural networks have been used successfully to identify damage based on a combination of damage indicators [11].

Solving an inverse problem will require a cost function to quantify the difference in the damage indicator, in addition to solution constraints and an optimization method. The selection of the most suitable constraints and the most reliable cost function is an active filed of research [1]. Due to complexity of the FEM updating problem, direct search methods are not a valid option. Evolutionary algorithms are considered ideal for this type of problems. Saada [12] applied model updating technique based on the frequency shifts between an intact and a damaged beam. In the course of his work Saada investigated two optimization schemes Particle Swarm Optimization (PSO) and Ant Colony Optimization (ACO) and concluded that ACO gave better optimization results.

1.3 Optimization Methods

Solving the inverse problem to find a structural mathematical model that represents the changes in the structure has been proven as a promising damage detection method [12]. The selection of an optimization method is of primary importance, since finding an accurate location is completely dependent on finding the true maxima or minima of the cost function used. As seen in the previous section researchers who attempted to tackle the inverse problem in damage detection used global optimization methods. In fact, this approach is completely justified for the following reason:

- Since damage detection algorithms are meant to be generic and should be applicable to any kind of structures. The exact behavior of the cost function can't be predicted. Hence, to maintain generality a global optimization method must be used.
- Research work done on inverse problem solutions have proven that even the simplest structures such as beams will have complex cost functions for damage detection [12]. The damage detection problem has been recognized to be a multi modal problem. Additionally, using optimization constraints might introduce cost function discontinuities.
- In direct search methods the final solution depends on the start location. So, unless a very lucky guess was made it would be hard to find the absolute maximum of a function with multi peaks or have discontinuities.
- Even for cost functions which can be handled using the direct search methods, if the number of variables being optimized was too large, the direct search methods will fall short of finding an acceptable solution.

The optimization method of choice for this research work is Genetic Algorithms (GA). The genetic algorithm is a member of the global optimization family. The GA evaluates multiple solutions each iteration. Finally, it is a search method capable of handling problems with relatively large number of variables.

1.4 Challenges Facing Damage Detection Algorithms

The challenges facing the available damage detection algorithms were discussed extensively in literature. The most important of these issues and challenges can be summarized as follows [1]:

- Some damage detection algorithms require a Finite Element Model (FEM) of the structure. In some applications, such as large existing civil structures, building and verifying a FEM might be tedious. However, in most aerospace and mechanical engineering applications building such a FEM is applicable. Verifying this model and eliminating the experimental errors will then be the major challenge.
- A group of algorithms proposed in literature use linear structure models to model the damaged structure. Assuming the structure would remain linear after damage may not be acceptable for all damage scenarios.
- Some algorithms tend to use an illogical number of sensors to detect damage. While in practice there will always be an upper limit to the number of sensors that can be employed.
- In most applications for the case of long term continuous health monitoring, relying on a measurable excitation force may not be achievable. There is a definite need for algorithms that rely on ambient sources of vibrations.

1.5 Research Objectives

Based on the challenges summarized in the previous section, the objective of this research work is to develop a vibration based damage detection algorithm that takes into consideration the following constraints:

- A model tuning phase should be included where a FEM is updated in reference to an intact structure to eliminate modeling and experimental errors.
- The algorithm should rely only on ambient sources of vibration for measurement. This constraint will be satisfied by using white noise as the only source of excitation. Additionally, no force feedback will be used since in fields of practice

measuring the ambient excitation force is a very complicated process and might not be always applicable.

- The algorithm should detect the damage accurately with a minimal number of sensors.
- Also, most vibration experimental work focuses on using accelerometers for modal testing. A promising alternative is strain gauges which can be very effective for the practical use in damage detection for the following reasons:
    - The strain gauge is compact in size and lightweight and can be accommodated in a structure without major design changes.
    - Strain gauges exhibit fast response and have a good sensitivity
- In order to ensure that the damage detection algorithm is applicable, all previous goals must be verified experimentally.

1.6 Thesis Organization

This thesis consists of five chapters. Chapter 2 covers the experimental setup and the signal processing algorithm used to adopt the strain gauge for dynamic testing. Chapter 3 discuses the GA used, the model updating process and the model tuning phase. Chapter 4 covers the damage detection process and the final results of the damage detection algorithm. The final chapter covers the conclusions and the recommendations for future work.

CHAPTER TWO
2. EXPERIMENTAL PROCEDURE

2.1 Experimental Setup

In order to provide a damage detection method that can be applied practically to structures in service such as aircrafts, ships and oil rigs, the conditions discussed in the research objectives should be imposed on the experiment design.

In order to investigate the feasibility of the proposed damage detection technique and satisfy the practical constraints, the modal response of intact beams were measured. Later damage was introduced to these beams and the modal response was measured again. The damage detection algorithm was based on comparing the damaged beam modal response to the intact beam modal response.

The experimental procedure Figure (2.1) is comprised of a Brüel & Kjær type 4809 shaker equipped with a fixture on the end of the shaker arm. The sample beam being tested is then fixed in a cantilever position using the shaker fixture. The shaker provides excitation to the beam as base motion Figure (2.2). A Brüel & Kjær type 1405 noise generator was used to generate white noise which is amplified by a Brüel & Kjær type 2706 amplifier and then fed to the shaker.

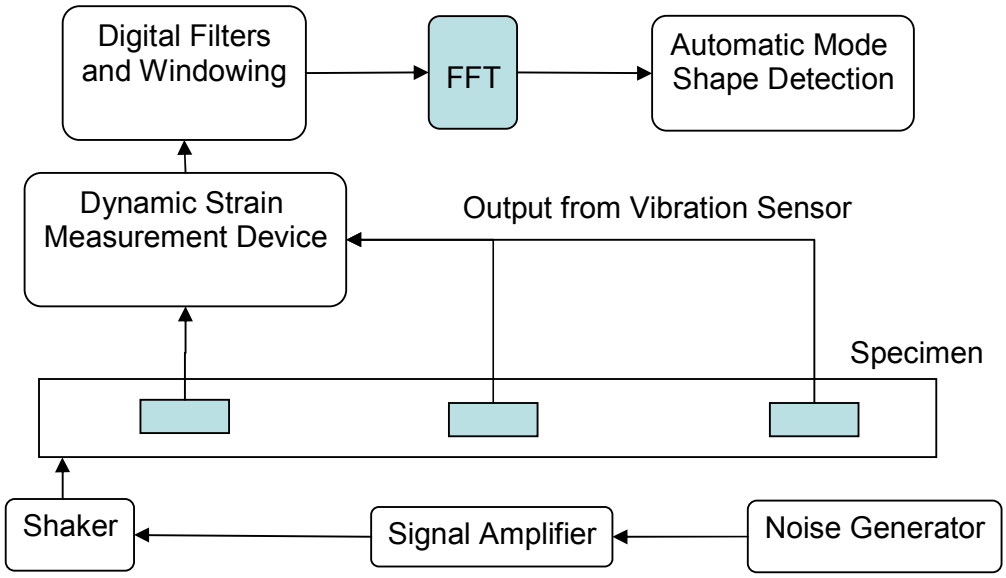

Figure (2.1) Experiment Schematic

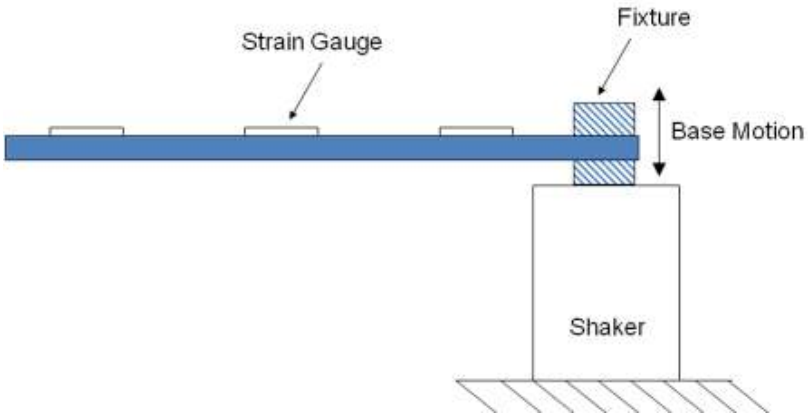

Figure (2.2) Sample Beam Fixation

Three strain gauges were fixed to each sample beam. The signal measured by these strain gauges was directly fed to a multi channel dynamic strain meter (Koywa PCD-300). The three strain gauges were calibrated using variable static loads. The experimental setup is shown in Figure (2.3). The signal acquired by the strain meter was fed online to a computer for signal processing and mode shape detection. These tasks will be discussed in detail in the subsequent section.

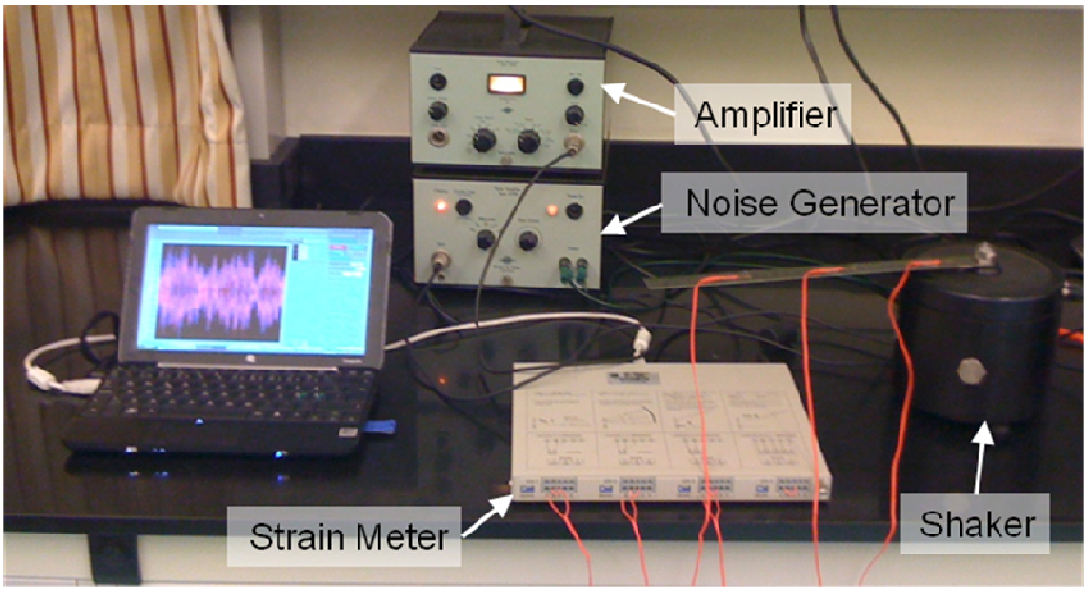

Figure (2.3) Experimental Setup

Table (2.1) shows the location of each strain gauge measured from the root of the beam.

Table (2.1) Strain gauges location on a sample beam

Channel Number	Strain Gauge location from root
1	2 cm
2	10.5 cm
3	20.5 cm

The modal analysis process was carried out for two identical intact beams. Later two damage scenarios were introduced to each beam making a total of four damage scenarios. Table (2.2) shows the sample beams specifications.

Table (2.2) Sample Beam Specifications

Length	32.5 cm / 30.5 cm from fixture
Thickness	0.7 mm
Width	26 mm
Material	Stainless Steel
Modulus of Elasticity	200 GPa
Density	7800 kg/m^3

Table (2.3) shows the details of the damage location measured from root and the damage size of the four damage scenarios tested in this research.

Table (2.3) Sample Beam Specifications

Damage Case	Beam Number	Damage Location from Root	Damage Size
1	1	19.5 cm	1mm X 10 mm
2	2	5.5 cm	1 mm X 10 mm
3	1	19.5 cm	1mm X 5 mm
4	2	5.5 cm	1mm X 5 mm

Figures (2.4, 2.5 and 2.6) show the damage introduced using a handsaw to cases 1, 2 and 3. As can be seen from figures the damage is not symmetric around the beam axis.

Figure (2.4) Sample beam no. 1 with damage case 1

Figure (2.5) Sample beam no. 2 with damage case 2

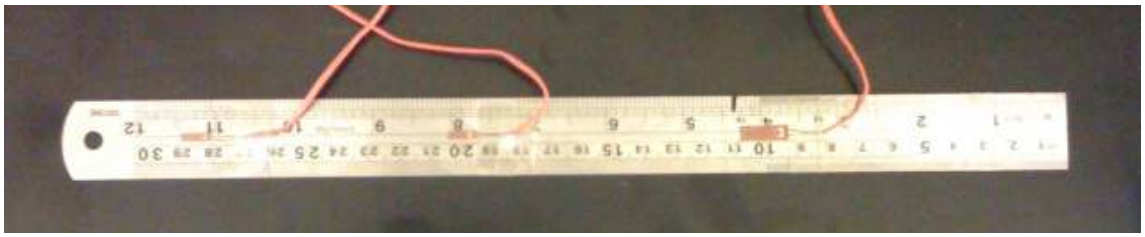

Figure (2.6) Sample beam no. 1 with damage case 3

The natural frequency of the intact beams was calculated using Finite Element Analysis (FEA). The results are shown in Table (2.4). Based on these results the frequency range for this experiment was taken form 1 Hz to 250 Hz to cover the first four mode shapes.

Table (2.4) Natural Frequencies of the sample beam calculated by FEA

Mode #	FEA Frequency (Hz)
1	6.16
2	38.57
3	108
4	211.6

2.2. Signal Conditioning and Processing

The strain meter used in the present work provides the necessary power input to the strain gauges and automatically balances the strain gauges bridge circuit electronically. The output is then converted to strain units and can be either displayed or stored with no option to further manipulate the data. For this reason all signal conditioning and processing had to be done separately since the use of conventional spectrum analyzers could not be facilitated as available models are adjusted to conventional vibration sensors. While this incurred a great deal of computation effort it resulted in better control of the signal processing through dedicated algorithms that were developed by the author. These are explained in the following sections.

2.2.1 Filtering

The experimental setup described in section 2.1 was used to measure the strain variation with time. Though the experiment was conducted in a laboratory environment, as expected, the acquired signal was contaminated by other ambient sources of noise. In order to remove unwanted frequency components form the signal, a digital signal filter was used [13]. For the purpose of this research work the MATLAB® built in implementation for Type 1 Chebyshev filter was selected [14].

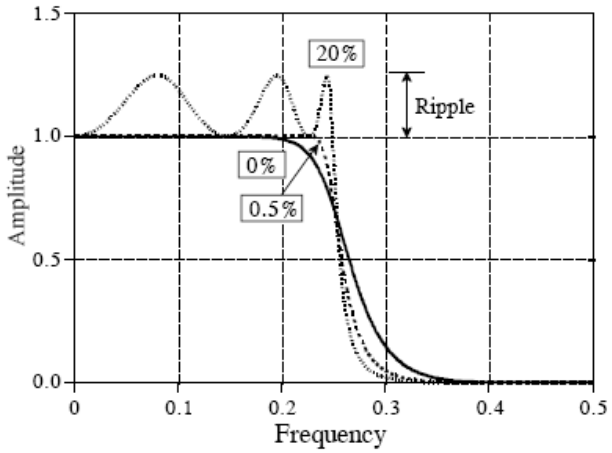

Figure (2.7) Chebyshev Filter Characteristics

The filter type is an important parameter to be determined during a filter design process. A low pass filter will allow only frequencies lower than the cutoff frequency and block all higher frequencies. On the other hand, a high pass filter will allow only frequencies

higher than the cutoff frequencies. While a stop band filter will block a certain band of frequencies and allow higher and lower frequencies to pass. For this experiment, two distinct filters were designed. The first filter removes low frequency ambient noise from the signal. This filter was designed as high pass filter with cutoff frequency of 1.14 Hz. The second filter is stop band filter that blocks the frequencies in the vicinity of 50 Hz which is the laboratory electricity supply frequency.

Another parameter for filter design is the ripple percentage in the pass band. As seen in Figure (2.7) a higher ripple will give a sharper transition between the stop band and the pass band but will affect the accuracy of the signal. While a lower ripple will provide a more accurate signal, it will make a gradual transition for the pass band to stop band; thus the filter will either allow a portion of the unwanted frequencies to pass or stop a portion of the desired frequencies form passing. The values of ripple and the filter order were determined through iterations. Table (2.5) summarizes the filter parameters utilized in the present work.

Table (2.5) Filters used to remove unwanted frequency ranges.

Filter	**Type**	**Range**
Chebyshev	High pass	< 1.14 Hz
Chebyshev	Stop band	48 – 52 Hz

2.2.2 Fast Fourier Transform

The Fourier Transform is a mathematical method used to decompose a general signal into a group of sinusoidal signals [15]. The Discrete Fourier Transform (DFT) is the part of the Fourier Transform family which handles non periodic discrete signals. There are many limitations for the DFT resulting from its discrete nature. Such limitations that could affect the accuracy of the experiment output were studied.

Periodicity: The mathematical nature of DFT enforces the fact the transformation output is periodic with a period length equal to the sampling rate [13]. Consequently, the DFT is only defined in the range from 0 Hz to the sampling frequency.

Symmetry: The DFT is known to be symmetric around the Nyquist frequency which is equal to 0.5 the sampling frequency [13]. The DFT output higher than 0.5 the sampling frequency is completely redundant. So, for this experiment the sampling frequency was chosen to be 500 Hz which is double the upper bound for frequency range of interest.

Leakage: The DFT must be carried on a finite number of sample points. For a given spectrum component at a given frequency ω, if the sampling period was not equivalent to a multiple of the spectrum, in such case, parts of the spectrum components while leak to frequencies in the neighborhood of ω. Such phenomenon is known as leakage [16, 17]. To minimize the effect of leakage, the full signal was divide into overlapping segments. Afterwards each segment was windowed and DFT applied to it separately. The final DFT output will be the average of all the segments' DFT.

Many types of symmetric windowing functions are available [16, 17]. Another available category of windows is the asymmetrical windowing functions which are characterized by a higher detection resolution [17]. The FEA done for this problem provided an insight to the nature of the modal response. Since all modes were sufficiently far from each other, no high resolution detection was needed. After testing a group of symmetric windowing functions, the Hann window was selected as it produced the best result for the problem in hand. Figure (2.8) shows a comparison between a group of symmetrical windowing functions. Figure (2.9) shows a comparison between the raw data and after the application of windowing and filtering.

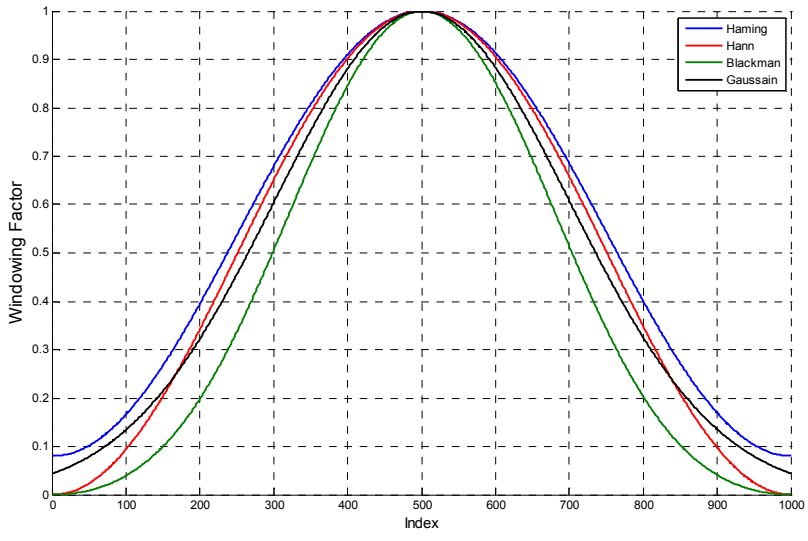

Figure (2.8) Comparison between Various Windowing Functions

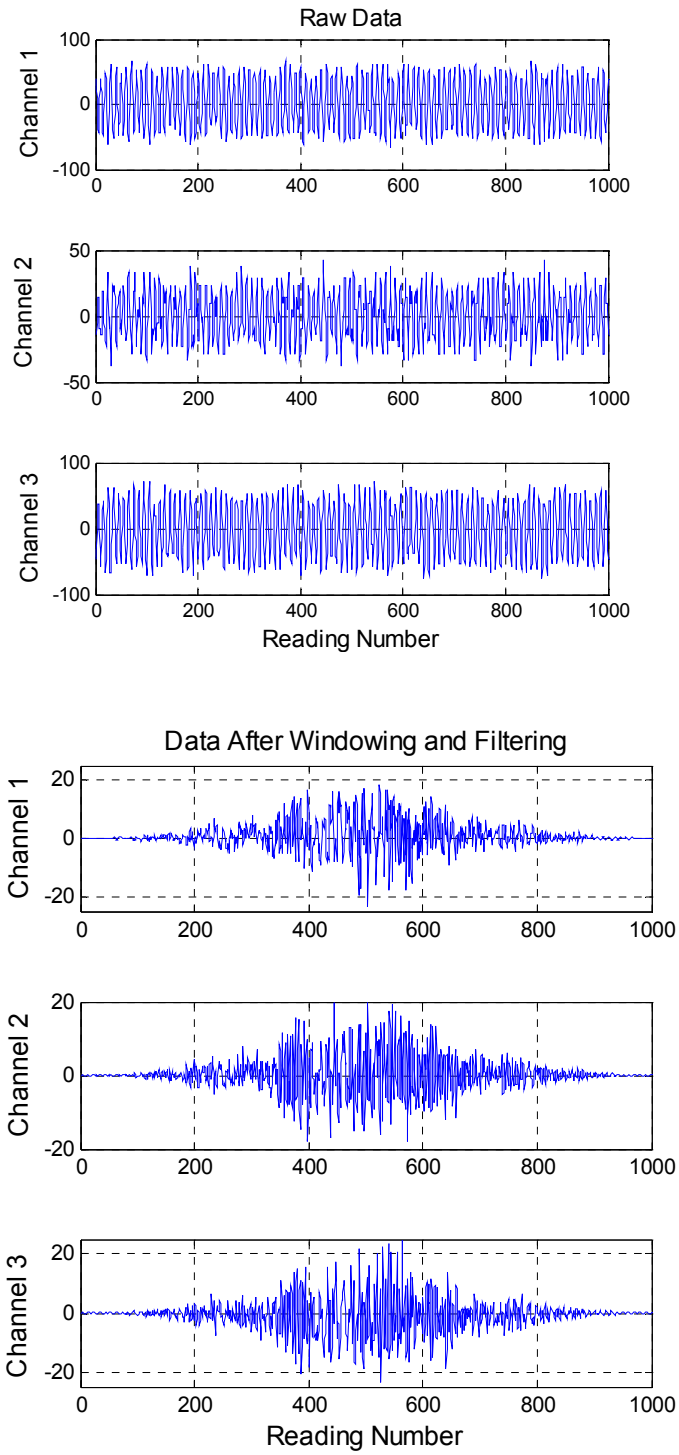

Figure (2.9): Comparison between Raw Strain Data before and after Filtering a) Raw Data, b) Data after Windowing and Filtering.

The DFT output after windowing and filtering is displayed in Figure (2.10). The results after the windowing were still unsatisfactory due to the presence of significant leakage.

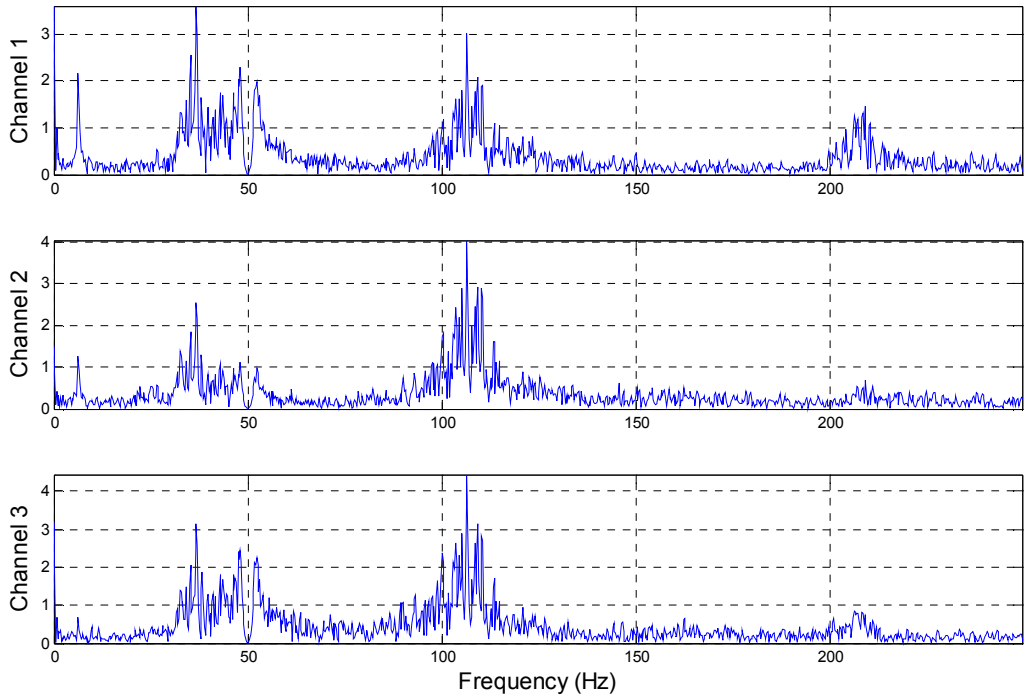

Figure (2.10) FFT for Data after filtering and windowing

To fully eliminate leakage an averaging process was employed. As stated earlier this process involved dividing the signal into overlapping segments. Figure (2.11) shows a signal divided into equal length segments.

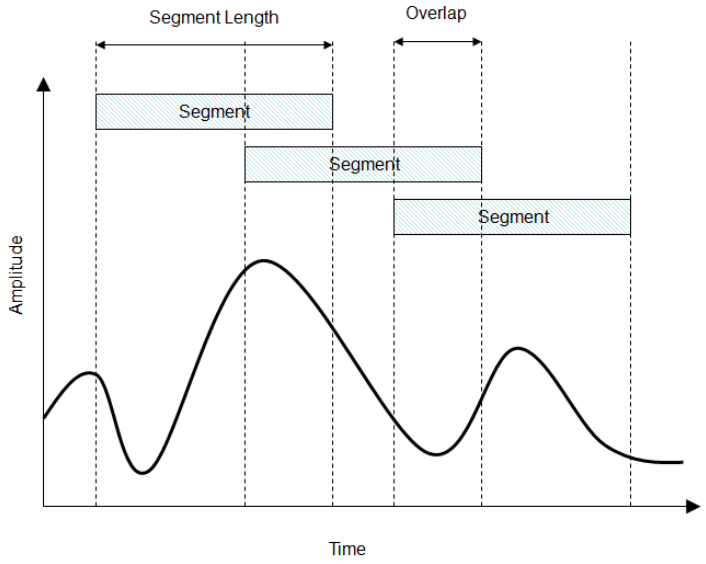

Figure (2.11) Averaging Technique

A factor of major importance is the overlap portion in each segment. Most commercial applications set this value to 0.66 and for this experiment it was found to be the optimal value. For a full sample length l, number of segments N and an overlap o the full length is can be given by:

$$l = (1-o)l_i N + x_s + x_e \tag{2.1}$$

Where x_s and x_e are the portions of the segments that will be truncated from the beginning and the end respectively. Assuming that:

$$x_s = x_e = x \tag{2.2}$$

$$2x = \mathrm{mod}\left(l, (1-o)l_i\right) \tag{2.3}$$

Where *mod* denotes the modulus after division. Solving for l_i we get:

$$l_i = \frac{l-2x}{(1-o)N} \tag{2.4}$$

For this experiment, averaging intervals of length 500 points were taken for 10 000 readings sampled at 500 Hz. A total of 117 intervals were used at an overlap of 0.66. The final FRF of an intact beam is shown in Figure (2.12).

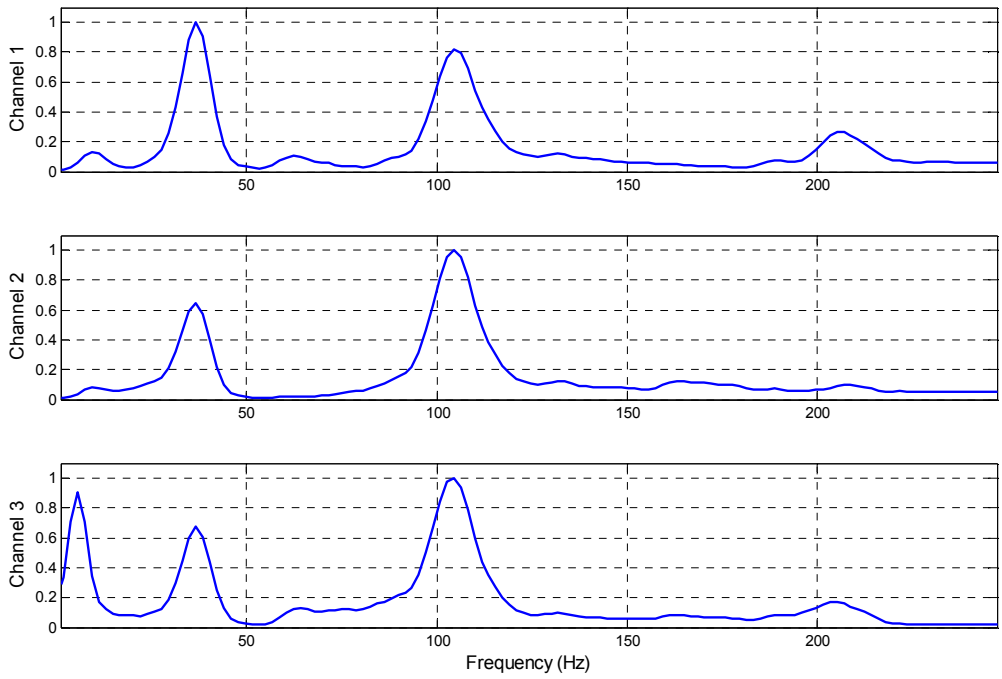

Figure (2.12) Final FRF for a sample beam

2.2.3 Automatic Mode Detection

There are many available methods for normal modes detection. A detailed listing of such methods can be found in [17]. For the purpose of this research work, a method known as The Peak Amplitude Method will be used. In this method the natural frequency can be determined by finding the peaks on the FRF graph. To implement the peak amplitude method, the local maxima for the FRF curves are calculated and sorted form the peak with higher amplitude and downwards. The highest four peaks are then selected and the rest of the detected peaks will be considered as numerical peaks and will be discarded. The next step is to sort the calculated peaks from the lowest frequency which is considered the first mode shape up to the highest frequency which is considered the fourth mode as illustrated schematically in Figure (2.13). This approach provided sufficient accuracy for the purpose of this research work. However, it should be noted that in case of a more complex structures a more advanced method should be used [18].

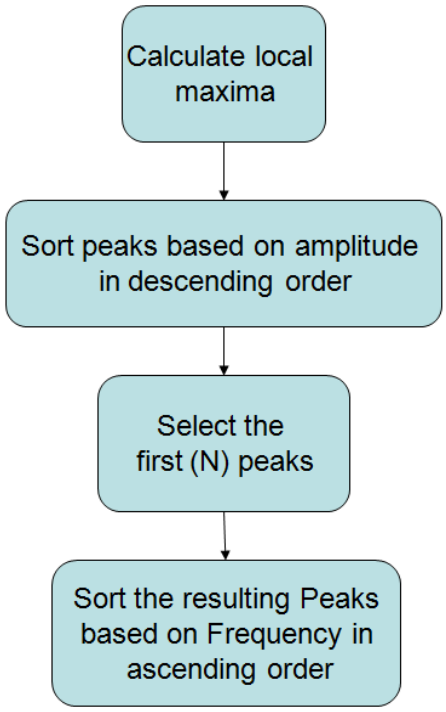

Figure (2.13) Automatic Mode Shape Detection Algorithm

Figure (2.14) shows a sample FRF for the intact and damaged beams showing the peaks used for mode shape detection. The peaks are detected correctly using the proposed Highest Amplitude Method.

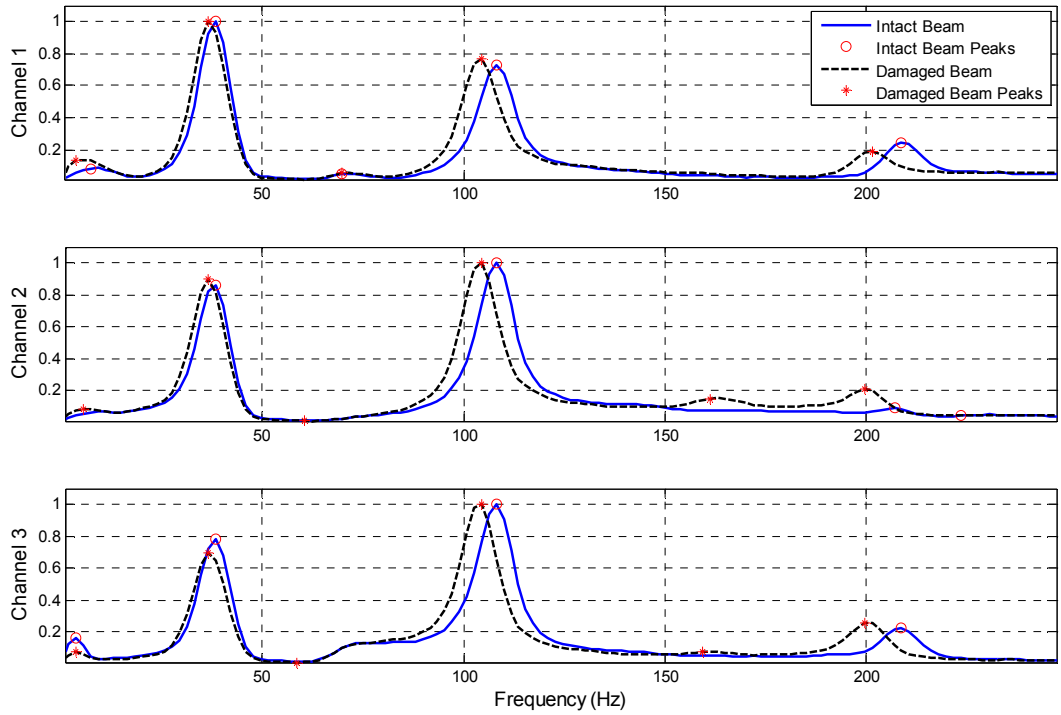

Figure (2.14) Highest Amplitude Method applied to an intact beam and Damage Case4

2.3. Vibration modeling

2.3.1 Response to a General Excitation

Even the most complicated system can be modeled as a group of single degree of freedom systems using the principle of superposition. For a simple mass – spring – damper system, the equation of motion is given by [15]:

$$m\ddot{x}+c\dot{x}+k=F(t) \tag{2.5}$$

Where m is the mass, c is the damping coefficient, k is the stiffness and $F(t)$ is the force applied to the system as a function of time. For the special case of a harmonic forcing function, the amplitude of the vibration can be given by:

$$X = \frac{F_o}{\left[\left(k - m\omega^2\right)^2 + c^2\omega^2\right]^{1/2}} \tag{2.6}$$

$$\phi = \tan^{-1}\left(\frac{c\omega}{k - m\omega^2}\right) \tag{2.7}$$

The derivation of equation (2.6) and (2.7) are provided in details in reference [15]. Viscous damping is one of the most widely used damping models for vibration problems and will be used through the rest of this research work.

Mutli-degree of freedom systems, like beams, are normally represented mathematically by system of coupled Ordinary Differential Equations (ODE). In order to find the system response to a given excitation, the system of simultaneous ODE has to be solved. Such systems can be solved as a group of second order ordinary differential equations using a multitude of numerical methods available for such purpose. Another approach is to uncouple these equations by transforming them to the modal coordinates as follows:

$$[P]^T[M][P]\{\ddot{z}\} + [P]^T[C][P]\{\dot{z}\} + [P]^T[K][P]\{z\} = [P]^T\{F\} \tag{2.8}$$

$$\{x\} = [P]\{z\} \tag{2.9}$$

Where the matrix [P] is the Eigen vectors matrix. Due to the orthogonal nature of eigenvectors, in the above equation the stiffness matrix and the mass matrix are both diagonal matrices. In order to guarantee that the damping matrix is diagonal as well the proportional damping assumption is used. This assumption states that the damping matrix takes the following form:

$$[C] = \alpha[M] + \beta[K] \tag{2.10}$$

Were α and β are constants characteristic for each system. The assumption used in equation (2.10) is widely used in commercial finite element packages and will be used

throughout this research work. Once the equation is transferred to the modal coordinates it can be solved as uncoupled system of equations by applying equation (2.6) to each degree of freedom separately.

2.3.2 FEM of Beam Element

Equations (2.8) and (2.9) relate the nodal displacement to the applied forces. However, in this experiment the measurement sensors used were strain gauges; thus, in order to compare the theoretical calculations with the experimental measurements the strain need to be calculated in terms of the nodal displacement. For the purpose of this research beam element is modeled as 2 node element with 2 degrees of freedom at each node a single lateral translation and one rotation.

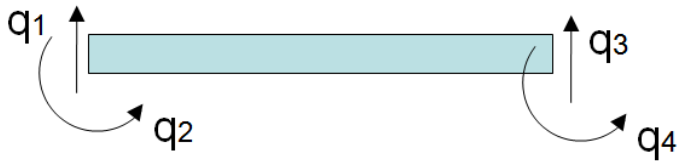

Figure (2.15) Beam Element

For the beam element shown in Figure (2.3), the strain can be related to curvature by the following relation [19]:

$$\frac{d^2v}{dx^2} = [B]\{q\} \tag{2.8}$$

Were $[B]$ represents the shape function of the beam and can be defined at the beam element centroid as:

$$[B] = \begin{bmatrix} 0 & -1/l & 0 & 1/l \end{bmatrix} \tag{2.9}$$

The stiffness and mass matrices of a beam element can be found in elementary finite element textbooks such as [19]. The stiffness matrix and mass matrix is calculated for each beam element separately and later the global matrices are assembled. The global damping matrix is directly calculated based on the proportional damping approach.

2.3.3 Calculation FRF using FEM

As discussed in chapter (1) the proposed damage detection technique relies on comparing the entire FRF elements rather than comparing a single element such as frequencies. Finding the FRF requires finding the amplitude of vibration when the beam is excited by a range of excitation frequencies. The FEM model built for a cantilever beam was subjected to a harmonic force acting at the beam tip as shown in Figure (2.16). Applying the modal analysis approach, the amplitude of vibration was tcalculated. This procedure is done for the range of frequencies of interest (1 -250 Hz). Using this approach the theoretical intact beam FRF for both beams being studied were calculated and a comparison between the theoretical and experimental results are displayed in Figure (2.17) and (2.18).

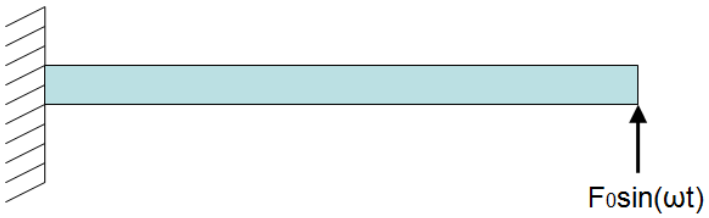

Figure (2.16): Force applied to finite model

The comparison between theoretical and experimental output show that most modes were calculated with high accuracy in terms of frequency and amplitude. However, the only exception is the first mode shape amplitude which was affected by the transition region for the high pass filter used to remove low frequency noise. It should be noted that the FRF calculated from the FEM is a result of tip excitation. However , the experimental measurements are a result of a base excitation. Since the FRF is dependent on the exciting force location, this contributed to the deviation in the first mode shape. This difference in exciting force location was intentional in order to verify that the damage detection algorithm can function without prior knowledge of the exciting force. Additionally, since the magnitude of the exciting force is unknown, the FRF was normalized in reference to the highest peak for each FRF.

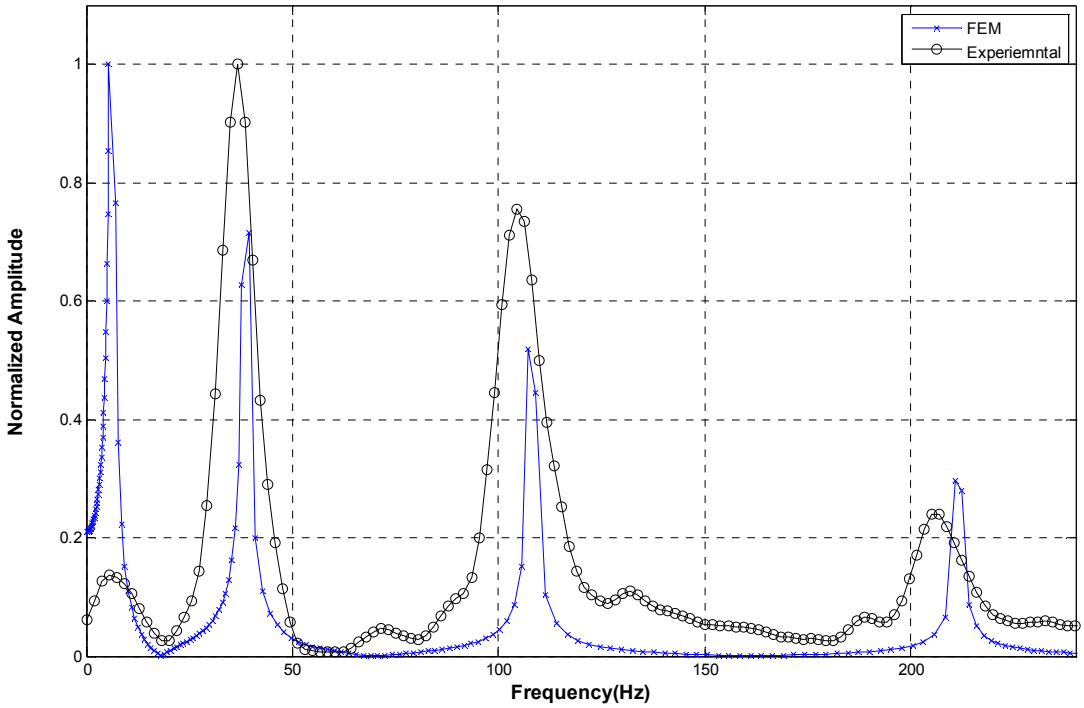

Figure (2.17): Comparison bet. Theoretical and Experimental FRF for Intact Beam 1

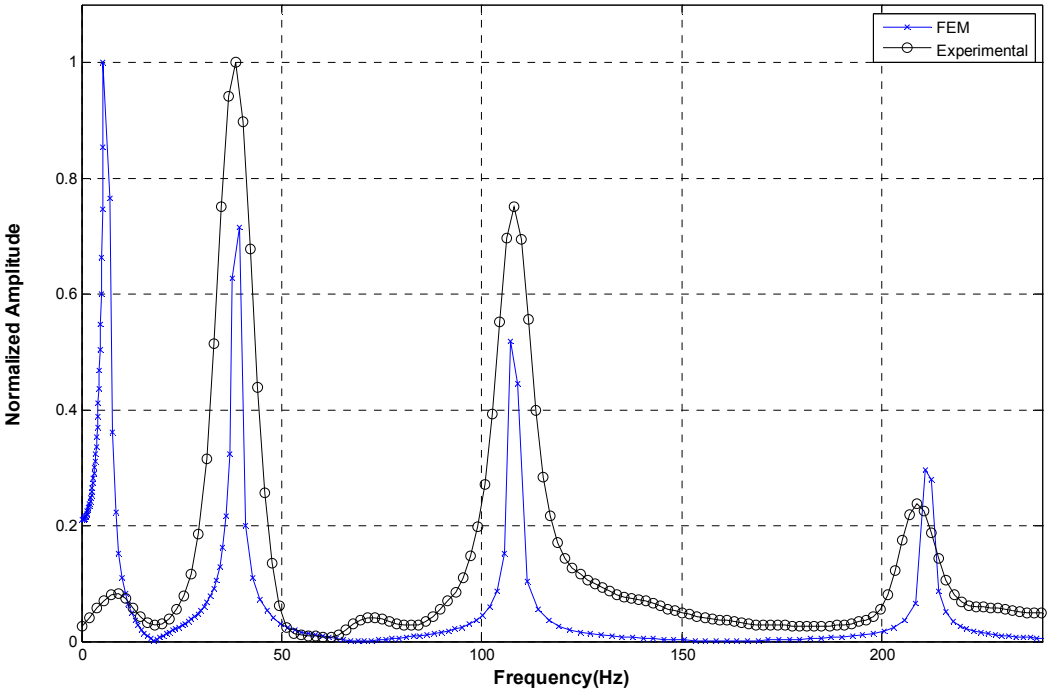

Figure (2.18): Comparison bet. Theoretical and Experimental FRF for Intact Beam 2.

CHAPTER 3
MODEL UPDATING USING GENETIC ALGORITHMS

3.1 Optimization Problem Definition

The genetic algorithms (GA) are a form of evolutionary algorithms that have been widely used in optimization problems recently. A typical implementation of genetic algorithms will start with a group of random solutions for a given problem encoded in the form of genes [20]. Each distinct group of genes represents a distinct solution for the problem. A common approach to model updating problems is using stiffness and mass matrices correction factors. In this approach correction factors are pre-multiplied with the elemental stiffness and mass matrix for each element of the FEM. Thus the stiffness and mass matrix of the i^{th} element is given by [10]:

$$[k]_i = P_{ki}[k_0]_i \tag{3.1}$$

$$[m]_i = P_{mi}[m_0]_i \tag{3.2}$$

The global mass and stiffness matrices are later assembled form the elemental matrices. However sensitivity analysis for correction factors given in [9 and 10] showed that the stiffness matrix correction factor and the mass matrix correction factors can balance each other. Such behavior might results in unnecessary redundancy when applying the damage detection algorithm based on the correction factors. For this reason, in this research work, only the stiffness correction factors will be used for model updating and hence damage detection.

3.2 Encoding

The majority of the research which involves GA uses real coding for genes which proved more efficient than the binary encoding used in the first genetic algorithms [20]. In order to select a chromosome that provides versatile encoding of the model updating problem, the chromosome was designed to consist of the proportional damping coefficients α and

β in addition to the stiffness correction parameters of each element. An illustration of the used gene is provided in Figure (3.1).

α	β	P_{k1}	P_{k2}	P_{k3}	-	-	-	P_{kn-1}	P_{kn}

Figure (3.1): GA Problem Encoding

3.3 Genetic Operators

3.3.1 Arithmetic Crossover

In the arithmetic cross, two individuals are selected based on the principle of elitism and the offspring is generated using interpolation.

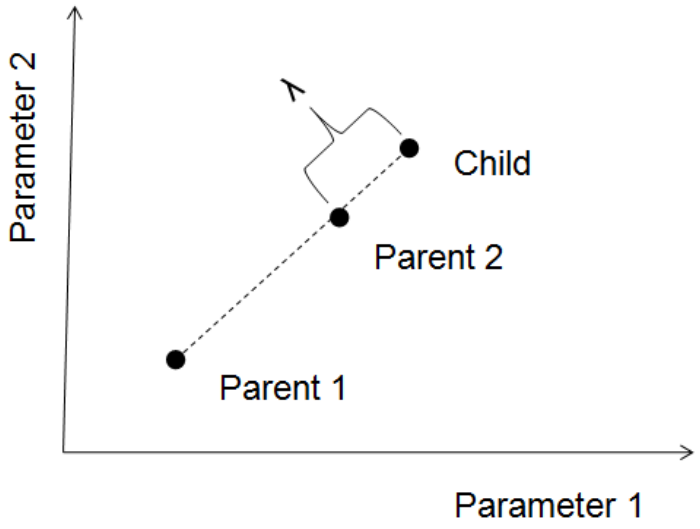

Figure (3.2): Arithmetic Crossover

The Offspring chromosome [G] is given by:

$$[G_1] = \lambda[P_1] + (1-\lambda)[P_2] \tag{3.3}$$

$$[G_2] = (1-\lambda)[P_1] + \lambda[P_2] \tag{3.4}$$

Were $[P_1]$ and $[P_2]$ are parents' genes and (λ) is a random variable selected between 0 and 1 for interpolation. Also, values of (λ) greater than 1 can be used for extrapolation.

3.3.2 Mutation

Mutation is a fundamental operator in Genetic algorithms. A random individual is selected. Then a random gene is selected within this individual and assigned a random value within the search space for this gene. Mutation is the operator that ensures the solver explores new sectors of the fitness function which could never be achieved using crossovers only.

3.3.3 Individuals Selection

The selection of individuals to be used for genetic operations and consequently produce offspring is done by giving individuals with higher fitness a higher priority. This can be guaranteed by using the geometric distribution. A sample of this distribution is shown in Figure (3.3). Unlike the normal distribution which favors the individuals in the middle of the population and unlike the uniform distribution which gives equal priority to all individuals, the geometric distribution favors the individuals to the left of the distribution. By proper sorting of each generation and by selecting the GA operators input using geometric the individuals with higher fitness will have a higher chance to be selected.

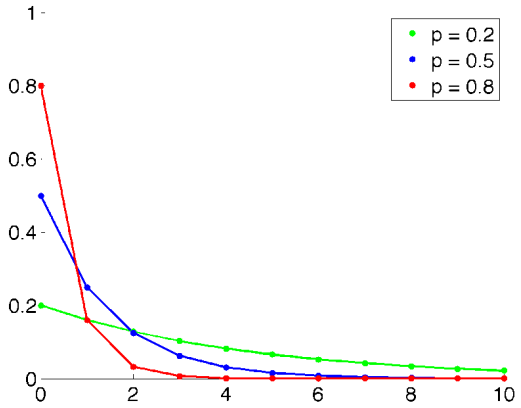

Figure (3.3): Geometric Probability Distribution

3.3.5 Elitism

To ensure convergence the element with highest fitness from each generation will be copied directly to the next generation without passing through any GA operators.

3.4 Algorithm

The GA solver starts the first generation by building the theoretical FEM of the beam being studied. Then the solver uses the mutate operator on the beam FEM to generate the whole first generation. The Fitness function is later evaluated for each individual within the population. The next step is to rank the population in ascending order based on fitness. Using the geometric distribution, individuals will be selected for mutation, crossover and copy. The fitness is then evaluated for the new generation and the solution continues on in this manner. In order to guarantee a GA solution convergence, the individual with highest fitness within a given generation must be copied directly to the next generation.

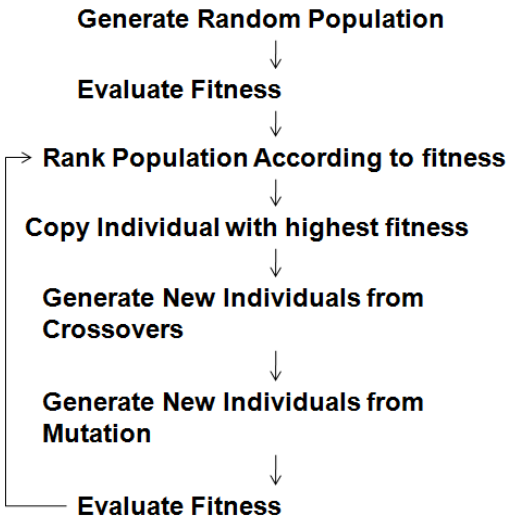

Figure (3.4): Genetic Solver Algorithm

3.5 Fitness Function

The fitness function is of primary importance in any optimization problem. The selection of such function determines the quality of the output regardless of the optimization method used. Many fitness functions were suggested in the literature for damage detection and model updating. In this work a new fitness function that combines the merits of both modal and frequency based methods is proposed for damage detection purpose. This method relies on the whole FRF rather than the frequencies or mode shapes only. Since there can be more than one sensor attached to the structure each operating on

a separate channel, the overall fitness function will be the given as the sum of the fitness function calculated for each channel separately and can be given by:

$$F = \sum_{nc=1}^{nc=Channels} F_{nc} \tag{3.5}$$

The fitness function F_{nc} can take many forms that would express the difference between the theoretical FRF and the experimental FRF. Minimizing this fitness function using model updating will result in a theoretical FEM closely representing the actual experiment. Several functions will be studied in the following sections.

3.5.1 Frequency Fitness Function

The first fitness function considered in this work is the difference between the peak frequencies representing the same mode shape for the theoretical and experimental FRF.

$$\boldsymbol{F_{nc1} = \sum_{i=1}^{i=n} \left| \left(\omega_T - \omega_E \right)_i \right|} \tag{3.6}$$

In equation (3.6) ω_E represents the expected frequency at which the i^{th} peak occurs, while ω_T is the frequency of the same peak calculated analytically. This function will be referred to as "cost function 1" henceforth.

3.5.2 Peak Vector

The research work done by [10,11 and 21] proved that for a cantilever beam the eigenvalues sensitivity for elemental correction factors does not have a unique value for each element. Based on this conclusion the results from the previous fitness function might show significant error for damage location. Since perturbations for a given element correction factor can cause the same effects as perturbations from an element at another position. Another fitness function was formulated which relies on minimizing the distance of the vector joining the two peaks V_p shown in Figure (3.5) and is given by:

$$F_{nc2} = \sum_{i=1}^{i=n} \sqrt{(\omega_T - \omega_E)_i^2 + \gamma (y_T - y_E)_i^2} \tag{3.7}$$

It should be noted that, this function takes into consideration the effect of eigenvalues, eigenvectors and damping. This fitness function will be referred to as "cost function 2" in later section of this thesis

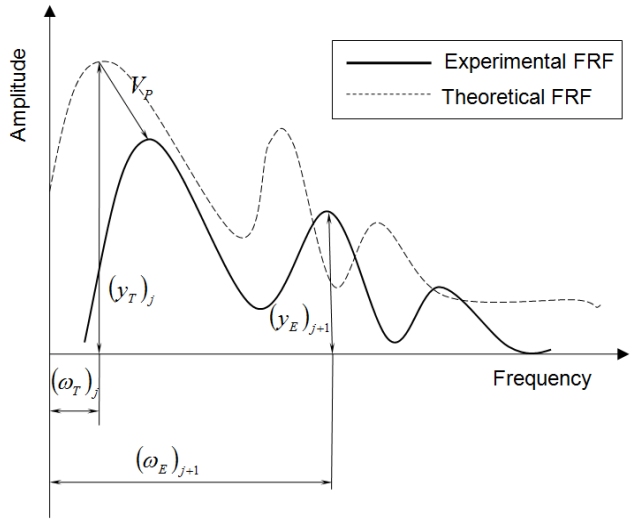

Figure (3.5) Peak Vector Definetion

3.5.3 Weighted Peak Vector

This weighted peak vector function is similar to the normal Peak vector function but takes into consideration the measured amplitude at a given mode shape. This function will give the error measured at a mode shape with higher experimental amplitude a higher weight than the error at a mode shape with lower amplitude.

$$F_{nc3} = \sum_{i=1}^{i=n} y_{E_i} \sqrt{(\omega_T - \omega_E)_i^2 + \gamma (y_T - y_E)_i^2} \tag{3.8}$$

3.6 Optimization Constraints

The constraints of an optimization problem are of extreme importance for the solution accuracy. For the model updating problem, the constraints ensures that the resulting FEM is physically meaningful and represents the model of a cantilever beam structure.

The first constraint is that all elemental correction factors must be positive. This condition ensures that the global stiffness matrix remains consistent.

$$P_{ki} > 0 \tag{3.9}$$

The second constraint is that within the frequency region of interest (1-250 Hz) the FEM should have a number of modes equal to or greater than the modes measured by the experiment in the same region. This constraint ensures that the cost function can be evaluated at each mode shape.

With every GA solver iteration new solutions are generated. These new solutions have an FRF with different characteristics from the original FEM. The third constraint ensures that the FRF peaks of the new solution lie on the peak vector V_p. Applying this constraint guarantees that solver gradually moves the initial theoretical solution towards the experimental measurements rather than coming up with a totally new solution that is unrelated to the original FEM. This constraint can be given as:

$$\left(\omega_T, y_T\right)_i \in V_P \tag{3.10}$$

The effect of applying the third constraint might not be visible for the normal model updating problem but was important when solving the damage detection problem.

These three constraints were applied by adding a fitness penalty to the solution violating the constraints. The first and second constrains were applied rigidly by adding a very large penalty rendering the solution unfit immediately. While solutions violating the third constraint were given a small penalty; thus allowing the solution to move in the vicinity of V_p rather than strictly on it. This approach significantly enhanced the solution convergence speed.

3.7 Solver Parameters

The GA solver uses a variety of parameters that affect the solution convergence and speed. The solver used in this research work was tuned through iterations to get the best

combination of speed and fitness. A list of those parameters and assigned values are given Table [3.1].

Table (3.1): Genetic Solver Parameters

Parameter	Value
Population Size	100
Maximum Number of iteration	100
Mutations	40%
Crossovers	40%
Copy	20%
Solution Convergence criteria	0.05
Number of Iteration for Convergence	25

The population size indicates the number of individuals created with each generation. Mutations, Crossovers and Copy indicate the percentage of individuals generated by each method for any given generation. Solution convergence criteria stop the solver when the solution does not show progress for a set number of generations.

An additional factor is the number of elements used to model the beam. The higher the number of elements the higher the number of correction factors. Consequently, the problem will be harder in terms of optimization. On the other hand, a larger number of elements will result in a more accurate FE solution and consequently overall accurate solution. Table (3.2) shows the optimization results using the first fitness function for different number of elements.

Table (3.2): Effect of Number of Elements on Solution Fitness

Number of Elements	Best Fitness
20	21.4
50	20.39
100	19.8

It can be seen from Table (3.2) that the model with 100 elements will reach the highest fitness. However, for the sake of solution speed all models used in damage detection were built from 50 elements.

Figures (3.8 and 3.9) show the model updating results for the first intact beam described in chapter (2). The theoretical FEM model is then updated using GA and fitness function number 2 with $\gamma = 1$. It can be seen that the GA solver did generate a significantly better solution in terms of mode shape locations and values. Detailed case study with analysis will be provided in the next chapter.

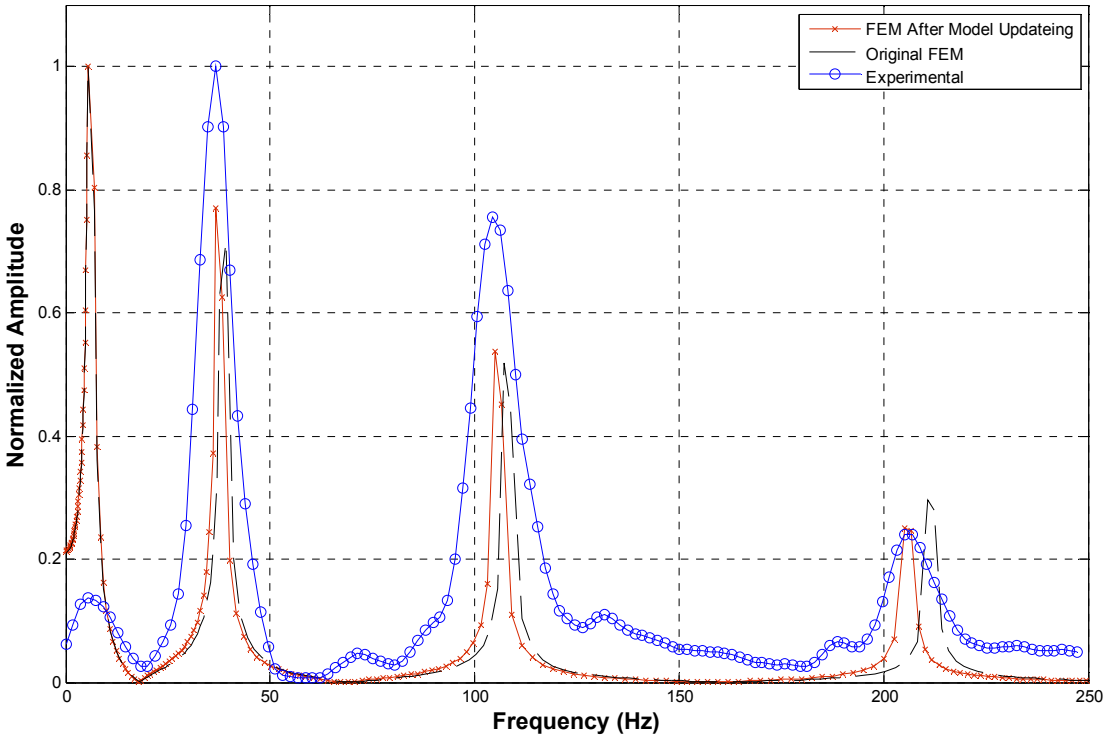

Figure (3.8): Model Updating Result for Intact Beam 1

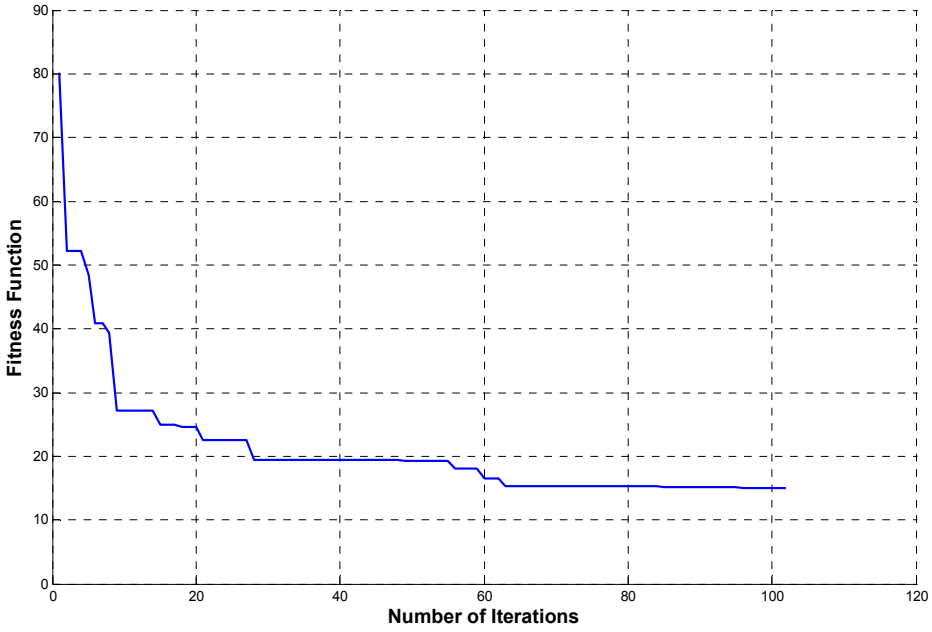

Figure (3.9): Model Updating Convergence for Intact Beam 1

CHAPTER FOUR
DAMAGE DETECTION

4.1 Introduction

The proposed damage detection method relies on matching the FEM response to the experimental results measured for a damaged beam. The first step eliminates the errors between the theoretical FEM and the intact structure through model tuning. In this step the model updating algorithm discussed in chapter (3) is used to match the intact FRF measured experimentally to the FRF calculated theoretically; thus eliminating the experimental errors. The next step is to match the FRF of a damaged structure to the update FEM from the model tuning phase. The difference between the correction factors from the tuning step and the damage detection step can be sued as an indicator of the location and magnitude of damage. This process is illustrated schematically in Figure (4.1).

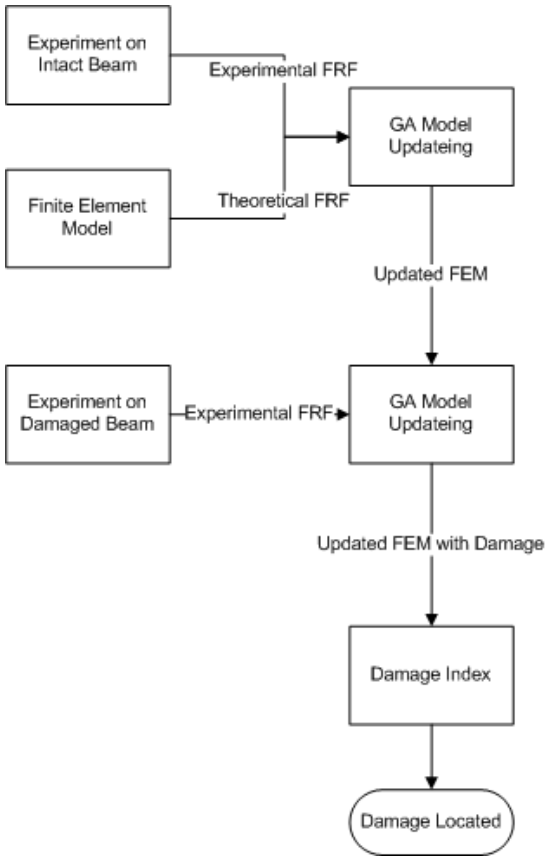

Figure (4.1): Damage Detection Algorithm

4.2 Damage Cases

Four different damage cases were studied in this research work. The first two cases represent a major structural damage while cases 3 and 4 represent a small structural damage. All damages were induced using a handsaw which resulted in an approximate width of 1 mm. For a FEM of the beams under investigation with 50 elements, a definition of damage size and location is given in Figure (4.2) and the corresponding element number for cases 1 to 4 are listed in Table (4.1).

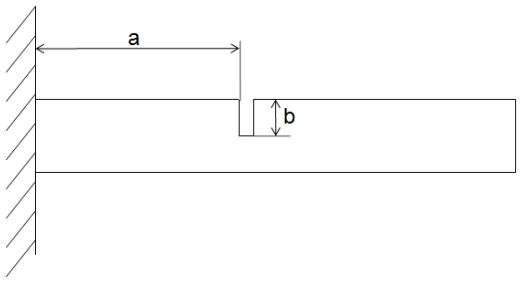

Figure (4.2) Top View of Damage Location and Size

Table (4.1): Damage Cases Details

Damage	a(cm)	b(mm)	Element no. for 50 element
1	20.5	10	34
2	5.5	10	9
3	20.5	5	34
4	5.5	5	9

A comparison between damaged and intact FRF measured for each case are shown in the Figures (4.3 – 4.6).

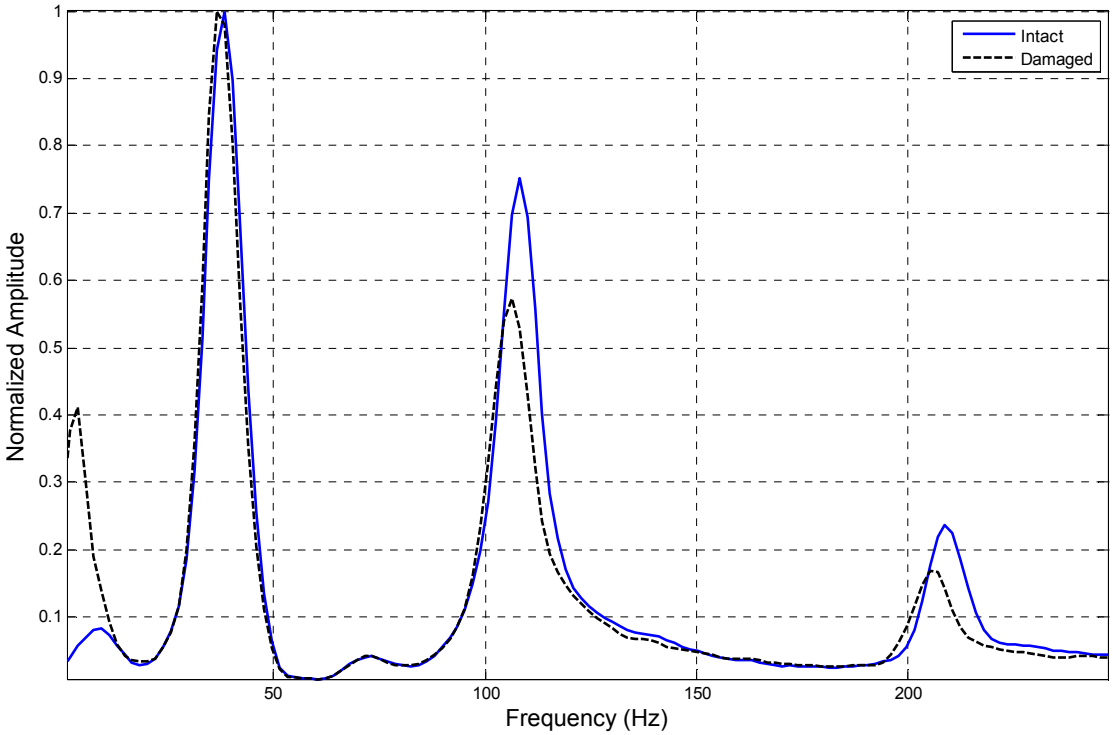

Figure (4.3) FRF Comparison for Case 1

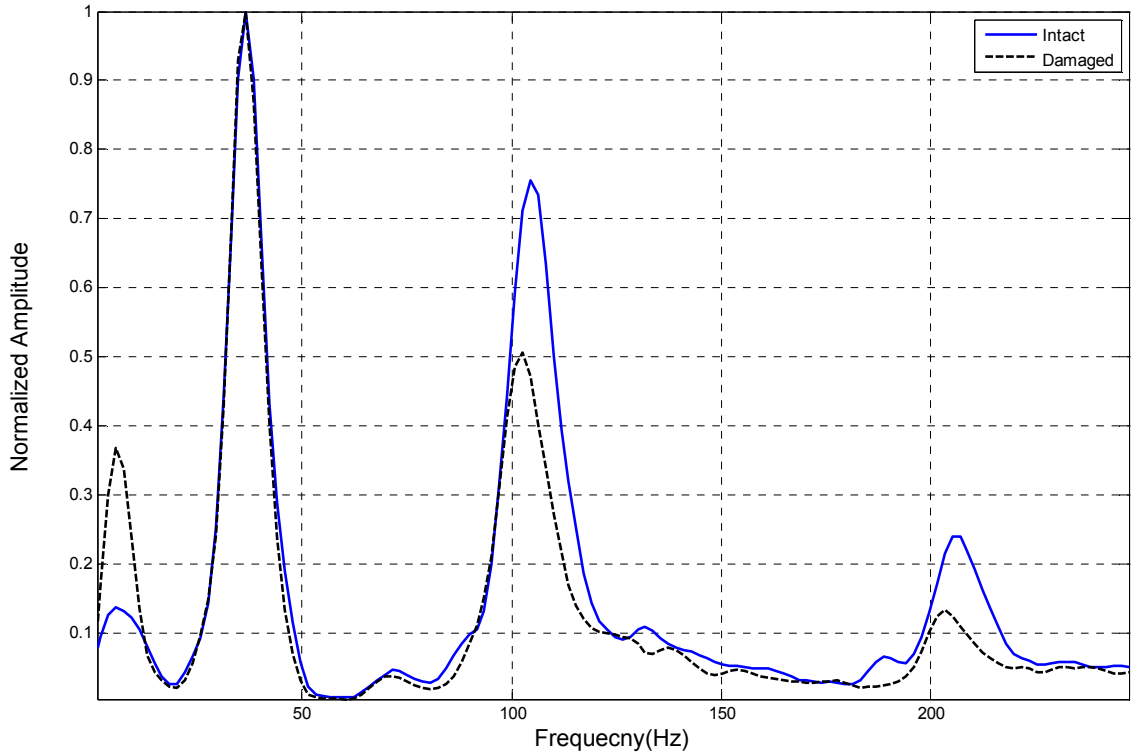

Figure (4.4) FRF Comparison for Case 2

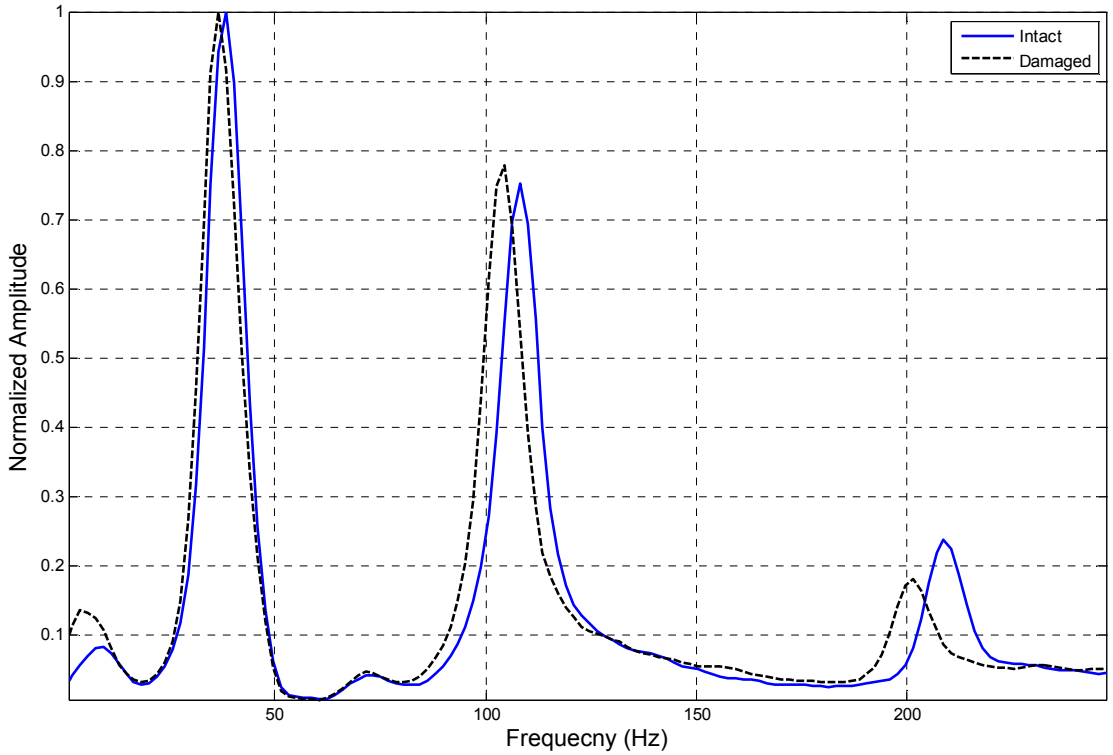

Figure (4.5) FRF Comparison for Case 3

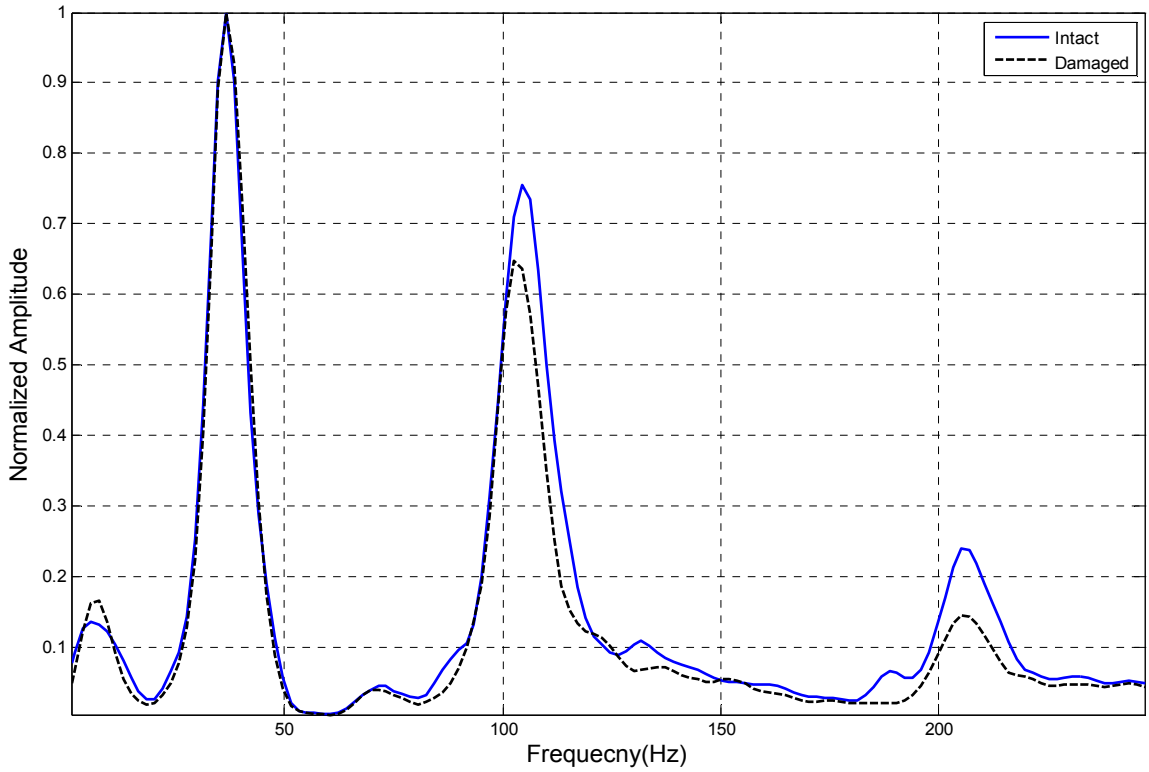

Figure (4.6) FRF Comparison for Case 4

4.2 Damage index

The final output of the model updating process is the stiffness correction factor. While the change in these factors might be a sufficient indicator in most cases. However, in some cases a more elaborate damage index might be needed. It is important to choose a fitness function that has equal sensitivity to changes in all elements. Additionally, after the model tuning phase the resulting FEM might have different characteristics than the original FEM. Consequently, at this point, the fitness function sensitivity could take any unknown form. In order to minimize differences in sensitivity effect, a damage index was formulated given by the following equation:

$$I_i = (P_{kT} - P_{kD})_i / S_i$$

Where I_i the damage index for the element number i. is P_{kT} is the element correction factor at the end of the tuning phase and P_{kD} is the correction factor at the end of the damage detection phase. S_i is the sensitivity of the fitness function to the correction factor at the given element. For this research work the sensitivity is defined as the amount of change in fitness function for a 1% change in the correction factor at a given element.

4.3 Large Structural Damage

The complete damage detection algorithm was used on damage cases 1 and 2 to determine which fitness function gives better results. The list of damage detection runs used for fitness function selection is given in Table (4.2).

Table (4.2) Large Structural Damage Detection Runs

Run	Cost Function	γ	Damage Case	Number of modes
1	1	0	1	4
2	1	0	2	4
3	2	1	1	4
4	2	1	2	4
5	3	1	1	4
6	3	1	2	4

Damage Detection Run 1

The first damage detection run used the fitness function #1 to detect damage in case 1. Since fitness function #1 relies only on the difference in frequencies, the frequencies from the model tuning and the damage detection phase are shown in Table (4.3). Both the model tuning phase and the damage detection successfully updated the frequencies of the FEM to closely match the frequencies measured experimentally. However, the damage index shown in Figure (4.7) showed an unacceptable amount of false detections far from the expected damage location which is marked by the black arrow.

Table (4.3) Results for Damage Detection Run 1

Model Tuning			**Damage Detection**	
Experimental Intact Frequencies (Hz)	**Original FEM Frequencies (Hz)**	**Updated FEM Frequencies (Hz)**	**Experimental Damaged Frequencies(Hz)**	**Updated FEM Frequencies (Hz)**
5.49	6.16	5.67	5.49	5.58
36.63	38.57	37.47	36.63	36.62
104.40	108.01	104.40	102.56	102.56
205.13	211.66	205.13	203.30	203.30

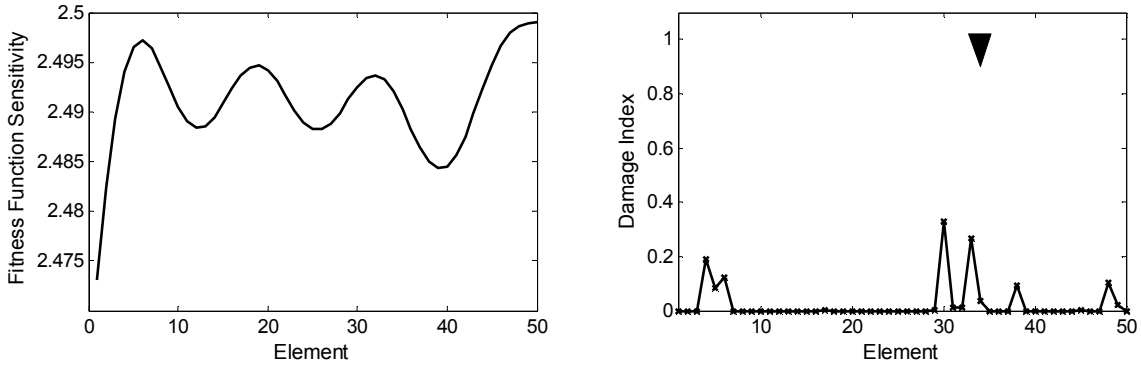

Figure (4.7): Damage Detection Results for Run1

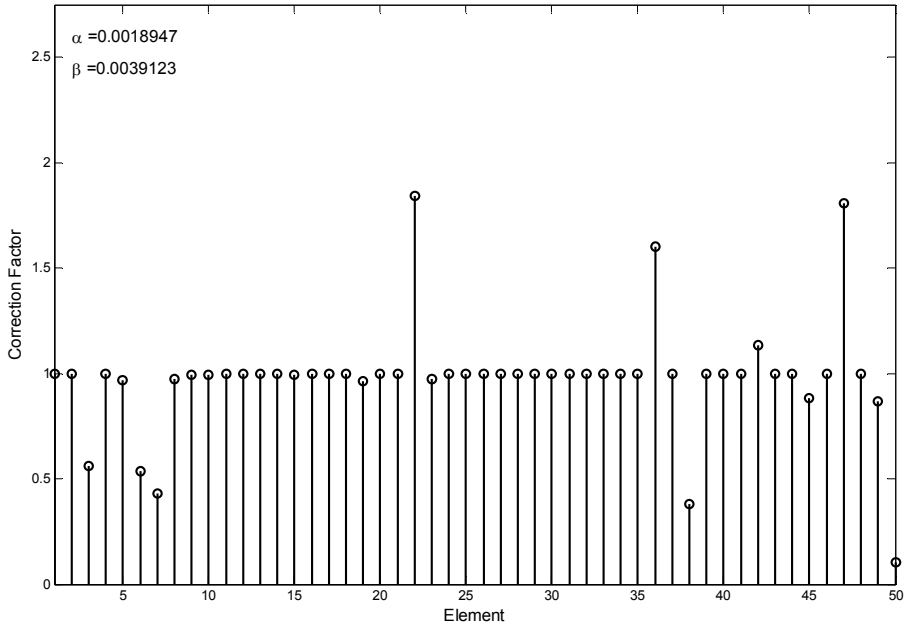

Figure (4.8) Final Correction Factors for Damage Detection Run 1

Damage Detection Run 2

The second damage detection run used the fitness function #1 to detect damage in case 2. The frequencies from the model tuning and the damage detection phase are shown in Table (4.4). Both the model tuning phase and the damage detection successfully updated the frequencies of the FEM to closely match the frequencies measured experimentally. Unlike run 1, the damage index shown in Figure (4.9) identifies the correct damage location despite negligible false detection towards the beam tip.

Table (4.4) Results for Damage Detection Run 2

Model Tuning			**Damage Detection**	
Experimental Intact Frequencies (Hz)	**Original FEM Frequencies (Hz)**	**Updated FEM Frequencies (Hz)**	**Experimental Damaged Frequencies(Hz)**	**Updated FEM Frequencies (Hz)**
7.33	6.16	6.16	3.66	4.92
38.46	38.57	38.57	36.63	36.32
108.06	108.01	108.01	104.40	104.42
208.79	211.66	211.66	201.47	201.44

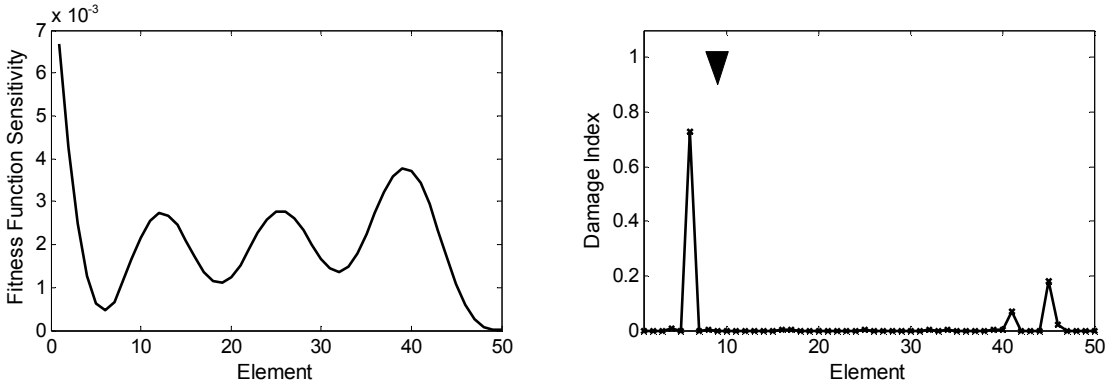

Figure (4.9): Damage Detection Results for Run 2

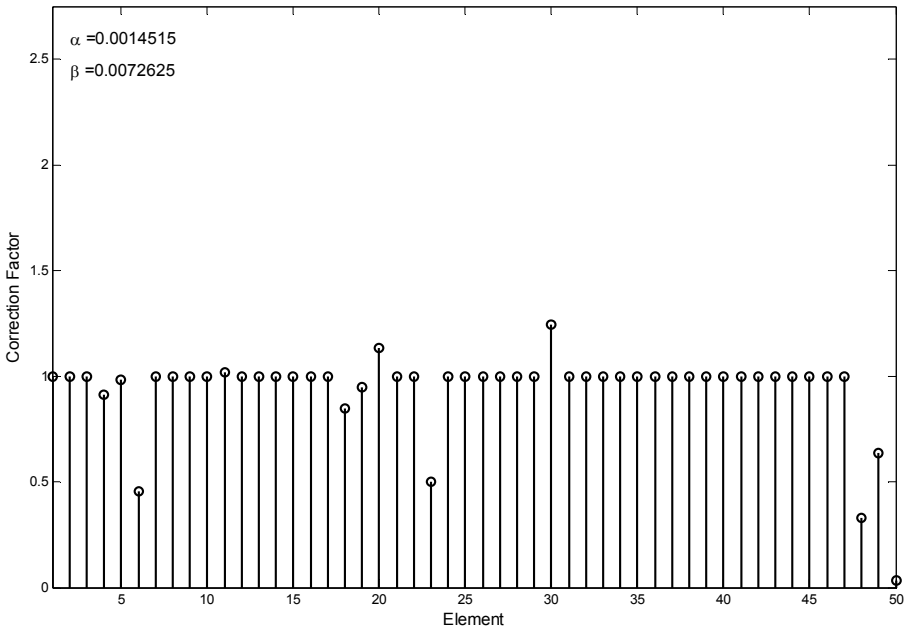

Figure (4.10) Final Correction Factors for Damage Detection Run 2

Damage Detection Run 3.

The third damage detection run used the fitness function #2 to detect damage in case 1. The model tuning and damage detection phase results presented in Figure (4.11) shows that the algorithm succeeded in updating the calculated FRF to a closer match of the experimental FRF. Additionally, the damage index shown in Figure (4.13) identified the correct damage location with negligible errors.

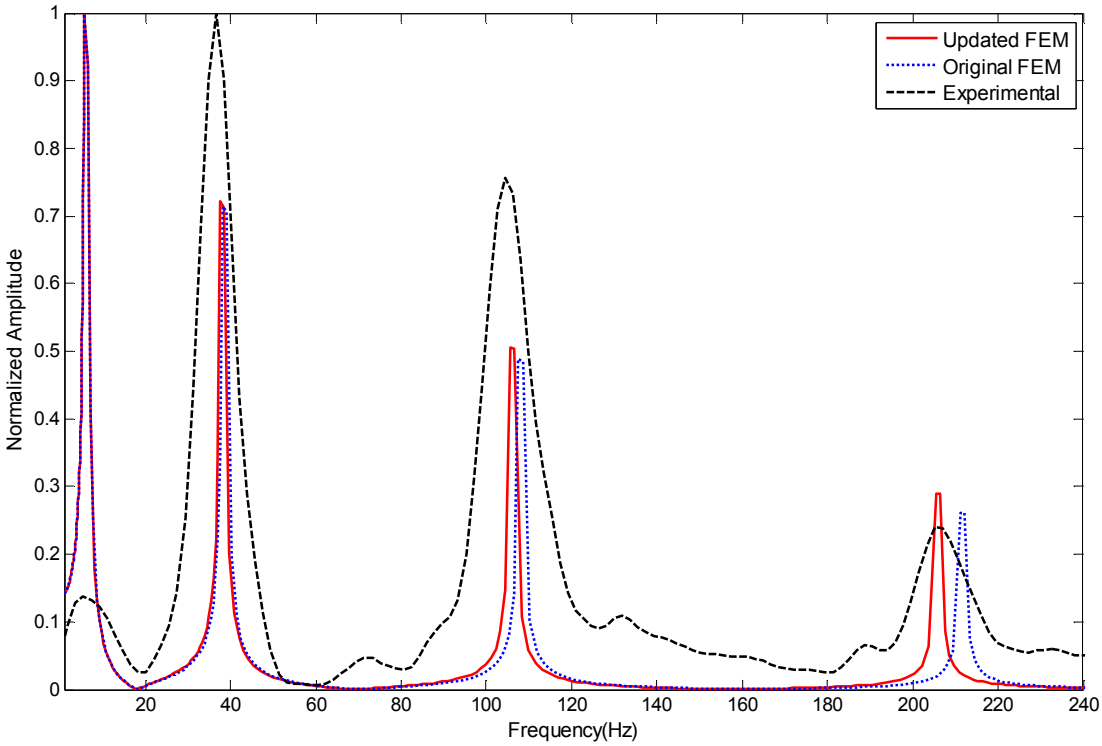

Figure (4.11): Model Tuning Results for Run 3

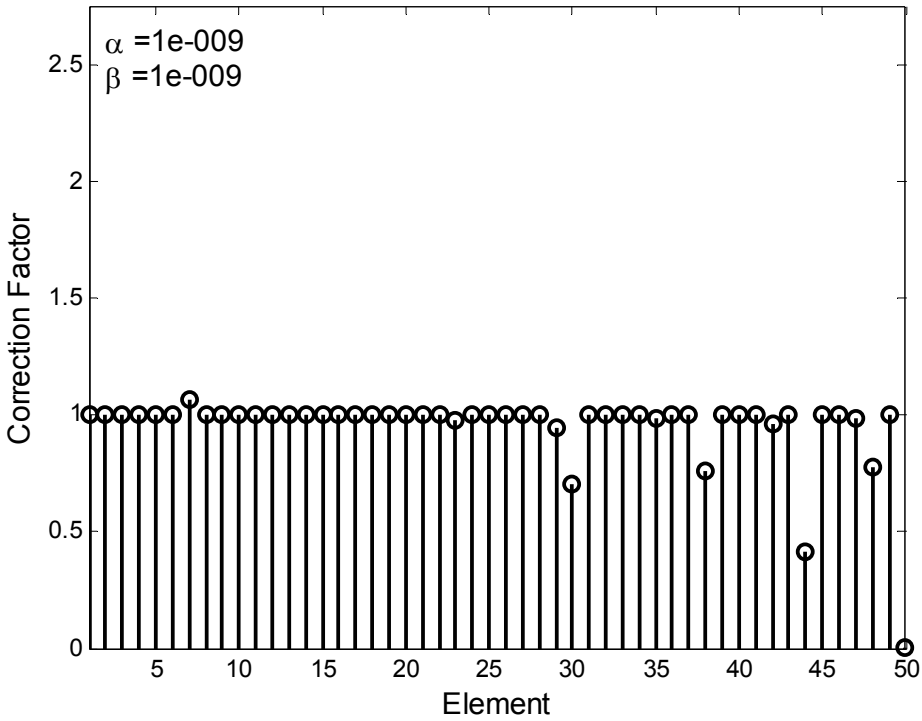

Figure (4.12) Final Correction Factors for Damage Detection Run 3

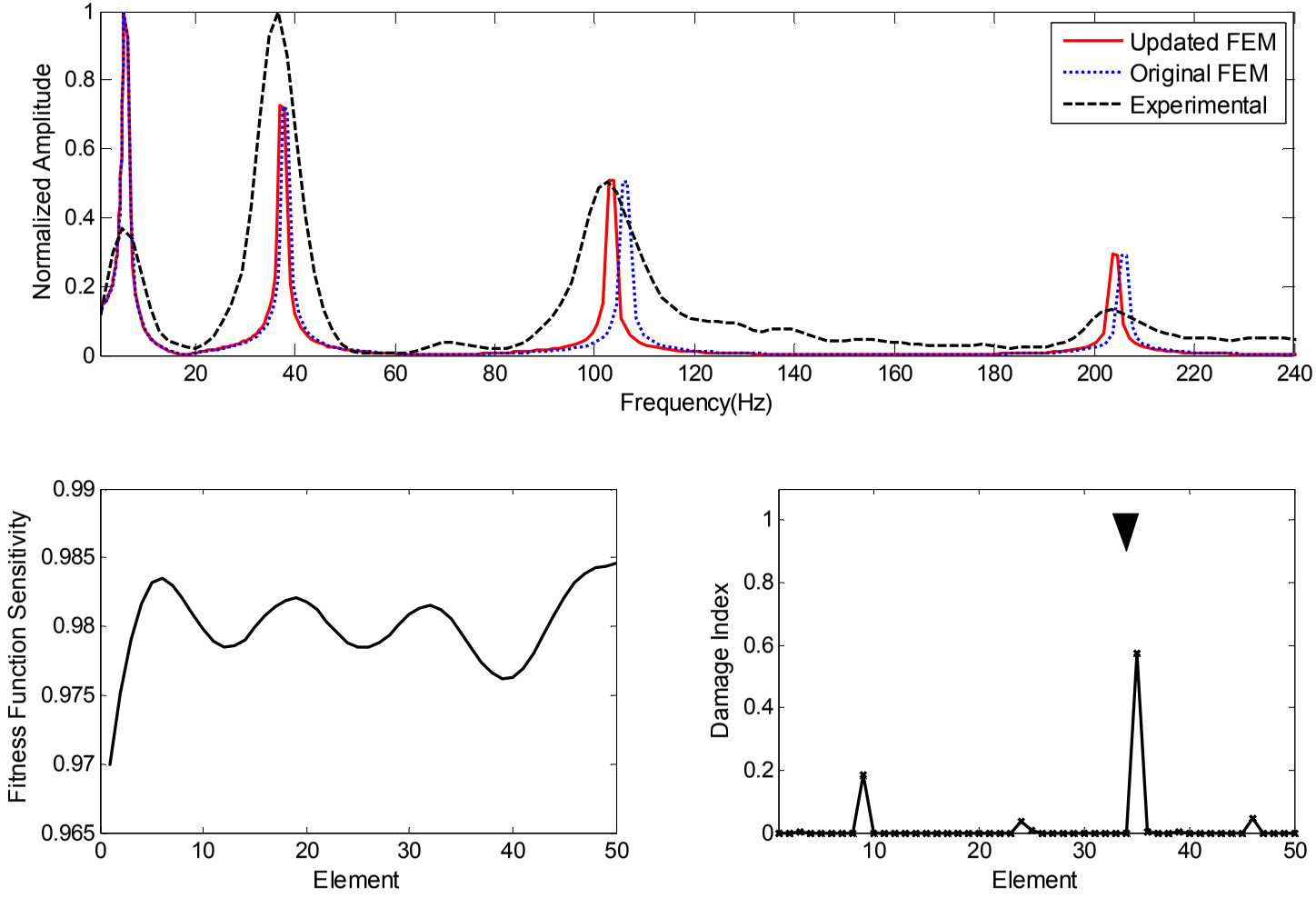

Figure (4.13): Damage Detection Results for Run 3

Damage Detection Run 4

This damage detection run used fitness function #2 to detect damage in case 2. The model tuning and damage detection phase results presented in Figure (4.14) shows that the algorithm succeeded in updating the calculated FRF to a closer match of the experimental FRF. The damage index Figure (4.16) displayed a group of peaks around the expected damage location rather than a clear single peak.

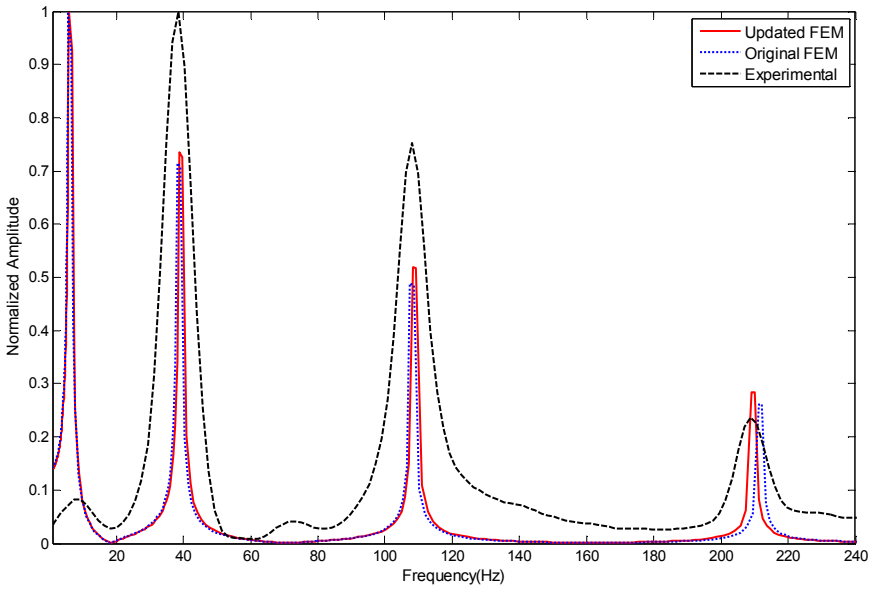

Figure (4.14): Model Tuning Results for Run 4

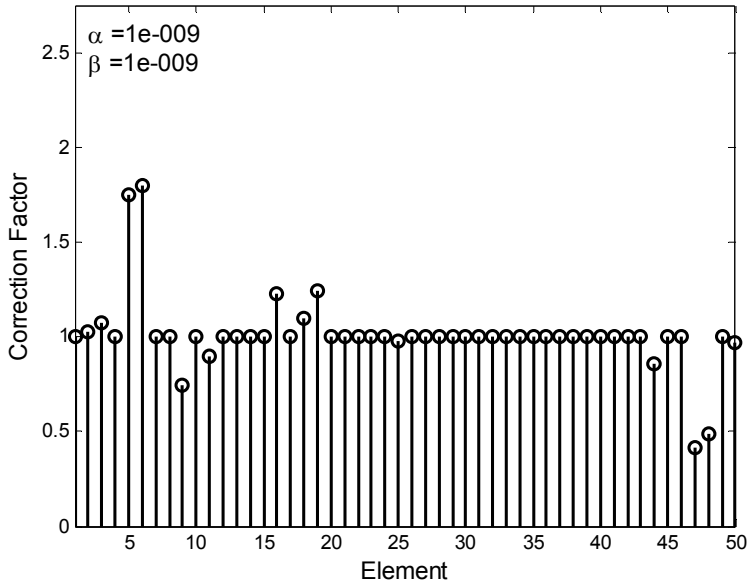

Figure (4.15) Final Correction Factors for Damage Detection Run 1

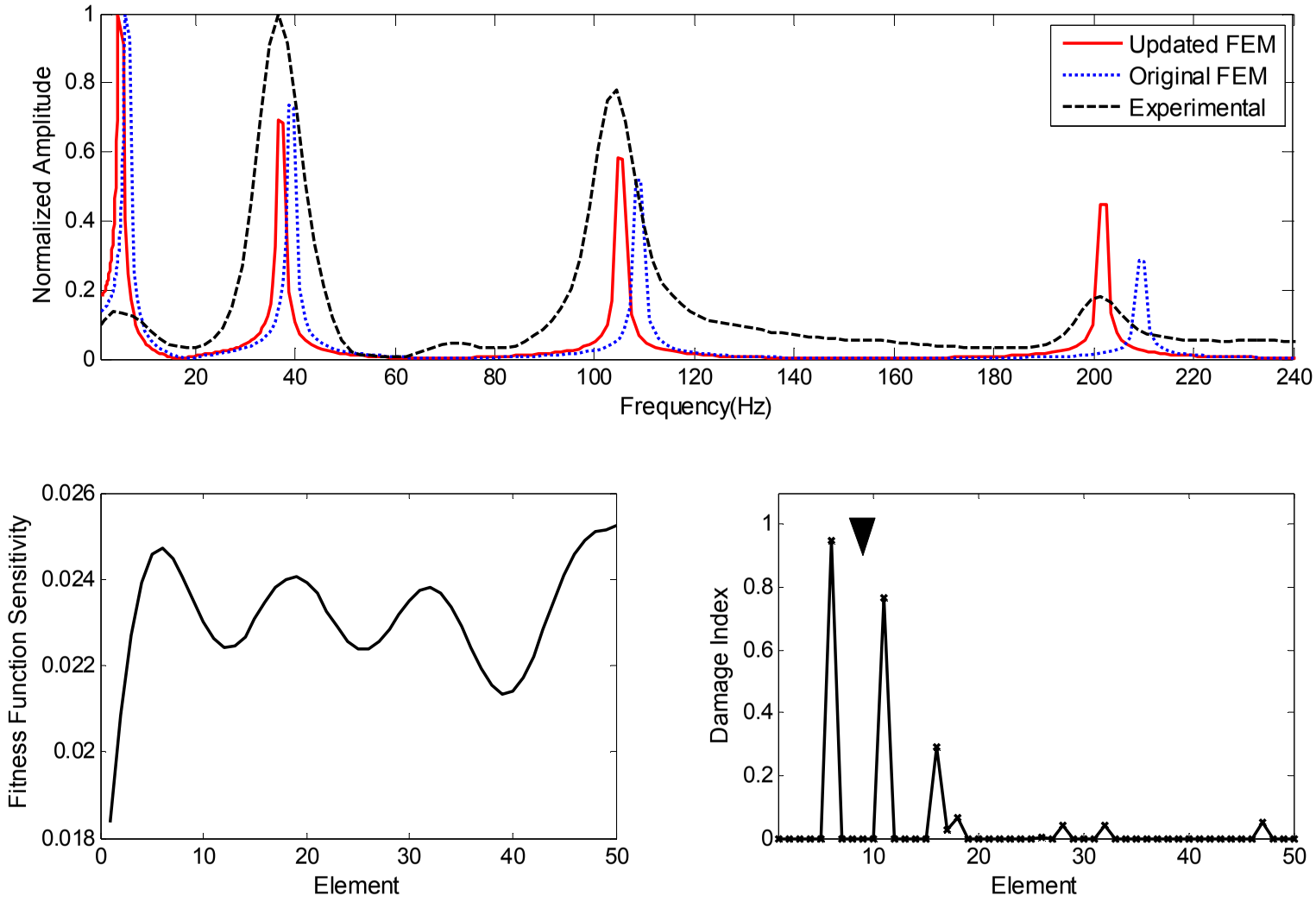

Figure (4.16): Damage Detection Results for Run 4

Damage Detection Run 5

For this run, cost function #3 was used to identify the damage in case 1. The model tuning results presented in Figure (4.17) shows that the error in amplitude for the third and fourth modes increased after model updating and with no significant improvements to the amplitude of the second mode. It should be noted that cost function #3 should focus on decreasing the error in the second mode since it has the highest amplitude. As for the damage detection results presented in Figure (4.19), it can be seen that no significant updates was introduced to FRF. As a result, the damage detection results showed unacceptable errors.

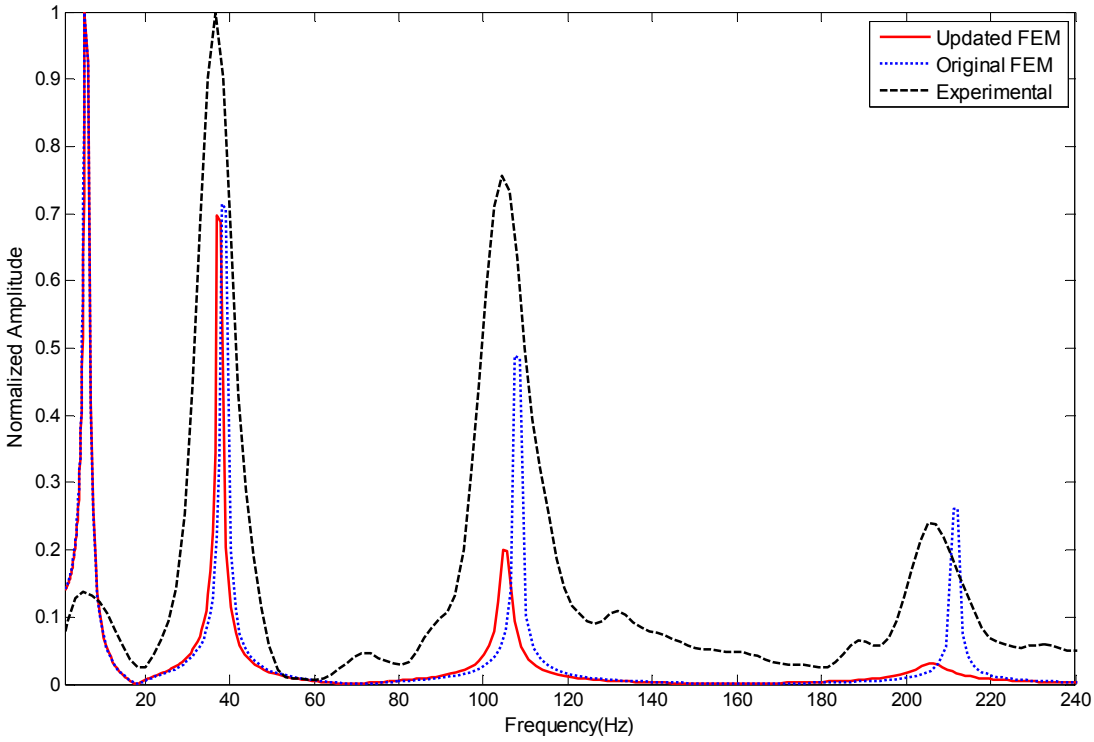

Figure (4.17): Model Tuning Detection Results for Run 5

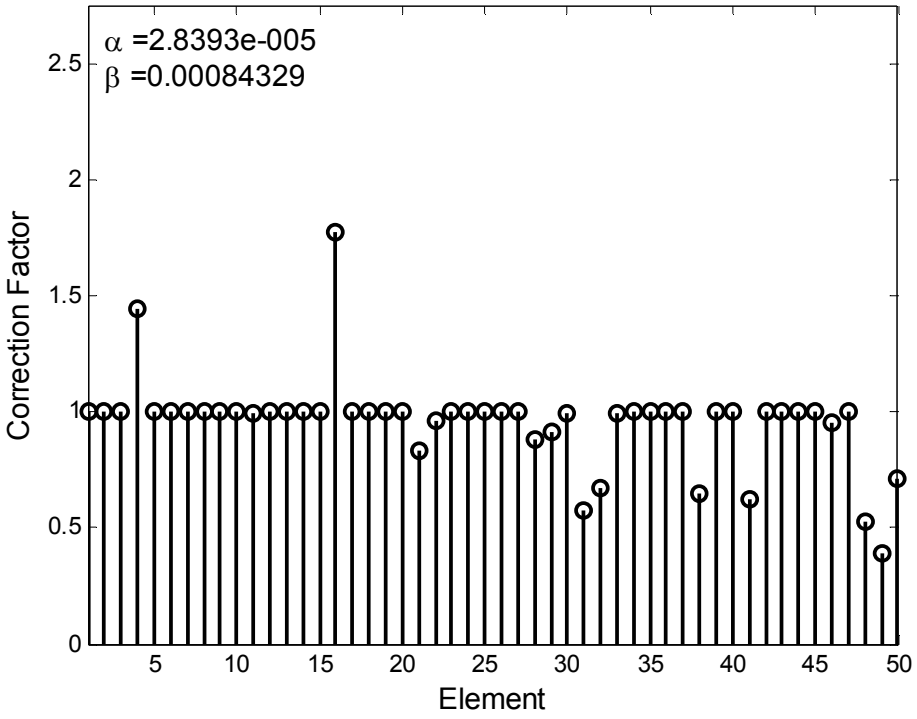

Figure (4.18) Final Correction Factors for Damage Detection Run 5

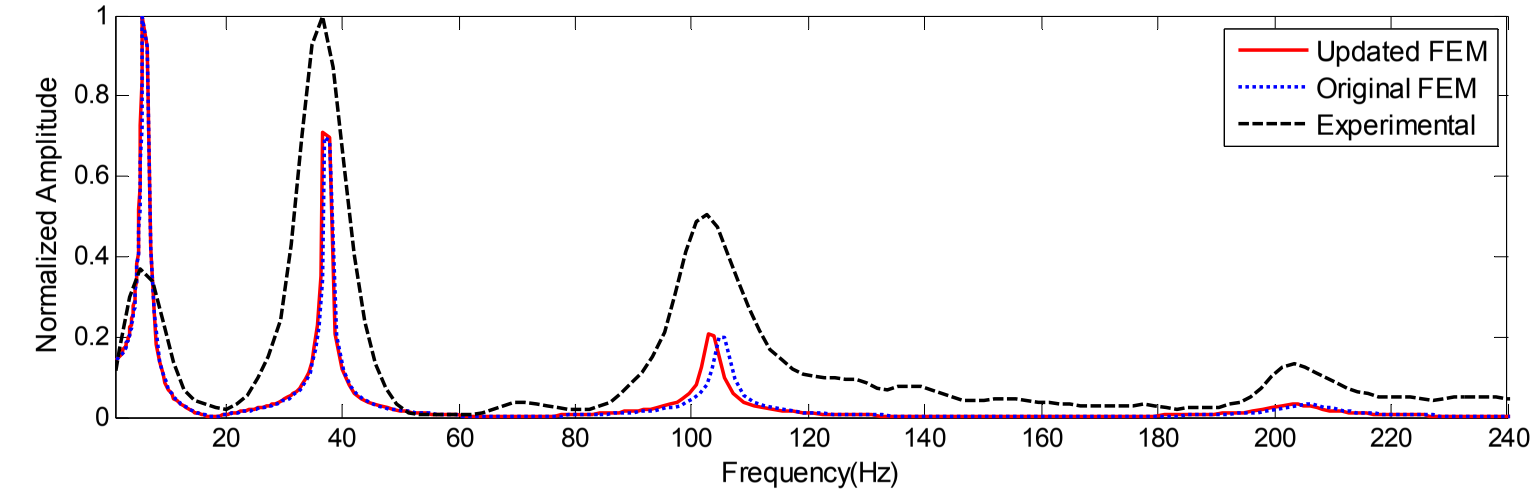

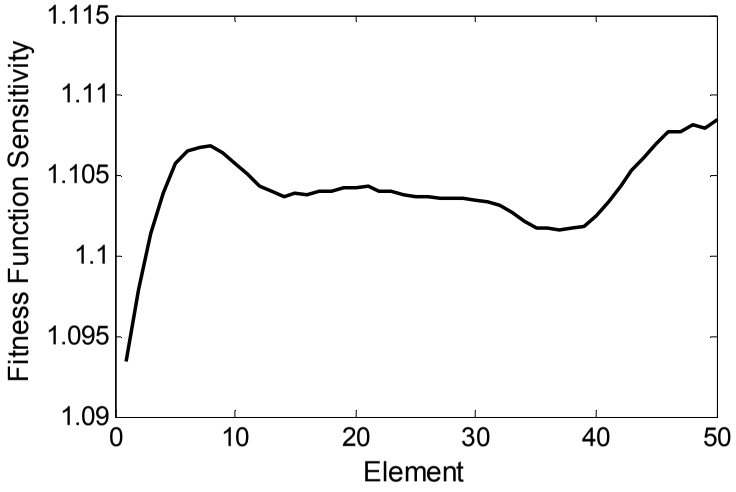

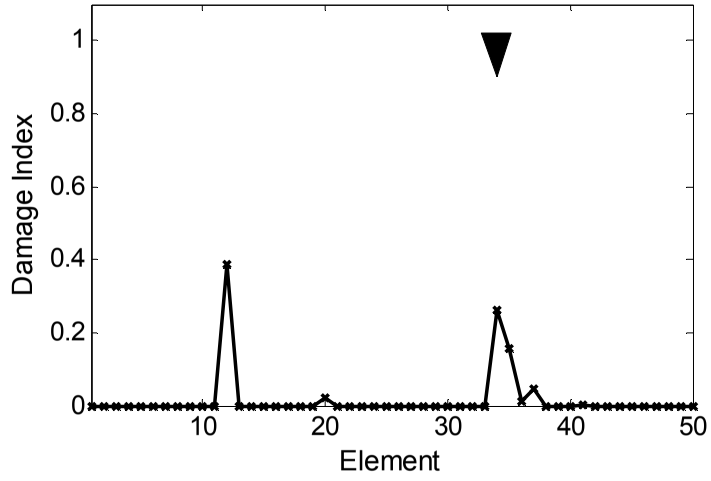

Figure (4.19): Damage Detection Results for Run 3

Damage Detection Run 6

For damage detection run 6, cost function #3 was used to identify the damage in case 2. The model tuning results presented in Figure (4.20) shows minor improvements to the theoretical FRF. But despite the significant improvement for FRF during damage detection phase shown in Figure (4.22) the algorithm failed to locate the damage.

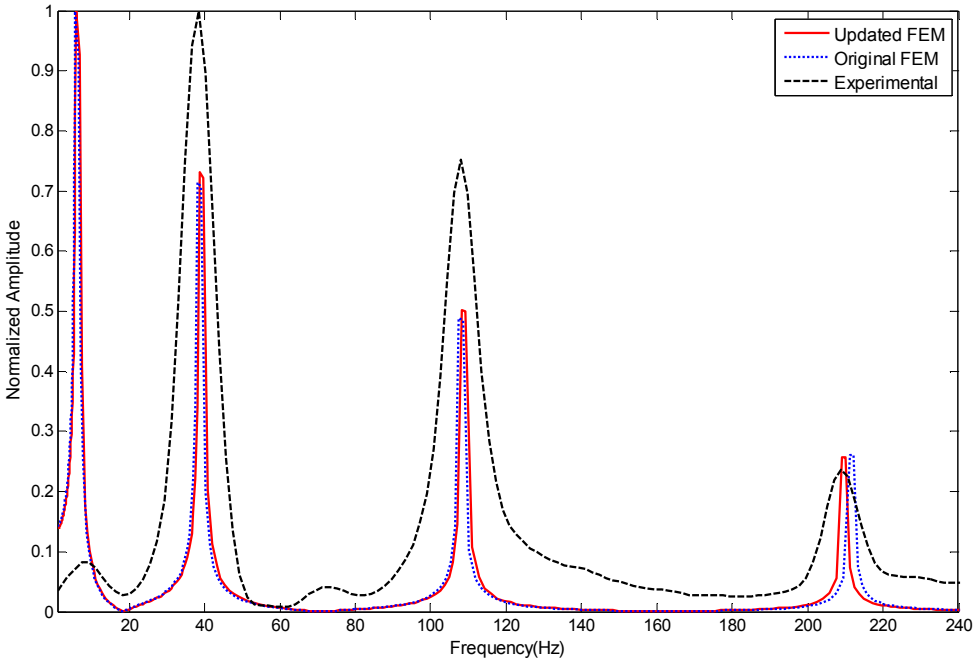

Figure (4.20): Model Tuning Results for Run 6

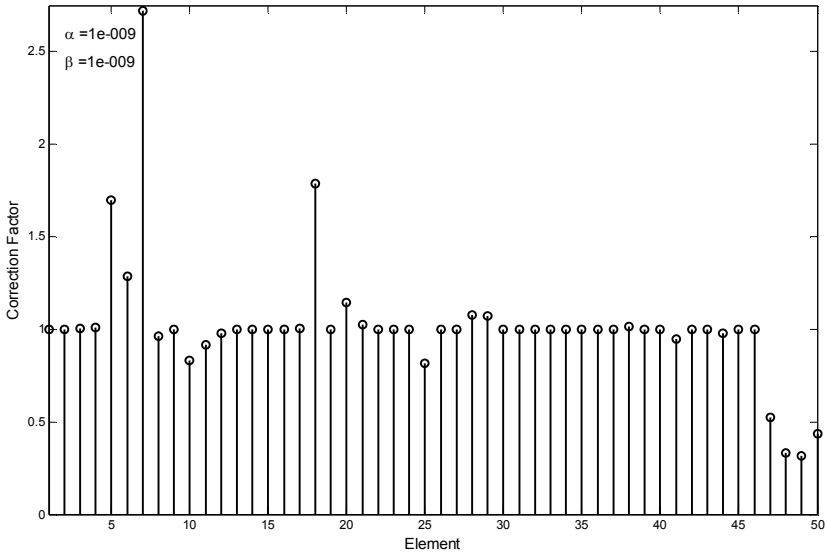

Figure (4.21) Final Correction Factors for Damage Detection Run 6

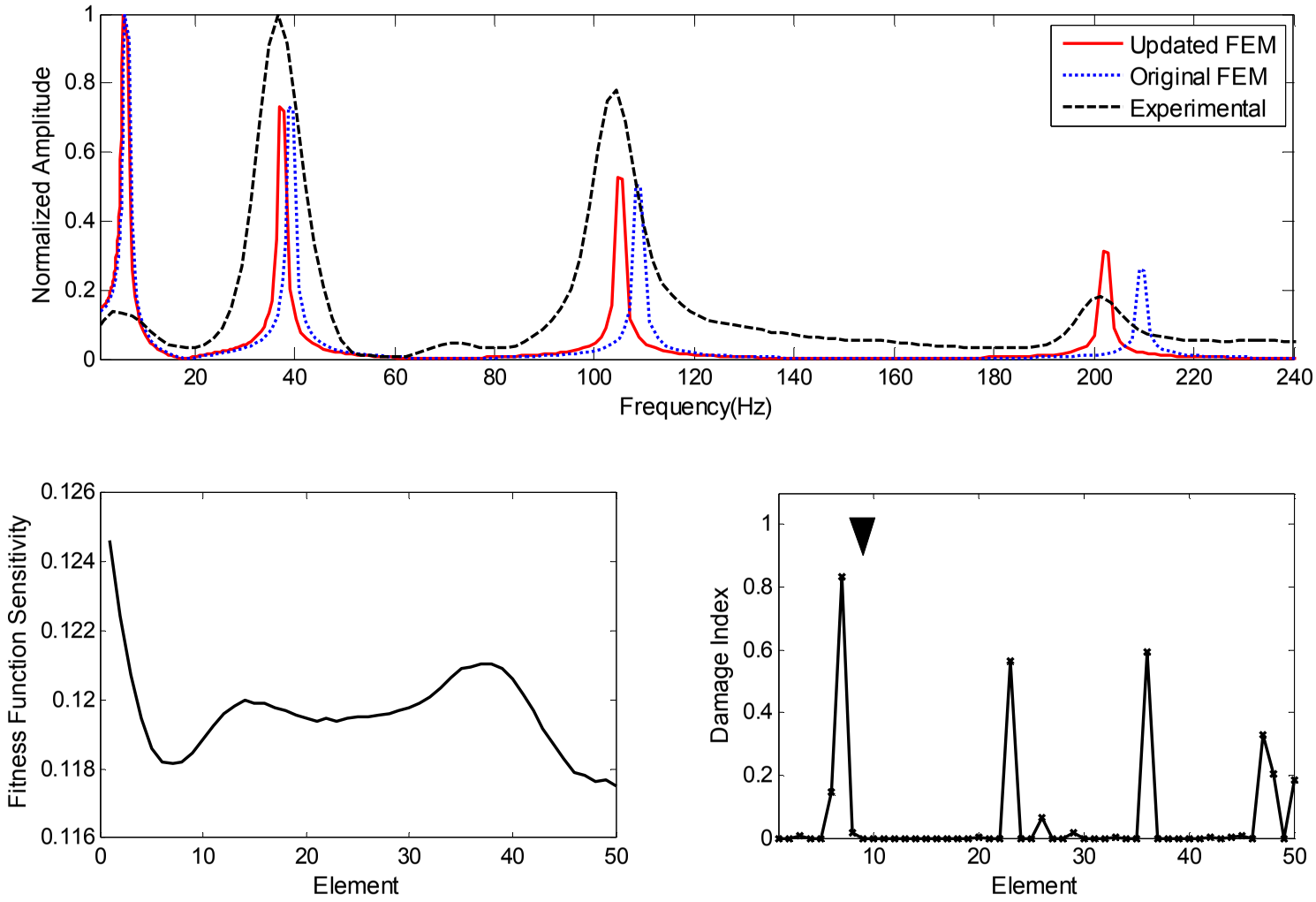

Figure (4.22): Damage Detection Results for Run 6

Discussion

By reviewing the results from damage detection runs 1 to 6, it is evident that cost function 2 which is given by equation (3.7) gives the most accurate results in terms of location. As for cost function 3 which is given by equation (3.8), since it will give more emphasis to the error on the mode with the highest experimental amplitude and since the first mode amplitude was affected by filtering, the low quality of results are expected.

4.4 Fitness Function Adjustment

As cost function 2 showed the best performance, the next step would be to determine the best value for the scale factor γ which adjusts the weight of the error in amplitude versus the error in frequency. Damage case 1 was used to adjust this value. Table (4.5) gives details for the damage detection runs done.

Table (4.5): Fitness Function Adjustment Runs Details

Run	Cost Function	γ	Damage Case	Number of modes
7	2	5	1	4
8	2	10	1	4
9	2	25	1	4

Damage Detection Run 7

This damage detection run used fitness function #2 to detect damage in case 1 with the scale factor γ set to 5. The model tuning and damage detection results presented in Figures (4.23, 4.24 and 4.25) respectively showed a significant improvement in damage detection accuracy when compared to the case of $\gamma = 1$.

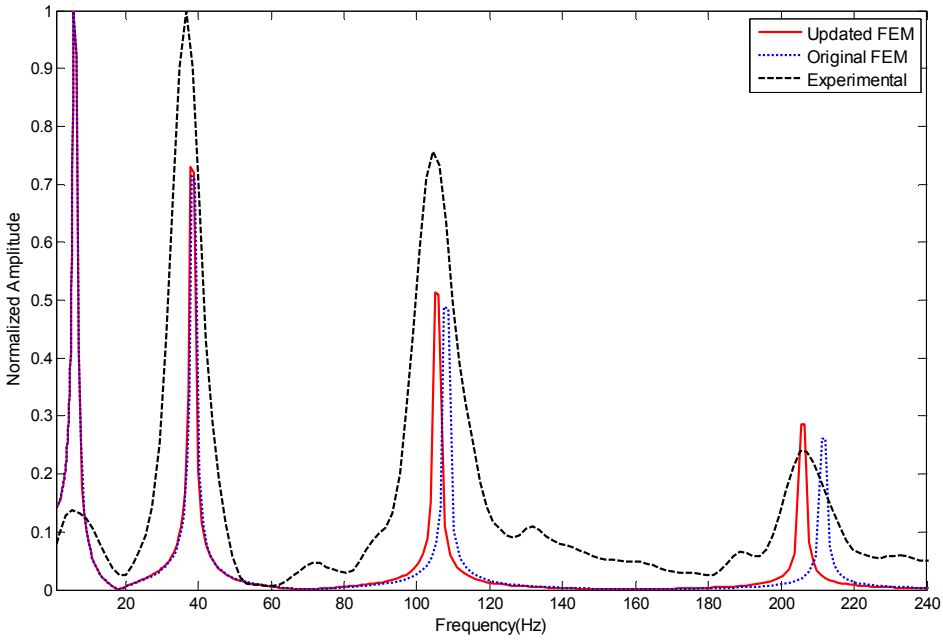

Figure (4.23): Model Tuning Results for Run 7

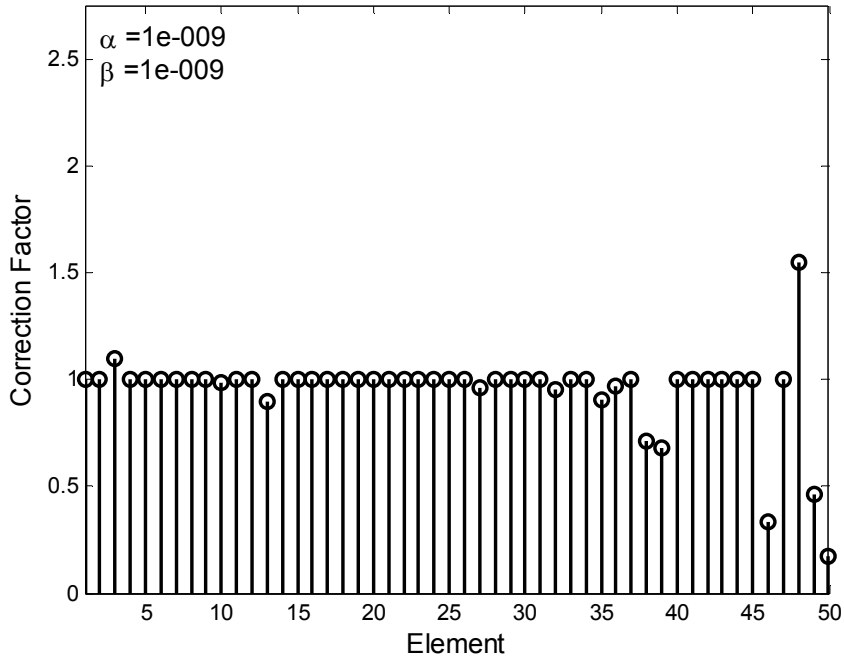

Figure (4.24) Final Correction Factors for Damage Detection Run 7

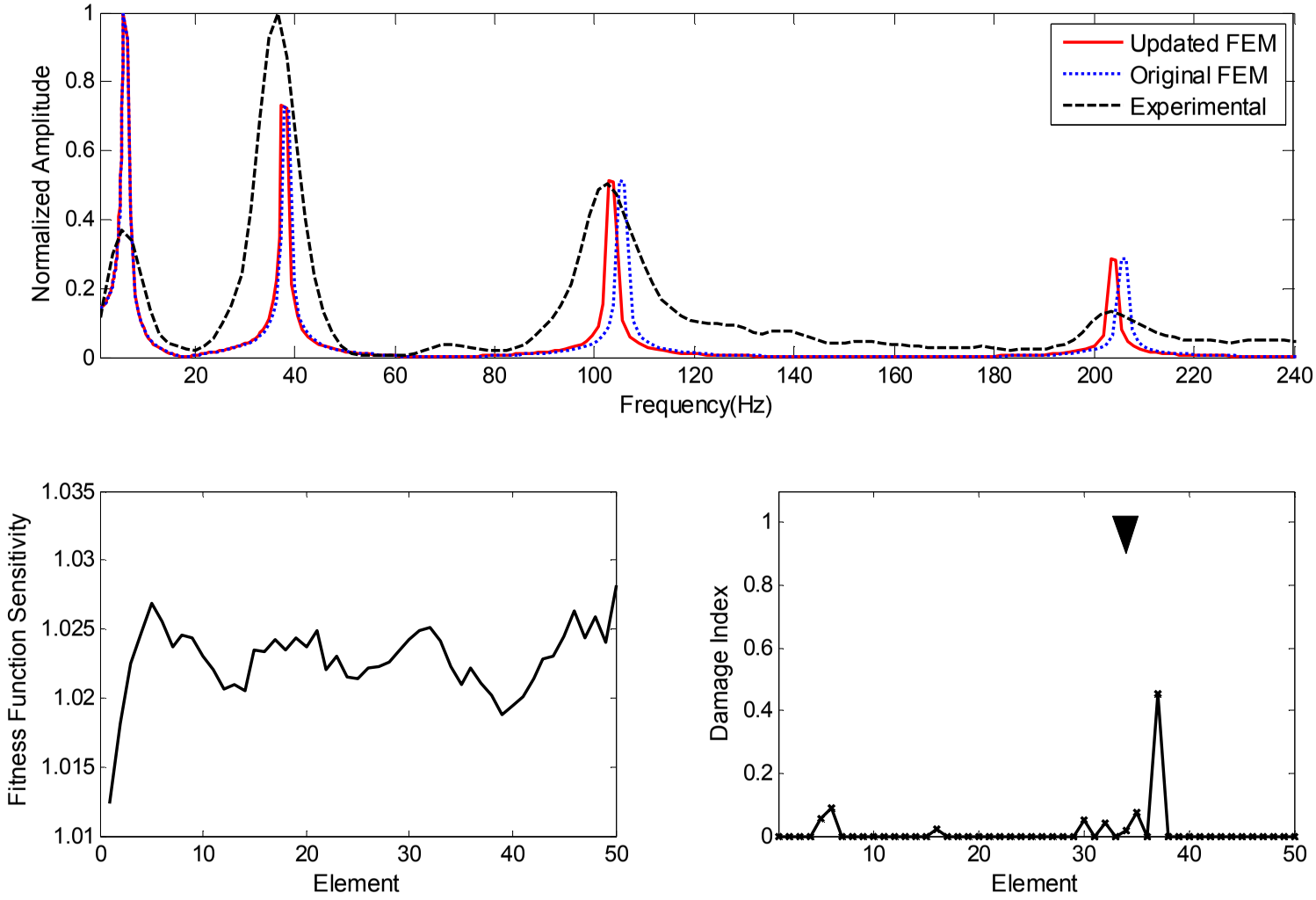

Figure (4.25): Damage Detection Results for Run 7

Damage Detection Run 8

This damage detection run used fitness function #2 to detect damage in case 1 with the scale factor γ set to 10. Figures (4.26, 4.27 and 4.28) shows model tuning and damage detection results which showed an improvement in damage detection accuracy when compared to the case of $\gamma = 1$ but not better than the case of $\gamma = 5$.

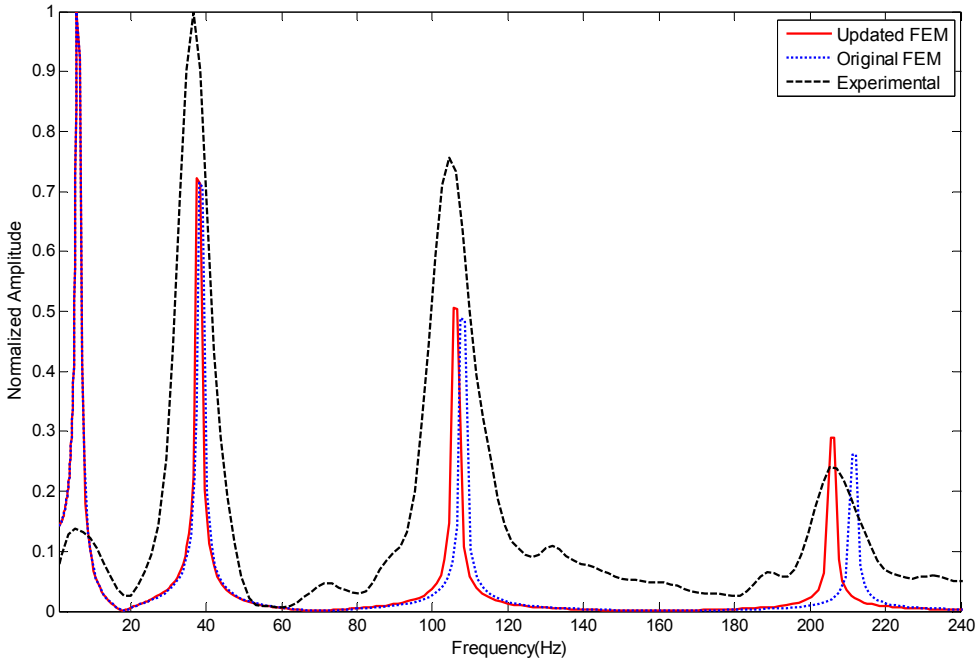

Figure (4.26): Model Tuning Results for Run 8

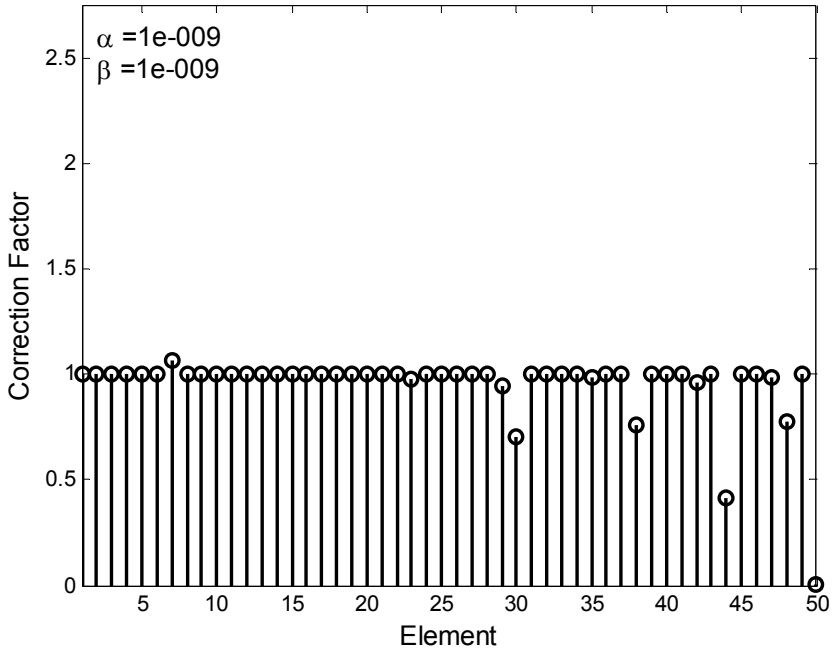

Figure (4.27) Final Correction Factors for Damage Detection Run 8

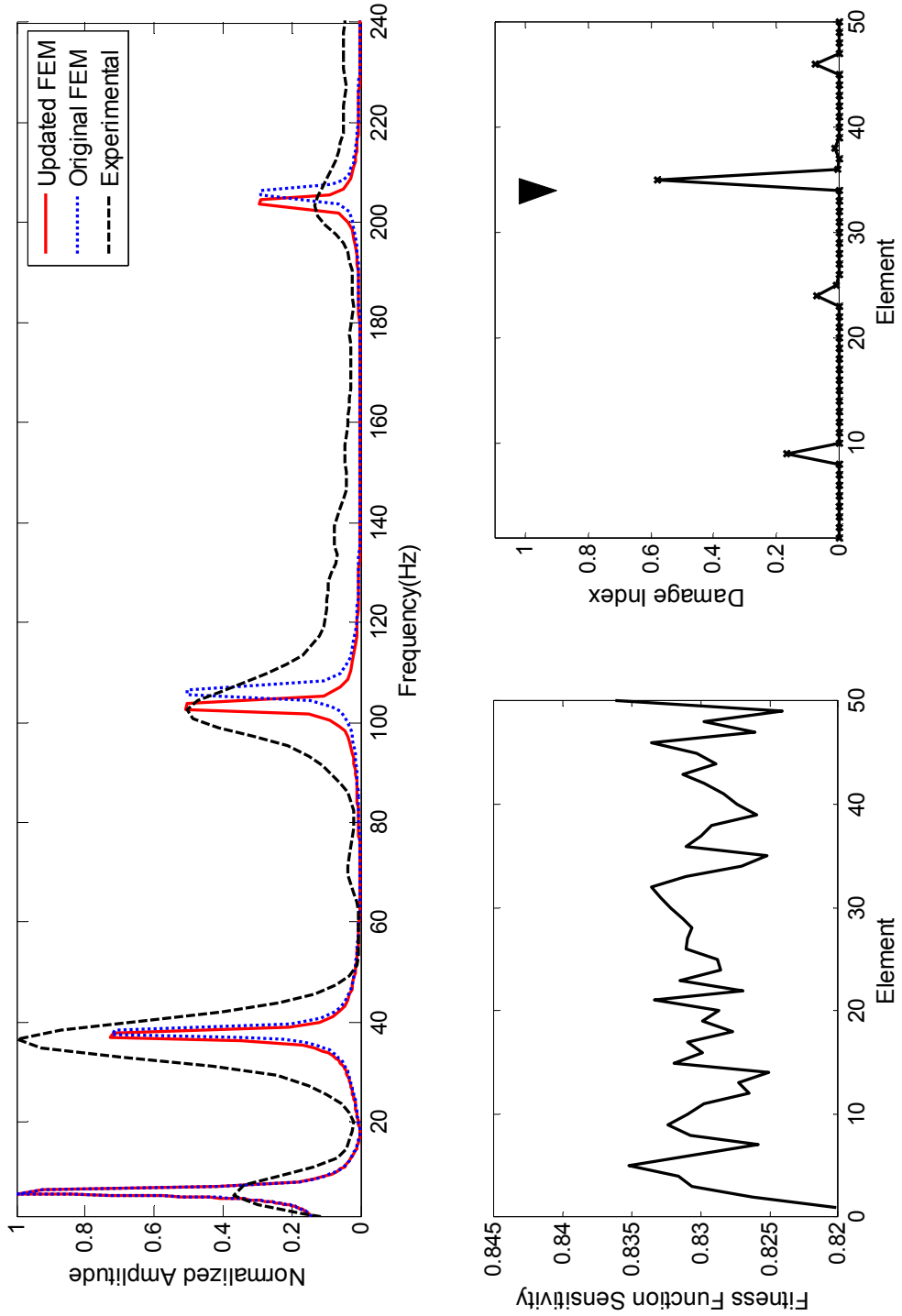

Figure (4.28): Damage Detection Results for Run 8

Damage Detection Run 9

For this run cost function # 2 was used with a scale factor of 25 to solve for the damage case1. Despite what appears to be good model tuning and damage detection FRF results which are shown in Figures (4.29, 4.30 and 4.31), the damage index was far from accurate. The algorithm detected a clear damage at the element number 16 while it should be located at element number 34.

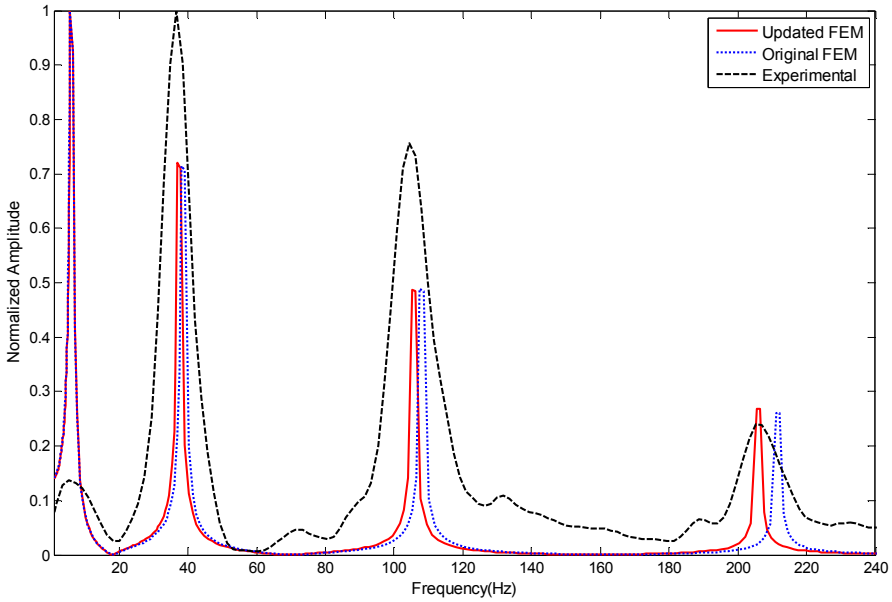

Figure (4.29): Model Tuning Results for Run 9

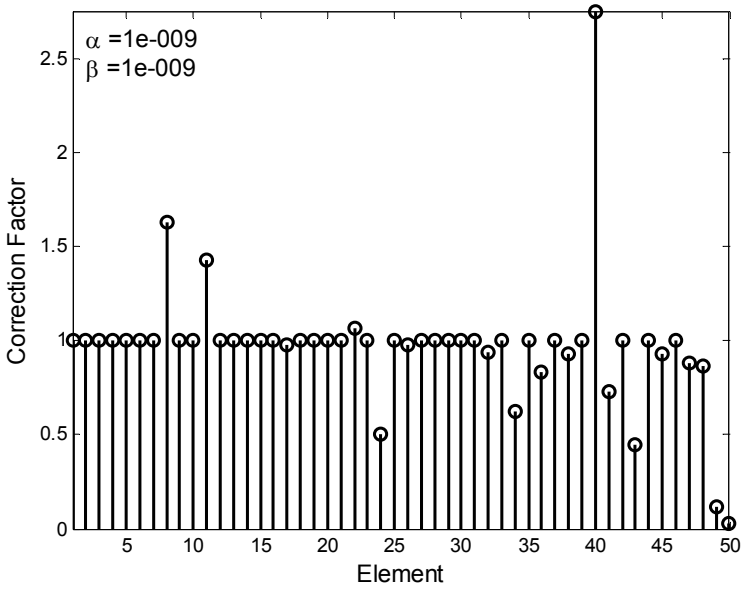

Figure (4.30): Final Correction Factors for Damage Detection Run 9

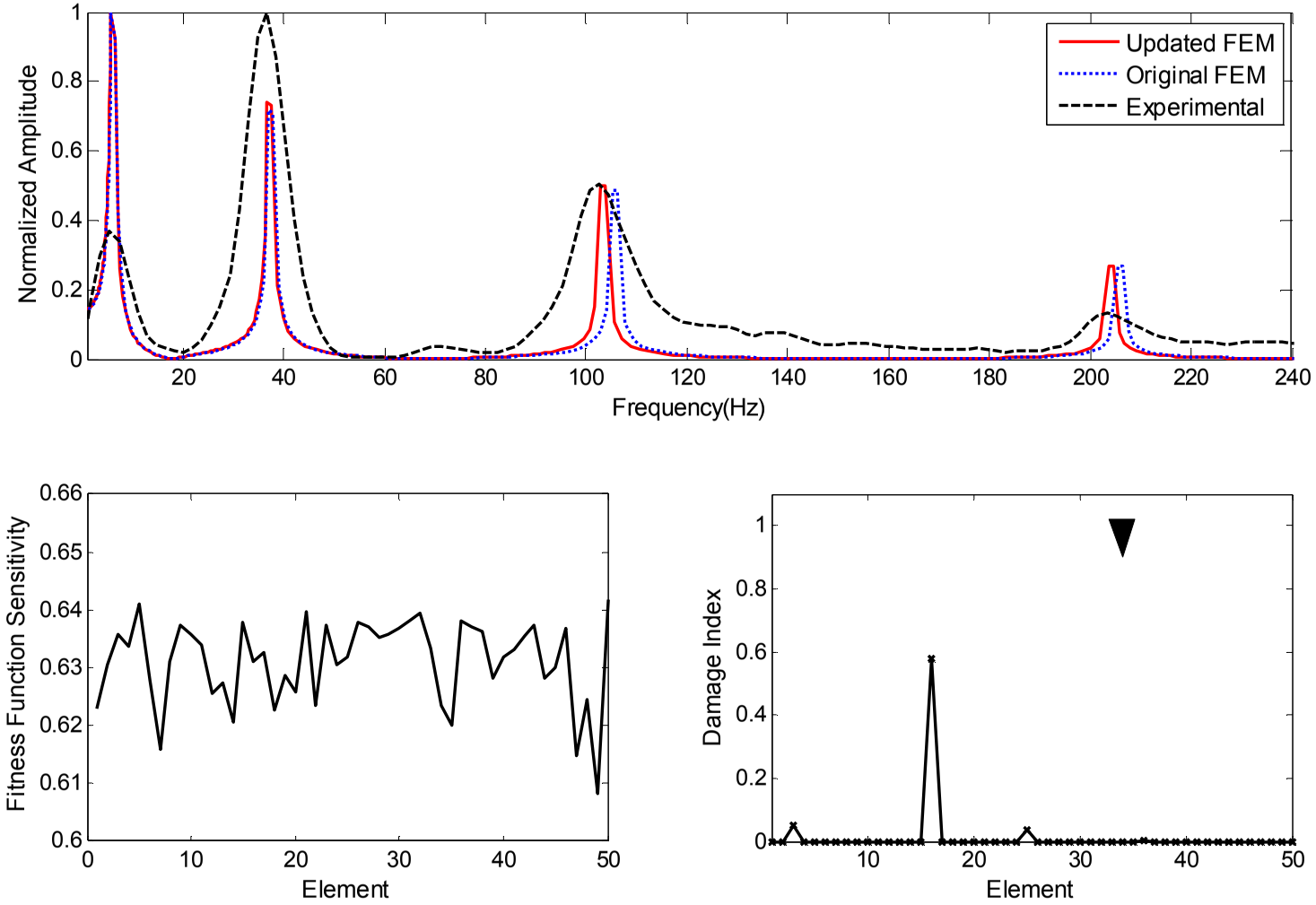

Figure (4.31): Damage Detection Results for Run 9

4.5 Small Structural Damage

Most available damage detection algorithms which rely only on changes in the natural frequencies tend to have accuracy problems with small structural damages. The proposed algorithm is characterized by detecting the location of small structural damages such as case 3 and case 4. In order to verify this accuracy, the adjusted cost function number 2 (equation (3.7)), the two cases were solved. The results are given in the following section.

Table (4.6): Damage Detection for Minor Structural Damage.

Run	Cost Function	γ	Damage Case	Number of Modes
10	3	5	3	4
11	3	5	4	4

Damage Detection Run 10

The results for this verification run are presented in Figures (4.32, 4.33 and 4.34). Despite the small damage size, algorithm was able to locate the damage with negligible errors.

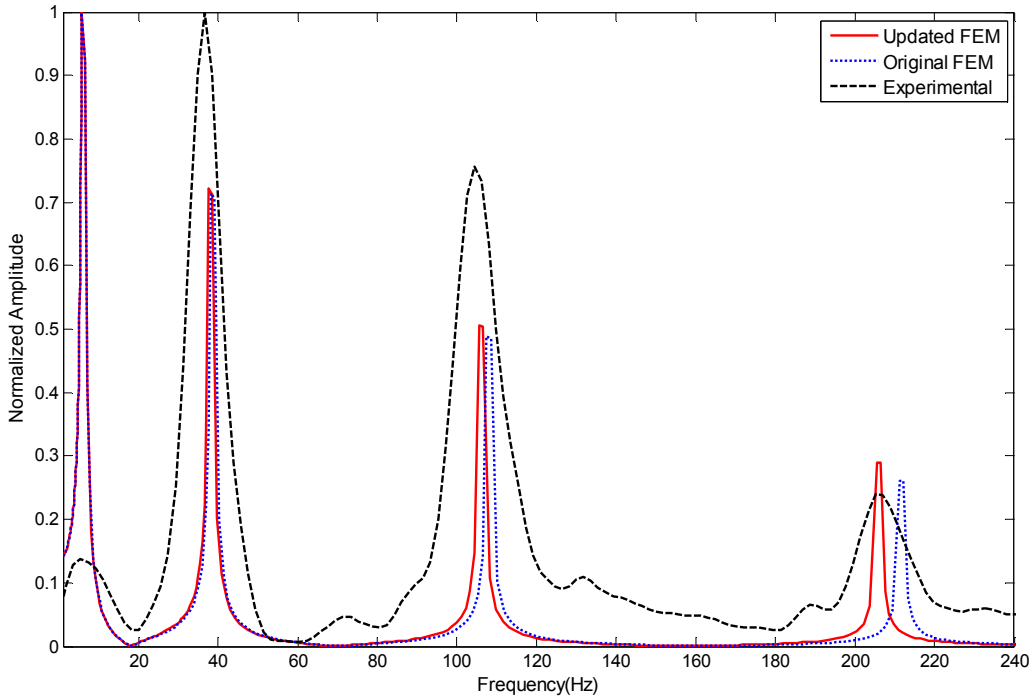

Figure (4.32): Model Tuning Results for Run 10

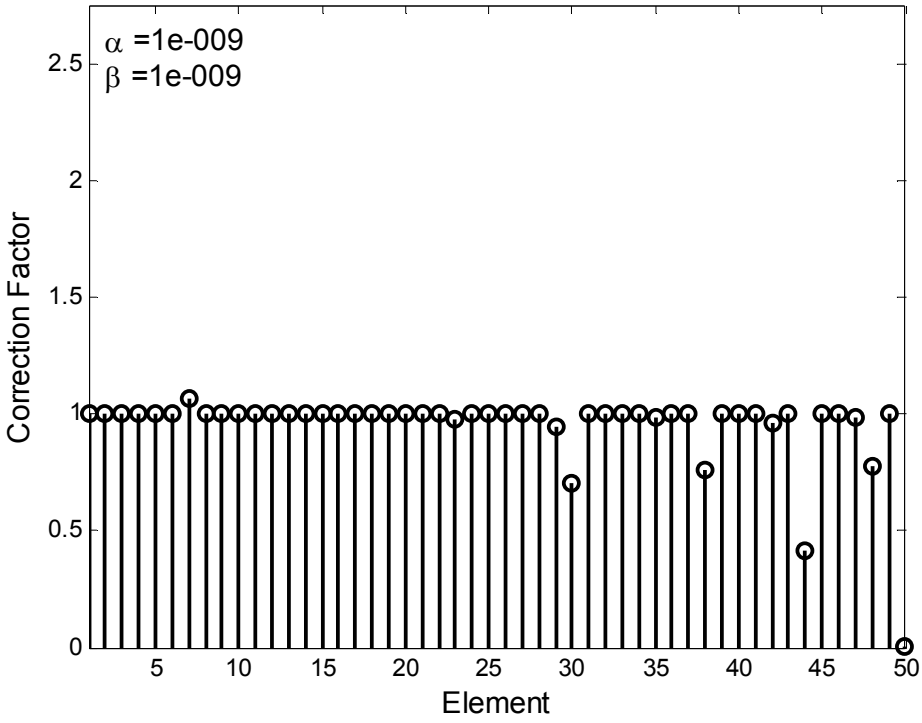

Figure (4.33): Final Correction Factors for Damage Detection Run 10

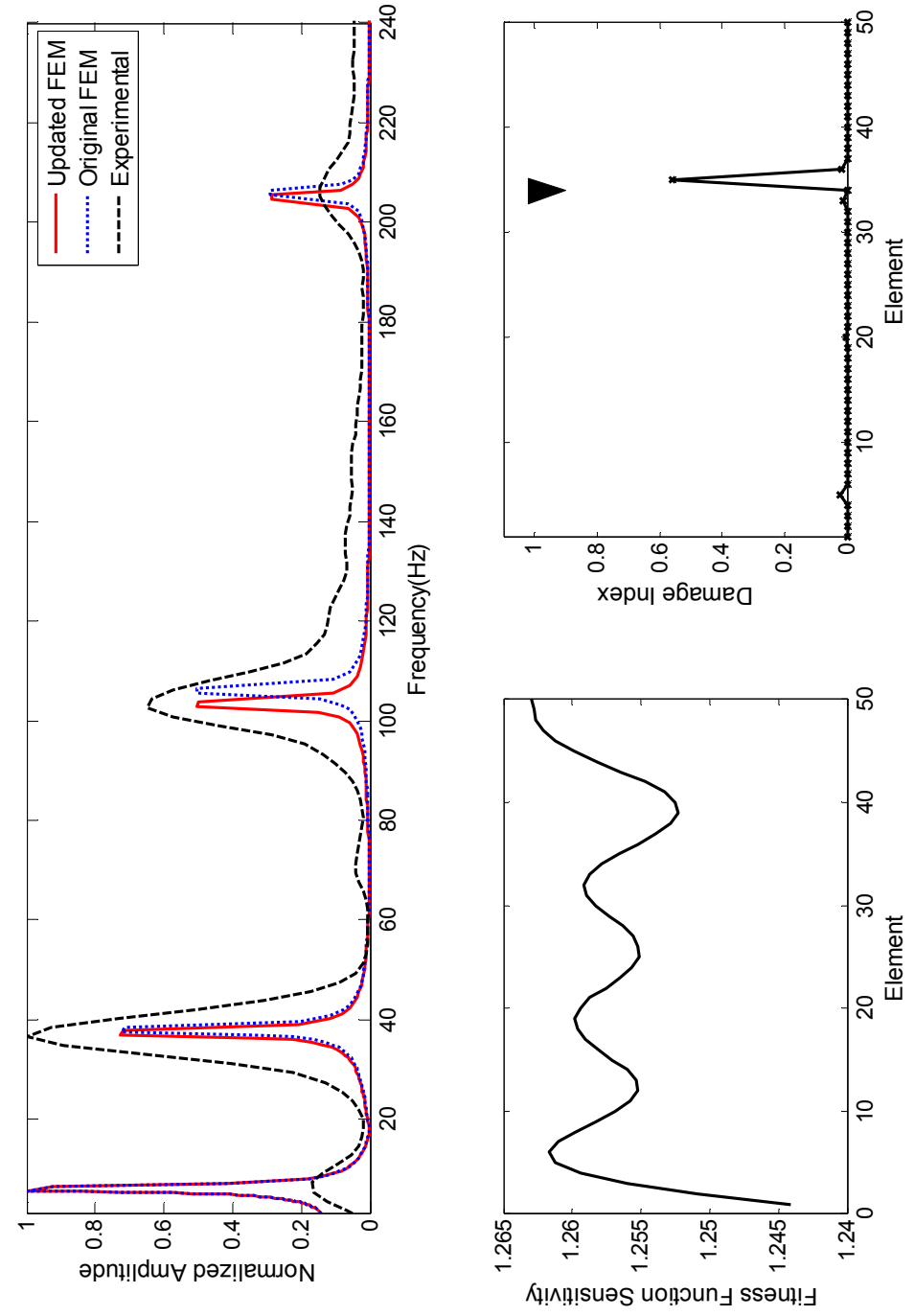

Figure (4.34): Damage Detection Results for Run 10

Damage Detection Run 11

This damage detection run used fitness function #2 to detect damage in case 1 with the scale factor γ set to 5. Figures (4.35, 4.36 and 4.37) shows model tuning and damage detection results. The model tuning phase was not able to add any significant improvement to the original FEM which can be attributed to experiment quality, since the theoretical FRF is close to the experimental FRF. The damage detection phase located the damage near the actual location. However, there is a minor false detection towards the beam tip.

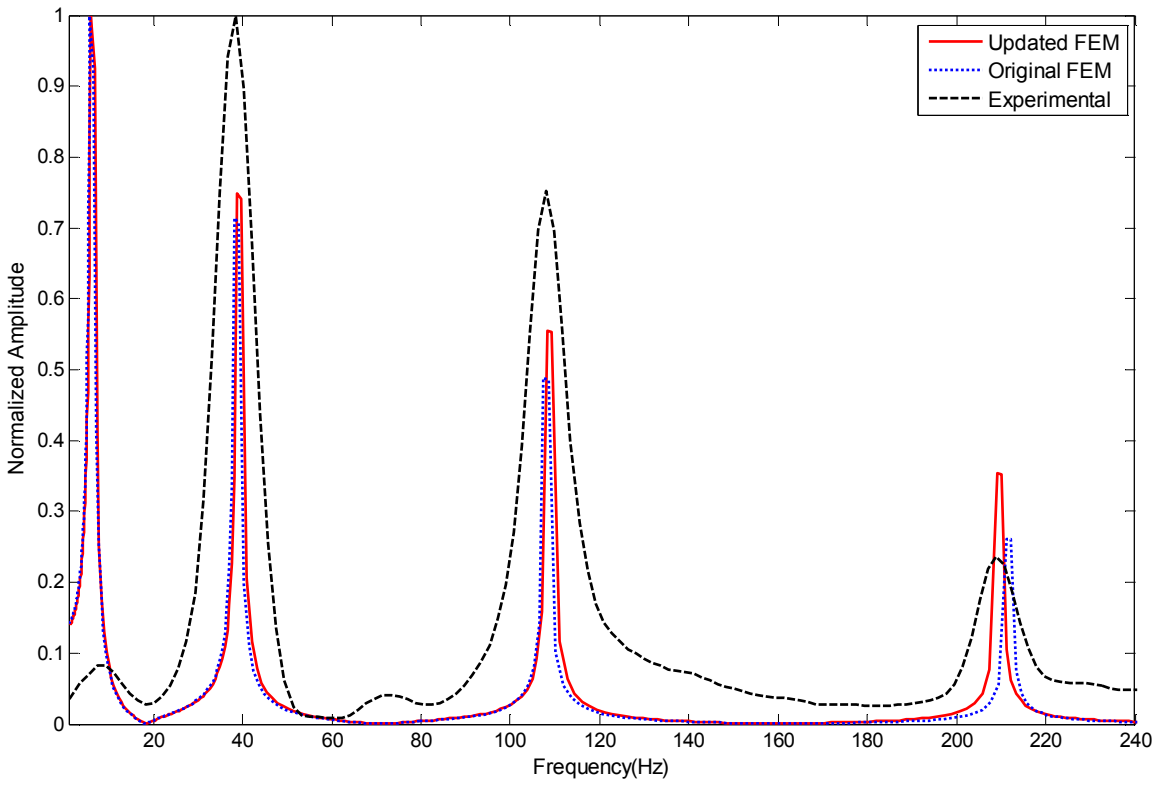

Figure (4.35): Model Tuning Results for Run 11

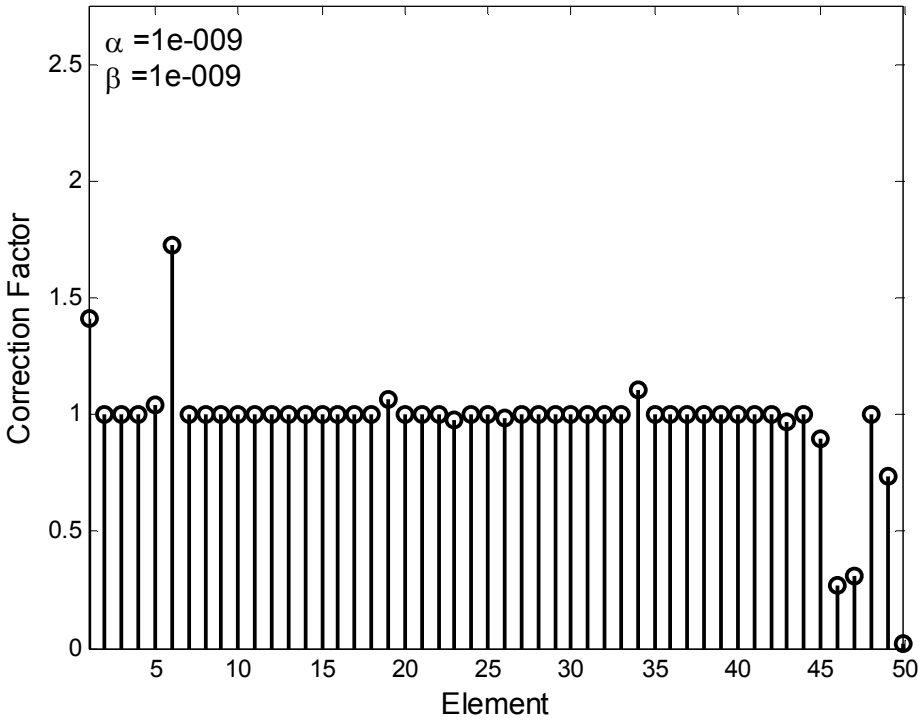

Figure (4.36): Final Correction Factors for Damage Detection Run 11

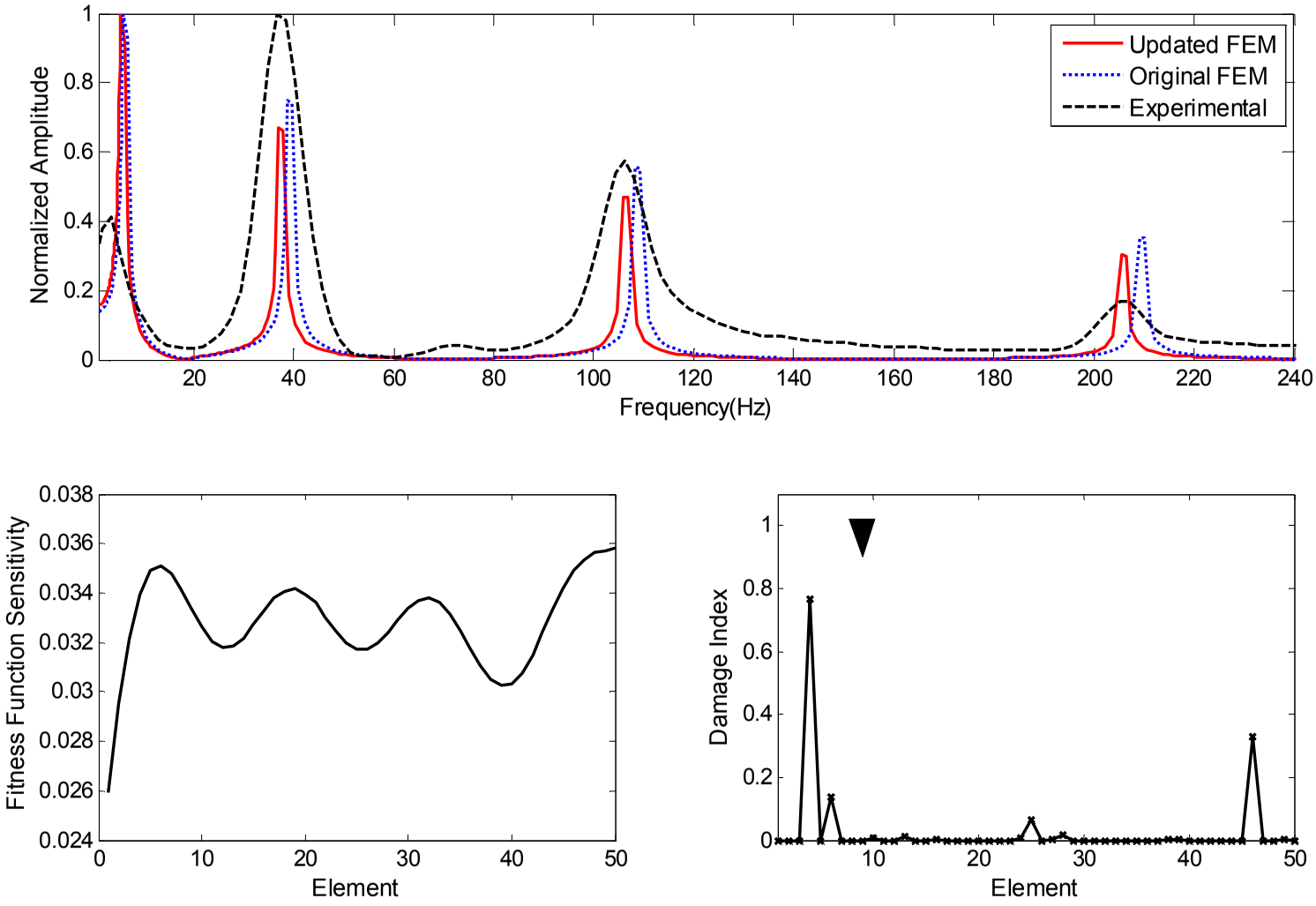

Figure (4.37): Damage Detection Results for Run 11

Discussion

The damage detection algorithm showed acceptable accuracy in detecting small structural damages. This accuracy is much appreciated in the light of the practical constraints imposed on the algorithm design such as: the absence of feedback and relying on white noise as the source of excitation.

4.6 Effect of Excitation Location

In the previous sections, the FRF measured experimentally was a result of base excitation. However, the FRF produced analytically from the FEM was a result of tip force excitation. According to Ertuk and Inman [22] the vibration resulting from base motion of a cantilever beam should be modeled as a distributed pressure reflecting the beam's own weight and not as a tip force. Also, it can be seen from results shown in previous sections that the theoretical FRF differs from the experimental FRF in terms of normalized amplitude while frequencies can be considered matching.

Despite the difference in FRF, the overall damage detection algorithm was able to detect damage with acceptable accuracy. This can be attributed to the model tuning phase. During this phase, the errors resulting from the difference in excitation location was neutralized. Thus, during the damage detection phase the damage detection algorithm was only sensitive to the differences coming from damage.

In this section, damage detection results are calculated from an FRF simulating base excitation. In this model the exciting force is applied as distributed pressure acting within the beam plane with a maximum at root and gradually decreasing to reach zero at the tip. This model was used to solve the two verification cases (scenario #3 and scenario #4). The results are shown in Figures (37-42).

The results show that using the base excitation model for theoretical FRF produced results closer to those measured experimentally. In addition, the overall damage detection produced more accurate results. Thus, it is advisable to use the same type of excitation force for both the experiment and theoretical model. However, if no prior knowledge of the exciting force location the model tuning phase can neutralize the errors resulting from

the difference in FRF and the damage detection algorithm can operate with acceptable accuracy.

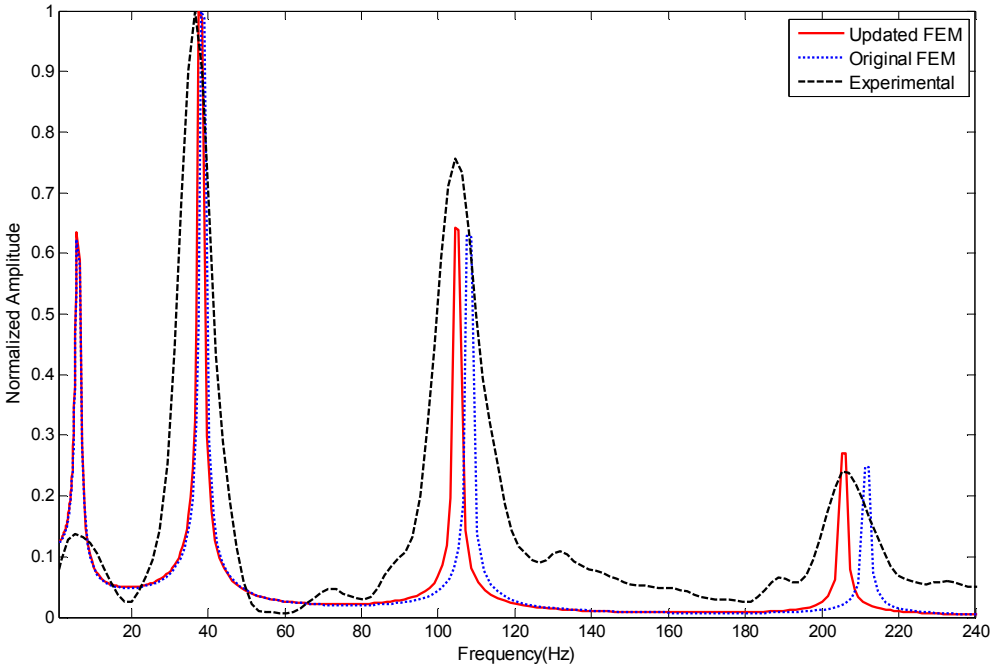

Figure(4.38) Model Tuning Results for Scenario #3 using Base Excitation

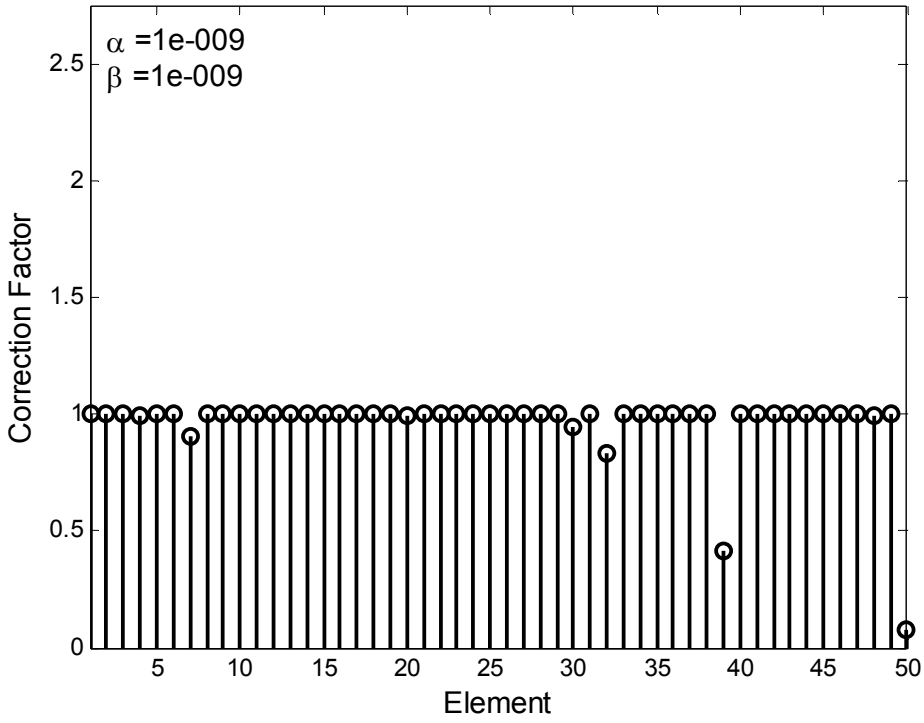

Figure (4.39) Final Correction Factors for Scenario #3 using Base Excitation

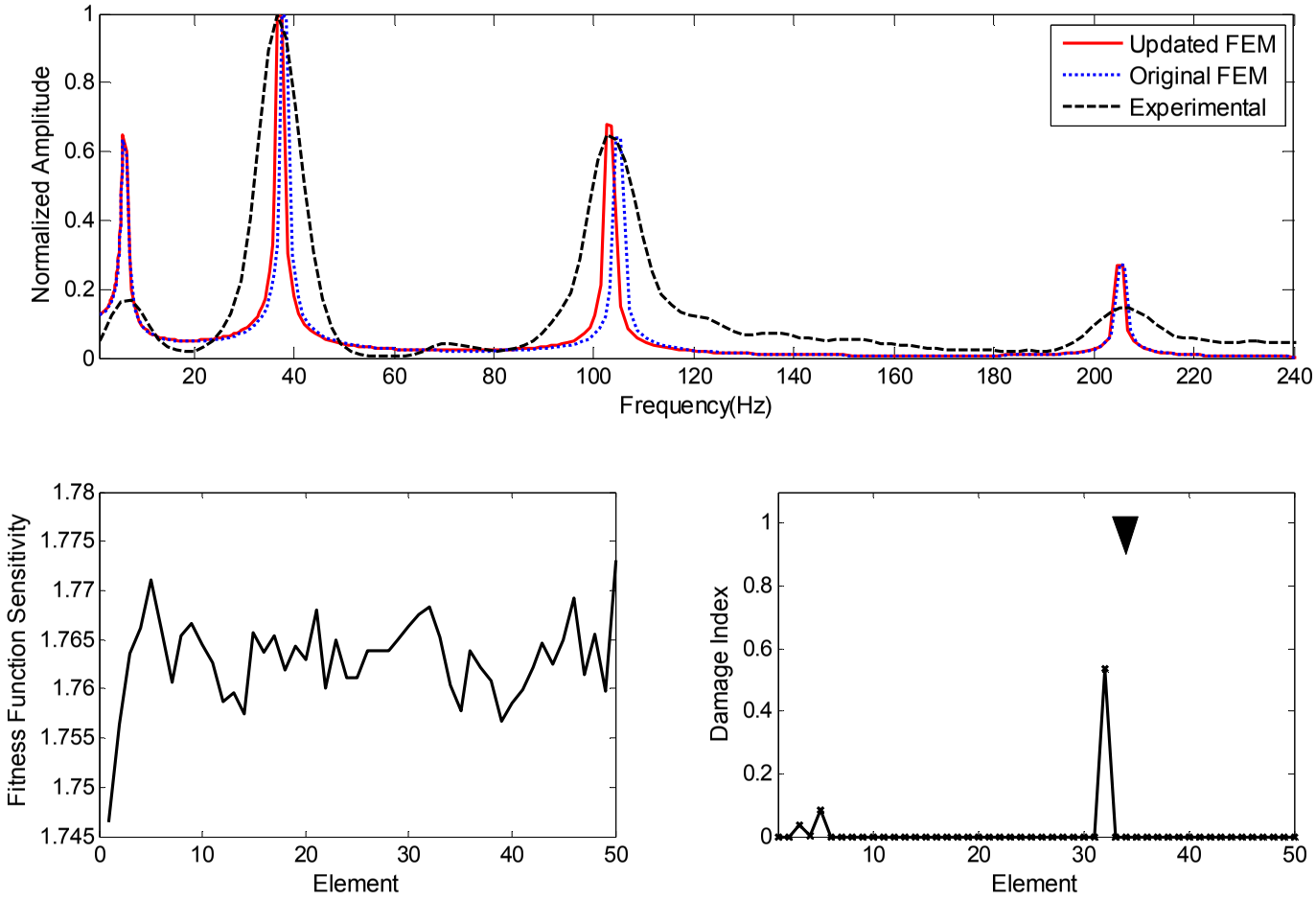

Figure (4.40): Damage Detection Results for Scenario #3 using Base Excitation

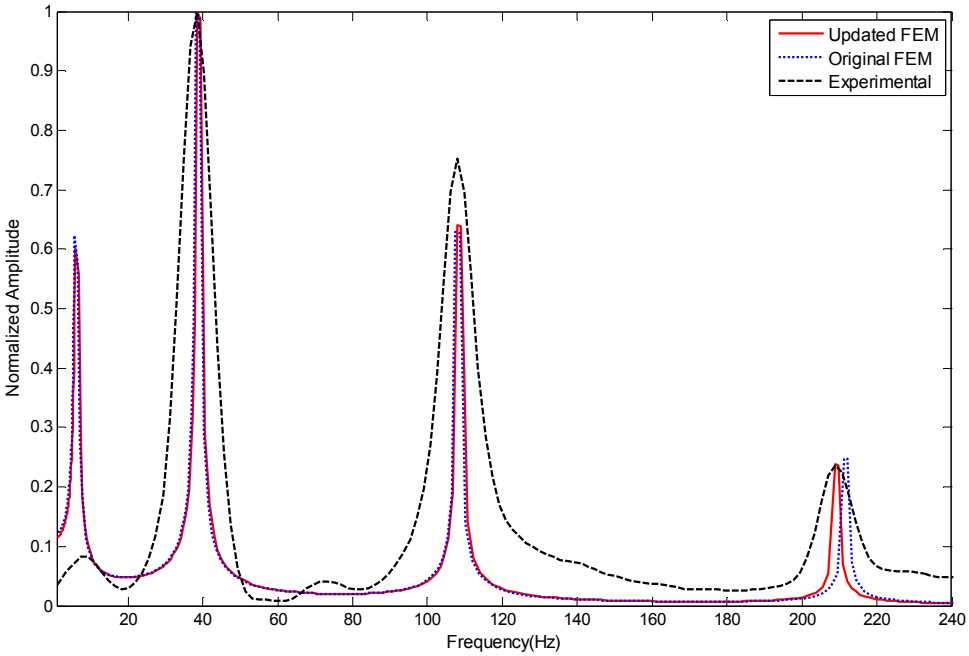

Figure(4.41) Model Tuning Results for Scenario #4 using Base Excitation

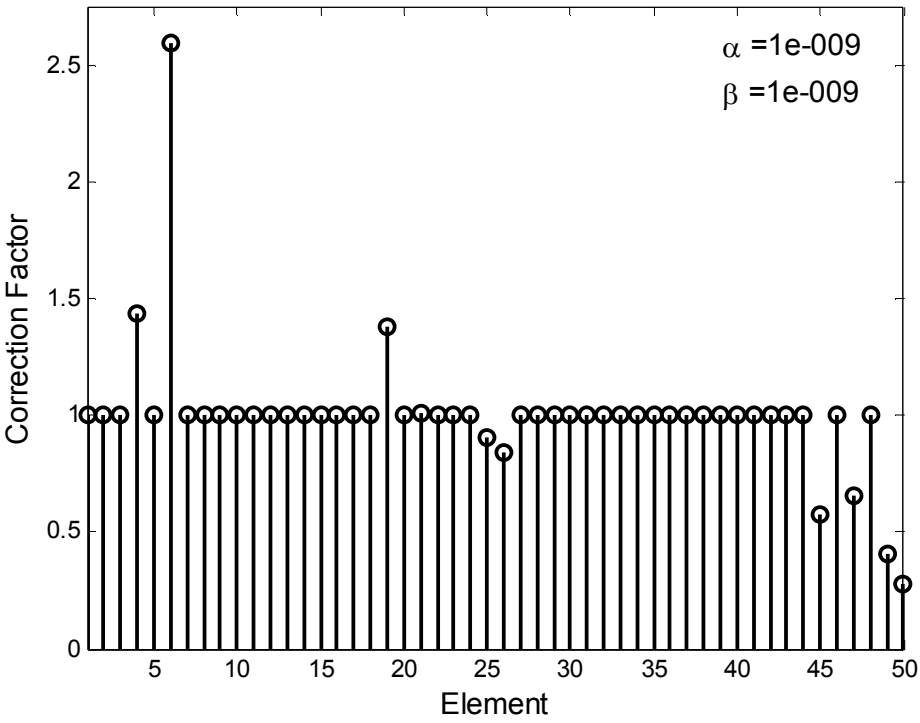

Figure (4.42) Final Correction Factors for Scenario #4 using Base Excitation

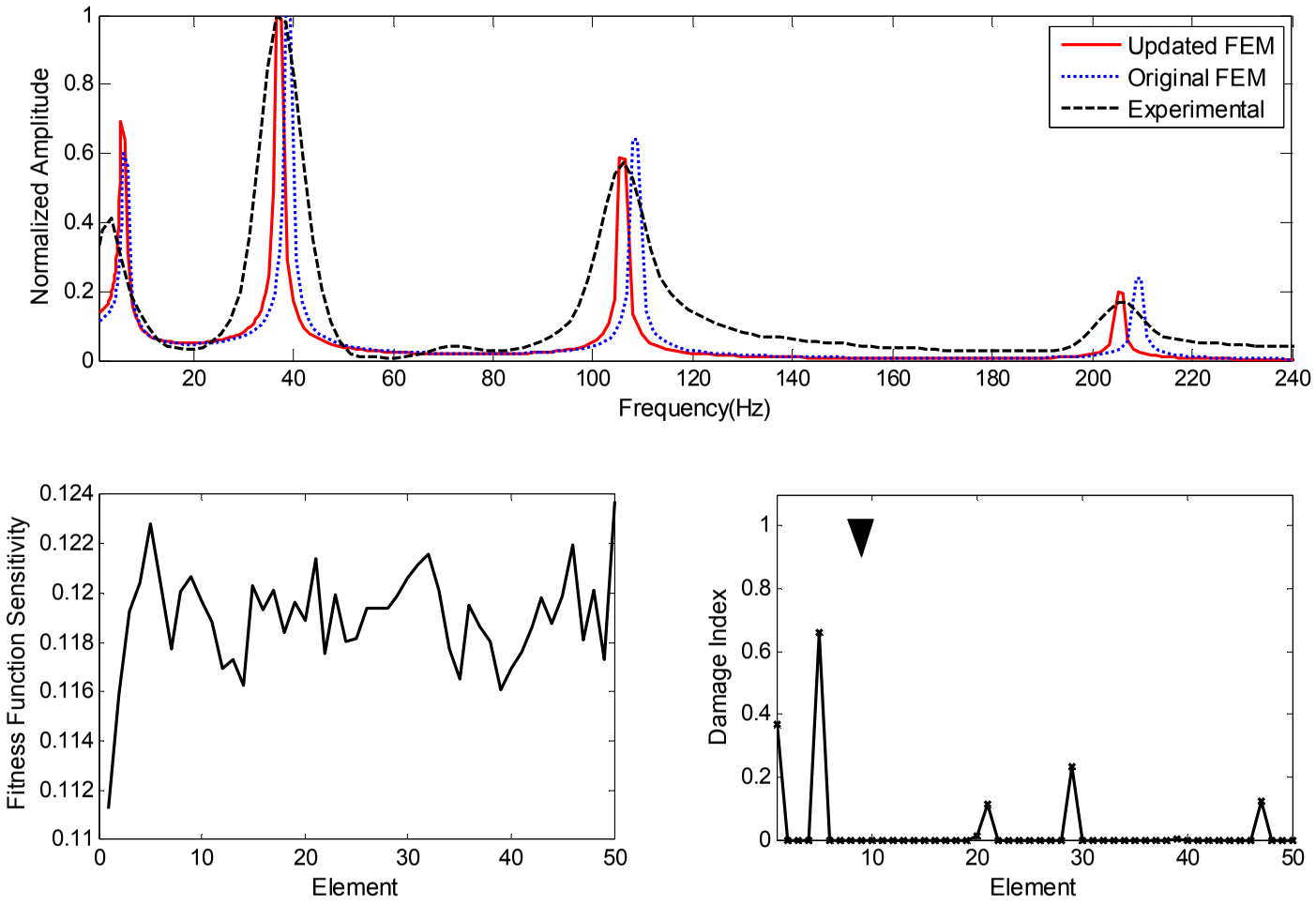

Figure (4.43): Damage Detection Results for Scenario #4 using Base Excitation

4.7 Multi-Channel Inputs

Despite the availability of the measurements from 3 channels, only 1 channel was used for damage detection in the previous. The reason behind this approach is that using the summation of the cost functions from all channels as a global cost function resulted in poor damage detection results. This can be attributed to the fact that optimizing more than one objective that might be competing by summing them will yield a solution that is not essentially the optimal [23].This multiple objective problem requires a different approach such as the Strength Pareto Approach [24]. Though the results were sufficient for the case of a simple beam, it is the assertion of this author that a single channel will not be sufficient for more complicated structure and the use of multiple sensors and multiple objective optimizations will be a necessity.

An alternate approach that will be used in the next section is using the average of the normalized strain measured from the three channels as a target for a single optimization function. Figures (4.43-4.48) shows the results of scenario #3 and #4 calculated using the averaged normalized strain and base excitation. The results show an improvement in damage detection algorithm accuracy when using normalized averaged strain form the 3 channels instead of 1.

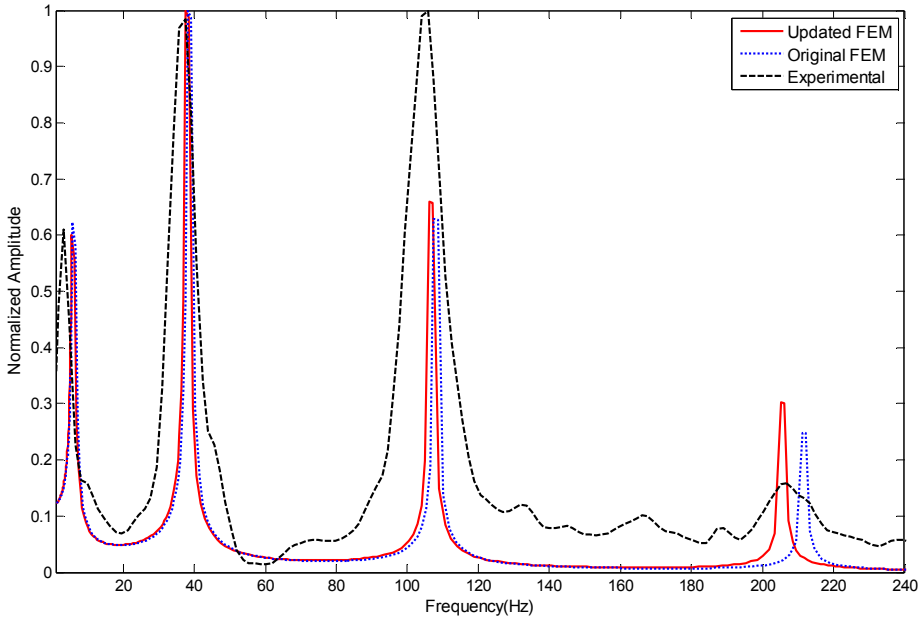

Figure(4.44) Model Tuning Results for Scenario #3 using Base Excitation and Averaged Normalized Strain

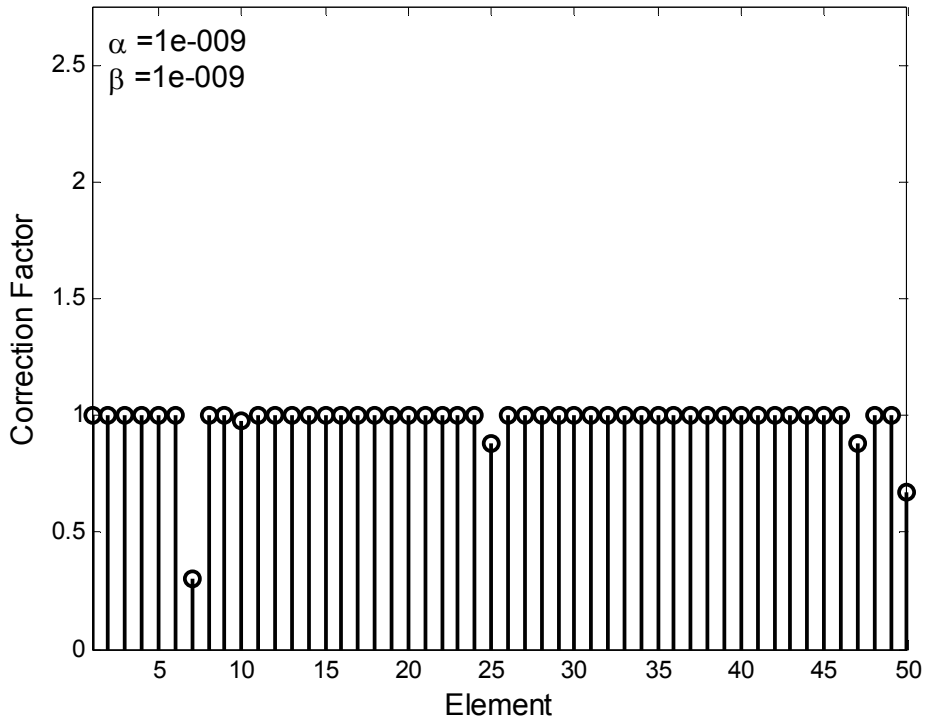

Figure(4.45) Final Correction Factors for Scenario #3 using Base Excitation and Averaged Normalized Strain

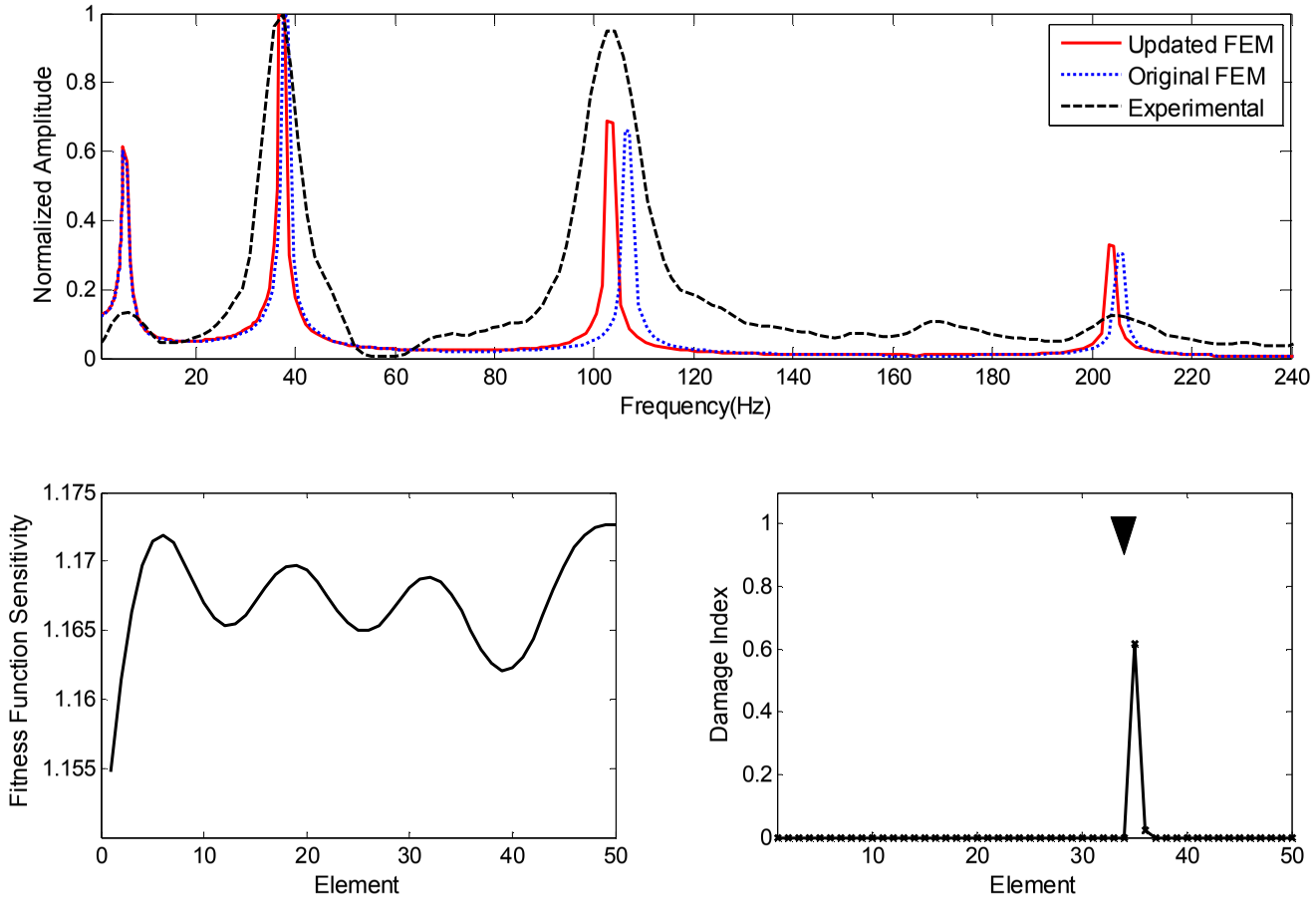

Figure(4.46) Damage Detection Results for Scenario #3 using Base Excitation and Averaged Normalized Strain

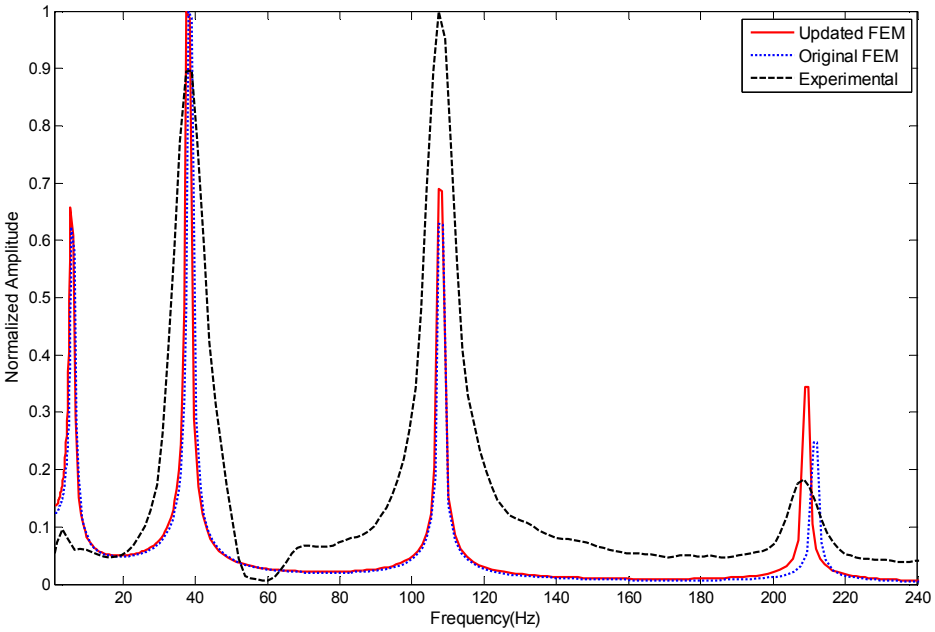

Figure(4.47) Model Tuning Results for Scenario #3 using Base Excitation and Averaged Normalized Strain

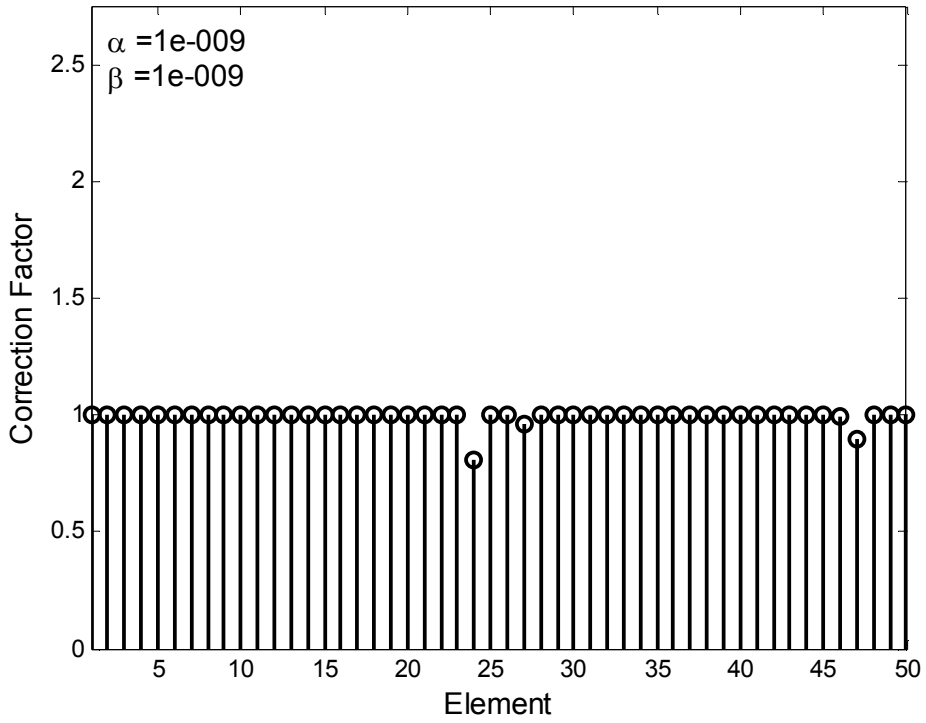

Figure(4.48) Final Correction Factors for Scenario #3 using Base Excitation and Averaged Normalized Strain

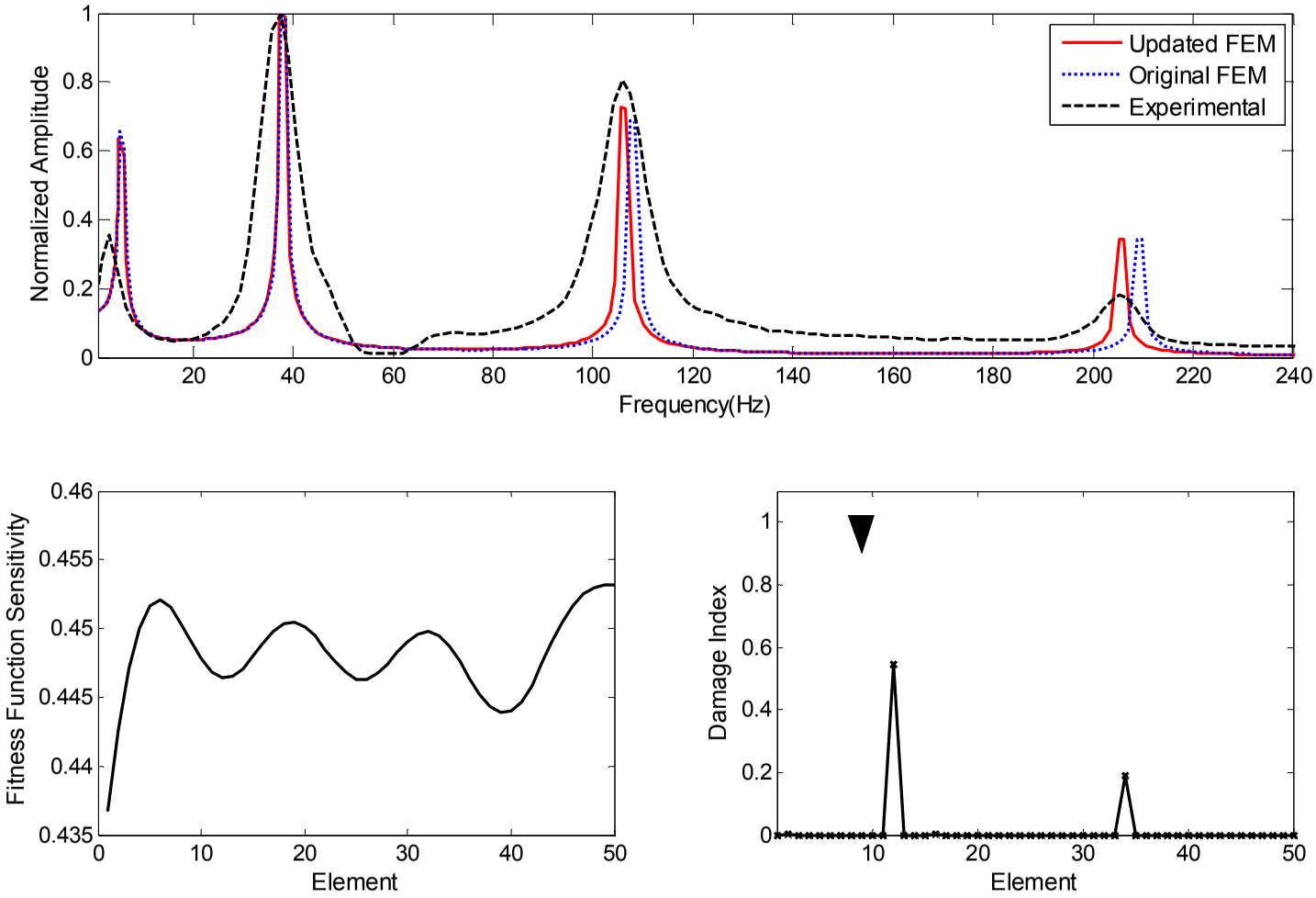

Figure(4.49) Damage Detection Results for Scenario #3 using Base Excitation and Averaged Normalized Strain

5. CONCLUSION AND RECOMMENDATIONS FOR FUTURE WORK

5.1 Conclusions

The Peak Vector cost function which includes both the amplitude and frequency showed high accuracy when used to detect damage in stressed and unstressed parts of the structure. On the other hand, the frequency cost function can only detect damages which have significant effect on the fundamental frequencies.

The model tuning phase is an important feature of the proposed damage detection algorithm. This phase will minimize the effect of modeling and experimental errors on the damage detection algorithm. The overall damage detection algorithm can be considered reliable and error resilient.

The proposed damage detection can function relying on ambient noise and without the need of excitation force feedback. Also, averaging the results from multiple sensors can enhance the damage detection accuracy.

Strain gauges have been shown as a reliable and convenient sensor for modal analysis when coupled with appropriate signal processing.

5.2 Recommendations for Future Work

Three Dimensional modeling of beams

While this damage detection algorithm is generic, it should be noted that the FEM model used doesn't include transverse displacement and torsion displacement. In order to verify that no transverse bending modes or torsion modes will interfere with the experiment results. The sample beam was selected of relatively high rigidity for torsion and bending in the transverse direction. Additionally, sweep modal testing was done for the frequencies between 1 and 250 Hz in, as well as, FEM models built using NASTRAN which all verified that there are no unwanted modes in the region of frequencies of interest. However, to deal with any kind of beams a 3 dimensional beam element should be used and sensors measurements directions should take all degrees of freedom into account.

REFERENCES

1. Doebling, S. W., Farrar, C. R. and Prime, M. B. (1998). "A Summary Review of Vibration-Based Damage Identification Methods". *The Shock and Vibration Digest*, Vol. 30, No. 2, 91-105.
2. Farrar, C.R. and Doebling, S.W. (1997). "An Overview of Modal-Based Damage Identification Methods". *In Proc. of DAMAS Conference, Sheffield, UK*.
3. Cornwell, P., Doebling, S. W. and Farrar, C. R. (1999). "Application of the Strain Energy Damage Detection Method to Plate-Like Structures". *Journal of Sound and Vibration*. Volume, Pages 359-374.
4. Jeong-Tae, K., Yeon-Sun, R., Hyun-Man, C. and Stubbs, N. (2003). "Damage identification in beam-type structures: frequency-based method vs mode-shape-based method*". Engineering Structures* Volume 25, Issue 1, January 2003, Pages 57-67.
5. Shi, Z. Y., Law, S. S. and Zhang, L. M., (1998). "Structural Damage Localization from Modal Strain Energy Change". *Journal of Sound and Vibration* 218.
6. Mayes, R. L., (1995), "An Experimental Algorithm For Detecting Damage Applied To The I-40 Bridge Over The Rio Grande". *In Proc. 13th International Modal Analysis Conference*, pp. 219–225.
7. Kim, J. T. and Stubbs, N. (2002). "Improved Damage Localization from Modal Strain Energy Change". *Journal of Sound and Vibration* Volume 252, Issue 2, 25 April 2002, Pages 223-238.
8. Huynh, D., He, J. and Tran, D., (2005). "Damage location vector: A non-destructive structural damage detection technique". *Journal of Computers and Structures*, Issue 83.
9. Gun-Myung, L. and Jae-Heung, K. (2007). "Short Communication, Effect of element thickness on the eigenvalues of beams". *Journal of Sound and Vibration* 300, Pages 414-421.
10. Gun-Myung, L. (2003). "Sensitivity of the eigenvalues of beams to the change of element correction factors"*, Journal of Sound and Vibration* 267, Pages 955-960.
11. Sahin, M. and Shenoi, R. A. (2003). "Quantification and localization of damage in beam-like structures by using artificial neural networks with experimental validation". *Engineering Structures*, Volume 25, Issue 14.

12. Saada, M. M. (2007). M.Sc. Thesis, "Finite Element Model Updating Approach to Damage Identification in Beams". American University in Cairo, Egypt.
13. Smith, S.W. (1997). "The Scientist and Engineer's Guide to Digital Signal Processing". California Technical Pub.
14. MATLAB (1998). "The MathWorks", MR Guide - Inc., Natick, MA,
15. Rao, S.S. (2004). "Mechanical Vibrations Fourth Edition". Pearson Prentice Hall.
16. Zivanovic, M. and Carlosena, A. (2006). "On asymmetric analysis windows for detection of closely spaced signal components". *Mechanical Systems and Signal Processing*, 20.
17. Maia, Silva, He, Lieven, Skingle, To, Ugrueira (1998). "Theoretical and Experimental Modal Analysis". Research Studies Press ltd.
18. Vanlanduit, S., Verboven, P. and Guillaume, P. (2003). "On-line detection of fatigue cracks using an automatic mode tracking technique". *Journal of Sound and Vibration* 266 .805–814.
19. Chandrupatla, T.R and Belegundu, A. D. (2002). "Introduction to Finite Element in Engineering", Third Edition. Pearson Prentice Hall.
20. Li, H. and Love, P. E. D. (1998). "Site-Level Facilities Layout Using Genetic Algorithms", *Journal of Computing in Civil Engineering*, Issue 227.
21. Lee, I. W., Kim, D. O. and Jung, G. H. (1998). "Natural Frequency and Mode Shape Sensitivities of Damped Systems: Part II, Multiple Natural Frequencies", *Journal of Sound and Vibration*, Issue 233.
22. Erturk A and Inman D J (2008). "Issues in mathematical modeling of piezoelectric energy harvesters", *Smart Materials and Structures*.
23. Metwalli S. M., Shawki G.S.A. , Mokhtar M. O. A. and Seif M. A. A. (1983), "Multiple Design Objectives in Hydrodynamic Journal Bearing Optimization". *The American Society of Mechanical Engineers*.
24. Zitzler, Eckart and Thiele, Lothar (1999). "Multiobjective Evolutionary Algorithms: A Comparative Case Study and the Strength Pareto Approach". *IEEE Transactions on Evolutionary Computation.*